University of Nairobi

School of Engineering

Department of Electrical and Information Engineering

**MODELLING RAIN ATTENUATION PREDICTION
FOR TERRESTRIAL LINKS AT
CENTIMETER AND MILLIMETER BANDS OVER KENYA**

Thesis submitted in partial fulfillment of the requirements for the award of the Degree of Master of Science in Electrical and Electronic Engineering in the Department of Electrical and Information Engineering of the University of Nairobi.

BY

Joseph Oyoo Onaya

BSc. Electrical and Electronics Engineering University of Nairobi

F56/88620/2016

February 2023

DECLARATION OF ORIGINALITY

NAME OF STUDENT: JOSEPH OYOO ONAYA

REGISTRATION NUMBER: F56/88620/2016

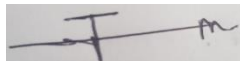**FACULTY/ SCHOOL/ INSTITUTE:** Engineering

DEPARTMENT: Electrical & Information Engineering

COURSE NAME: Master of Science in Electrical & Electronic Engineering

TITLE OF WORK: Modelling rain attenuation prediction for terrestrial links at centimeter and millimeter bands over Kenya

1) I understand plagiarism and am aware of the university policy in this regard.
2) I declare that this research is my original work and has not been submitted elsewhere for examination, award of a degree, or publication. Where other people's or my work has been used, this has been acknowledged and referenced following the University of Nairobi's requirements.
3) I have not sought or used the services of any professional agencies to produce this work
4) I have not allowed and shall not allow anyone to copy my work to pass it off as their work
5) I understand that any false claim in respect of this work shall result in disciplinary action, per the university anti- plagiarism policy
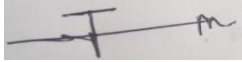
Signature:

Date: 6th February 2023

DECLARATION

This thesis is my original work and has not been presented by any other university for a degree award.

Signature: Date: 6th February 2023

JOSEPH OYOO ONAYA

F56/88620/2016

This thesis has been submitted for examination with our approval as university supervisors.

Signature: Date: 9th February 2023

DR. PETER ODERO AKUON

University of Nairobi

Signature: Date: 10th February 2023

PROF. VITALIS KALECHA ODUOL

University of Nairobi

Acknowledgement

Name: Joseph Oyoo Onaya

Registration Number: F56/88620/2016

Thesis Title: Modelling rain attenuation prediction for terrestrial links at centimeter and millimeter bands over Kenya

Abstract

The wireless sector of telecommunications networks has seen the development of more data-hungry products and services due to the industry's ongoing growth. The radio network's constrained bandwidth must support these services and products. However, radio network systems still under-utilize the frequency spectrum, particularly in the higher frequency bands, because rain substantially attenuates high-frequency signals through methods of absorption and dispersion.
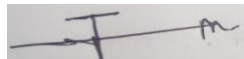
Prediction of rain attenuation has remained an active research problem for implementing radio links. The International Telecommunications Union Radio Sector Recommendation (ITU-R) periodically updates its model based on new research approaches that lead to better rain rate prediction models.

Based on two years' worth of rainfall data, this thesis presents the cumulative distributions of rain intensity for 87 locations across various areas of Kenya. According to ITU-R standards, the rain rate with a 60-minute integration time is changed to an integration period of 1 minute. The resultant cumulative rain intensities and their relationships are evaluated against the global data published in ITU-R Recommendation P.837 and against the work in other African nations.

Given that raindrops are not spherical and are flattened at the base, the results demonstrate that the specific rain attenuation for horizontal polarization is more significant than for vertical polarization. As a result, the horizontally polarized waves are attenuated more than the vertically polarized waves. Additionally, it is also determined that the ITU-R mapping of Kenya as $50 mm/hr$ underestimates rain attenuation in certain parts of the country and over estimates in other parts.

Contour plots of specific attenuation are modeled based on the collected data and the outcomes, which reflect the true rain rate for the various locations in Kenya where these values should be used by Mobile Network Operators for link designs.

Signature:

Date: 6th February 2023

Table of Contents

List of Figures

List of Tables

Nomenclature

1. TLC   Telecommunications

2. FSL   Free-Space Loss

3. LOS   Line of Sight

4. RSD   Raindrop Size Distribution

5. RF   Radio Frequency

6. PDH   Parallel Digital Hierarchy

7. SDH   Synchronous Digital Hierarchy

8. CCDF   Complementary Cumulative Distribution Function

9. RCDD   Rain Cell Diameter Distribution

10. ITU-R   International Telecommunication Union-Radio

11. UPC   Uplink Power Control

12. MNO   Mobile Network Operator

CHAPTER 1

1   INTRODUCTION

This chapter includes an overview of the ITU-R perspective on rain attenuation, a general background on attenuation due to rain and its effects on point-to-point terrestrial links, as well as a problem statement, research objectives, research questions related to the objectives, research justification, the scope of the research work, and a description of the thesis organization.

1.1   Background

The telecommunications (TLC) industry is continuously expanding, leading to the inception of goods and services with data-intensive demands within the wireless TLC systems. The limited bandwidth of the radio network must support these goods and services. However, radio network systems still underutilize the frequency spectrum. Indeed, rain negatively attenuates high-frequency transmission lines through absorption and scattering methods [1]. Therefore, at the planning stage for links, the TLC design engineers must consider the extent of attenuation due to rain that is expected in a transmission link located worldwide in any place. Understanding the properties of precipitation rate and attenuation is essential for this procedure.

In wireless telecommunications systems that use radio frequency (RF) as the primary transmission medium, microwave links play an important role. Point-to-point (multipoint) microwave links typically use the Synchronous Digital Hierarchy (SDH), but most of the underlying and eventual terrestrial communication systems use the Digital Hierarchy. Parallel digital (PDH). When designing a microwave link, TLC engineers often pay attention to the following factors: (a) systems that are reliable; (b) designs that are cost-effective; c) current and future frequency selection and planning; (d) limiting the quantity of extra wireless sites to reduce frequency charges; and (e) flexible, multi-level and adjustable communications system.

Due to signal attenuation along the line of sight, microwave links are susceptible to a variety of signal interference challenges; The path of microwave transmission is generally due to physical variations occurring in the troposphere and tropics. We have hydrometers, i.e., rain, fog, humidity, and oxygen, in the path of a radio signal (propagation path), which can significantly weaken signals by absorbing them. Rain is the chief source of signal loss from path attenuation within the hydrometers, proving to be a substantial issue in link designs for microwave radios, mostly for

operations at upper frequencies, typically over 10 GHz [2]. Therefore, the rain-persuaded decline is the most important in causing propagation loss because it usually attenuates the propagation of radio waves along the conduction line. This elicits that rain attenuation negatively affects the path lengths of terrestrial microwave links. Therefore, their use is severely restricted for the point-to-point microwave transmission systems at high frequencies for these terrestrial links

We are able to measure the effects that rain has on the design of terrestrial point to point (multi point) that relies on electromagnetic radiation. This can be done for waves from 10km of the earth's atmosphere. The total attenuation due to rain is usually added together with losses due to free space (FSL) along the path of propagation, this helps in determining the total path loss. This is considered in conjunction with the expected rain rates. These rates are usually measured in millimetres per hour. This rate is usually determined by the size, shape, and frequency of drops of the rain. The rate of the rain together with raindrop size distribution usually varies the total value of the path loss. Rain rate has a dissimilarity in its profile. The area occupied by rain referred to as rain cell will be considered along the propagation path. Heavy rainfall leads to small rain cells.
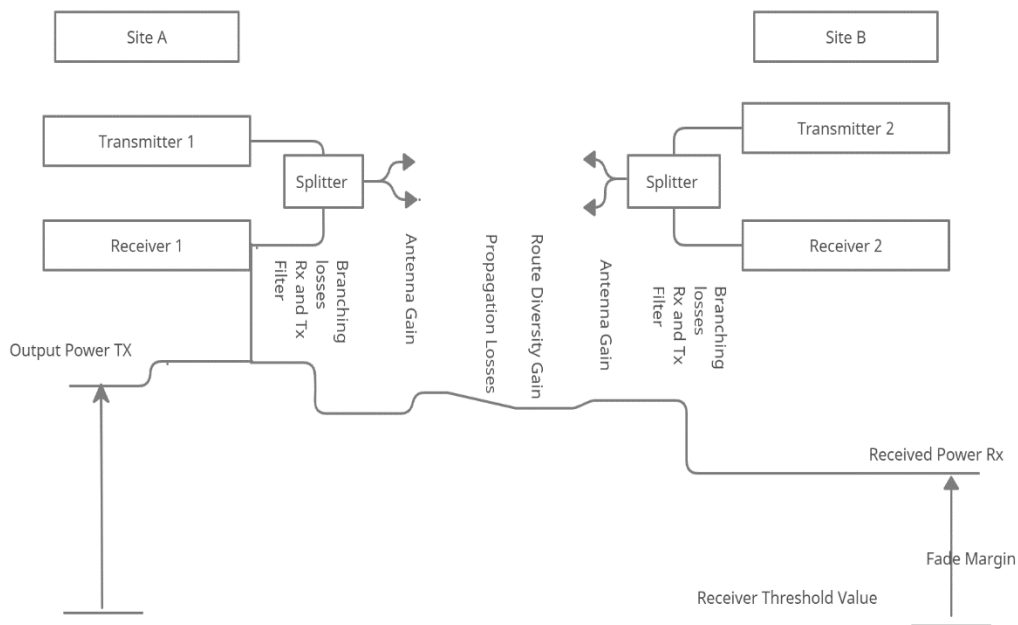
Figure 1.1 Sample attenuation margin allocations

Fig. 1-1 summarises the fade margin calculations often met in the link planning process. The receiver threshold value is set, so the radio equipment runs a constant bit error rate, BER. A distinctive value for BER is 10^{-6}. Another solution to this is the employment of forward error-

correction methods. The transmitted power suffers branching and propagation path losses, but the gain of a transmitting antenna and the reception antenna provides for some losses. Various mitigation methods have been suggested to achieve higher power levels on the receiver. Route or site diversity is used to increase the effective fade margin. Uplink power control, UPC, or automatic transmitter power control are also some of the practical mitigation techniques, but their operation bandwidth is limited due to the non-linear amplifier characteristics under increased power levels [8].

Besides, the significant contribution of the fade margin depletion comes from rain attenuation especially for shorter wavelengths or frequencies higher than 10 GHz [9 –12]

In an effort to understand the characteristics of rain, several research ideas have been brought forward by many authors and studies conducted by ITU-R. Observations have been made that the growth in rain rates is non-uniform, inhomogeneous, and characterized by spatial variation of rain drops depending on the geographical area. Rain rates depend on the number of rain drops, rain drop diameters (which can be measured directly from the disdrometer), and the size of the spacing between rain drops. Theoretically, the spacing between the rain drops may be estimated by `listening' to the time intervals between the drops in measuring equipment. It can be said that if the drops coalesce, then the packing density of rain drops is unity which means that any wave that traverses this unity drop density will always be intercepted for all the cell length. Such rain forms have been reported to be of convective nature. Stratiform rain drops do not coalesce, and therefore the rain drop packing density can be assumed to be less than unity. The general inference of this rain drop packing density is that within a rain event, a radio wave does not always undergo attenuation in the whole length of the rain cell. This is because, depending on the rain structure, there are spaces between rain drops, and therefore the effective length that is responsible for attenuating the waves will always usually be less in length than the observed rain cell diameter. This is to be referred to as rainy cell diameter. As a result, if the size of the rainy cell diameter is known, then attenuation along a propagation path caused by rain in a link is derived from the size of this cell diameter only. The rainy cell diameter is estimated as the measured rain cell diameter (which includes spatial variation of rain drops) minus the spacing between rain drops. However, there is an inherent difficulty in directly measuring the spacing between rain drops in a rain event, especially for point rain measurements or even in rain field measurements from radar observations.

1.2 ITU-R Perspective

There are fifteen climatic rain zones in the world, according to research from the ITU-R 837-7. Utilizing the cumulative median distribution of rainfall rate for the rain climate area, this was accomplished [10]. The figure below depicts the rain intensity in various climatic zones. These are to be utilized to obtain the rain intensity for estimating attenuation caused by rain on both terrestrial radio links and earth satellite microwave links for areas without adequate data on the cumulative rain intensity distribution [30].
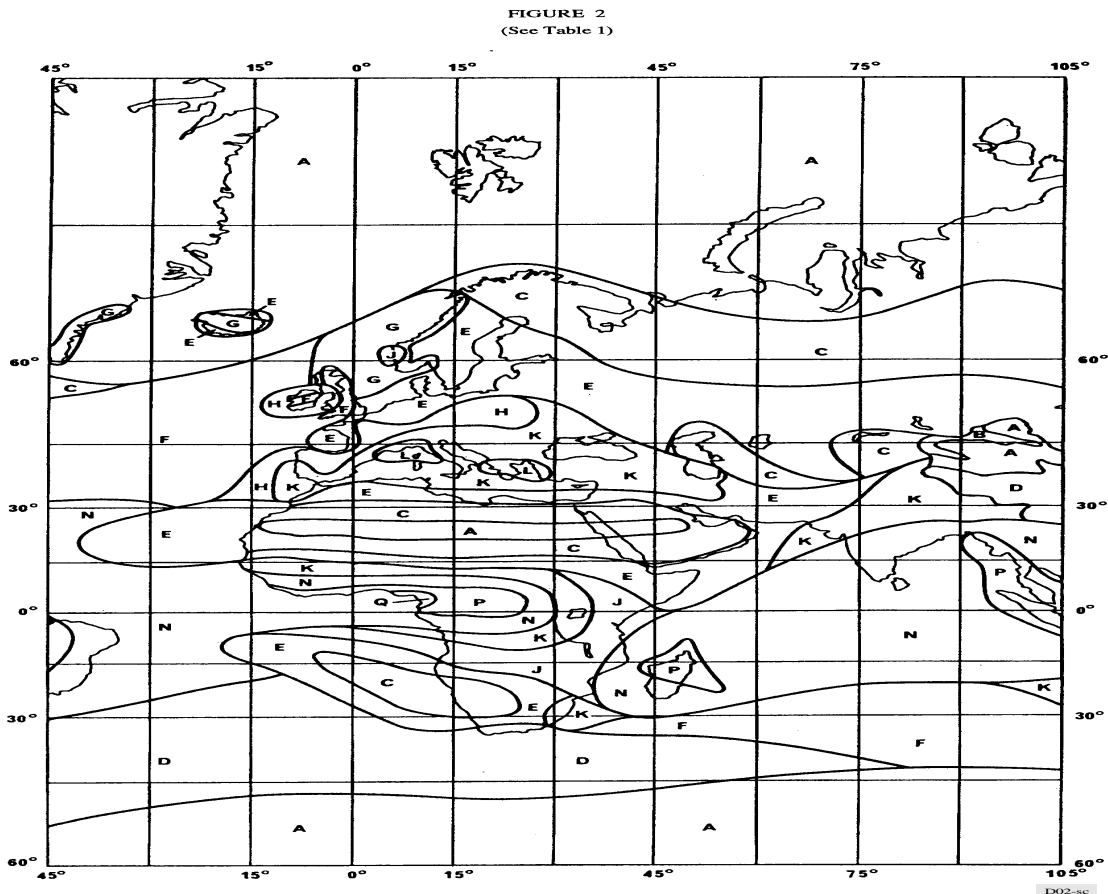
Figure: 1.2 ITU-R rain climatic zone boundaries in Europe and Africa

Sub-Saharan Africa is divided into six rain zones according to the ITU-R classification: D, C, J, E, N, and K. It is abundantly obvious that these ITU-R designations are frequently insufficient for attenuation prediction [30]. From this map it ca be seen that Kenya is in zone J and E with a little portion in K.

The discrepancy in the ITU-R has been pointed out by Migliora et al. [31], [30] in Brazil, where from rain rate measurements, they obtained 11 rain climatic zones as opposed to two rain climates

(N and P) classified by ITU-R. Similarly, according to ITU-R, China is designated by 5 types of rain (E, F, G, H, K); Zang et al. [32], [30] were able to obtain 12 rain climatic zones for China. Hence, a great need exists that based on local actual collected rain data, we can redefine the ITU-R regional rain climatic zones [30], especially in equatorial and tropical climates.

1.3   Problem Statement

Studies due to the effects of rain attenuation have been done all over the world in the past decades, and several models for finding a solution to the problem have been offered. However, lower atmosphere propagation conditions that do exist in tropical and equatorial parts of the globe offer a huge constraint on terrestrial radio communications. Therefore, there is a need for accurate prediction of propagation as over or under prediction of propagation effects due to rain can result in costly over-design of systems or unreliable systems.

There exist databases of propagation measurements; however, most of these data are based on measurements taken in the northern hemisphere temperate zones. It is clear that in the tropical and equatorial zones, the factors that impair signal strength are different from those used in the temperate regions. This therefore means that actual data collected from both the tropic and the equatorial region should be used to build more solid databases of propagation measurements to improve on link reliability; as we will get more accurate results desirable for every particular area. Kenya, in particular, has no known model based on local rain information; we wish, therefore, to develop a model based on rain data collected locally.

1.4   Objectives

We aim to formulate and propose a suitable rain attenuation model for Kenya based on local rain data; then, using global conversion factors, we will obtain the desired rain rates, and the results achieved will be measured against the existing ITU-R P.530-17 models.

The specific objectives are:

i.   To obtain accurate rainfall rate data at selected geographical locations in Kenya for several years and convert it into a 1-minute time of integration

ii.   To determine the cumulative dissemination of the rate of rainfall and the rain rate past 0.01% of the time in the selected locations

iii.   To classify Kenya into different zones of climatic rain on account of the available data and draw contour maps.

iv.   To calculate the specific attenuation of rain for the chosen locations based on the available rain data and approximate the path factor r for the selected locations using ITU-R P.530-17 model.

1.5   Research Questions

To accomplish the above-stated objectives, the following research questions were examined:

(i) How can we convert the 5-minute rain data into 1-minute rain full data to enable analysis using ITU-R P.530-17 model?

(ii) How can we calculate the rain rate in Kenya at 0.01% of the time?

(iii) How are horizontally and vertically polarized signals fair in rain-induced attenuation?

1.6   Justification for the Study

Rain attenuation is a major stumbling block to the good performance of high-speed wireless communication networks. This attenuation affects their degree of robustness and reliability. Therefore, this attenuation must be considered during the design process of such networks, which are robust, reliable, and have good performance. It is a clear fact that rain causes attenuation of signals with different levels of intensity based on the rain drop size, rain intensity, rain rate, transmit/receive frequencies, and power of the transmission. Terrestrial point-to-point microwave radio links in most cases suffer complete signal outages/loss at higher rain rates and at 10 GHz and above.

There is, therefore, a need to determine exactly the total amount of attenuation on the propagated signal on a point-to-point microwave links due to rain rate and raindrop sizes that vary in nature. We appreciate that considerable studies have been carried out on this subject; there still exists gaps, and the studies are inconclusive in certain cases. Consequently, there exists a need to get better and more accurate prediction models for rain rates, raindrop size distributions, rain attenuation signal phase shift, and signal depolarization effects caused by raindrops along the microwave terrestrial radio links

In fact, ITU-R continues to carry out studies on propagation modelling specific to rain attenuation, namely ITU-R 530, 837, and 838 recommendations.

1.7   Scope of Work

The research project has the following scope and input to the knowledge body.

- To examine the current rainfall rate models and, using the available data, determine $R_{0.01}$ that is applicable in Kenya for the various locations model that offers better results based on rain data collected from local stations.

- To determine specific rain attenuation, rain attenuation, and the fade margins for select locations based on the data available for Kenya and compare the results to ITU-R mapped value of 50 mm/hr.

1.8   Limitations and assumptions

This research work does not include details of meteorological studies, that is, types of rainfall (convectional, stratified and relief, etc.) and environmental features. Antenna size, metallic properties, and design, which also greatly influence signals during rainfall, are not considered within the scope of the rain model.

1.9   Thesis Organization

There are five main chapters in this thesis; the first comprises an introduction, a problem definition, research objectives, justification for the research, and a description of the work done, limitations, and assumptions. Chapter 2 focuses on the review of the literature. Estimating rain attenuation along a communication link requires using rainfall rate modeling, which is significant. Physical models, analytical models, and empirical models are all treated. To estimate the relevant parameters that will best characterize the patterns of rainfall rate distribution, a good methodology is needed. Additionally, this section looks at several rain rate conversions.

Chapter 3 focuses on the methodology used to and how data was collected and ultimately analysed, the rain rate measurements and cumulative distributions, and specific attenuation. After modifying the data in accordance with the ITU-R model, the results and analysis are presented in Chapter 4. Conclusion and recommendations for further research are included in the subsequent chapter.

CHAPTER 2

2 LITERATURE REVIEW

This chapter overviews the atmospheric effects on wave propagation on a point-to-point terrestrial link. It briefly describes the types of rain and models used in rain rate prediction, summarises attenuation due to rain, reviews previous research studies, and the problem formulation.

2.1 Introduction

There is a huge demand for already congested radio spectrum, and broadband services have grown in volumes, putting pressure on the need to explore frequencies above 20 GHz. However, at frequencies above 20 GHz, radio signals suffer strong distortion since the rain drop size and the signal wavelength become comparable.

In tropical countries like Kenya, we have great diversity in the conditions of climate in relation, particularly to rain, we would like, therefore, to investigate a prediction model that would be very useful to all ranges of rain fall rates. We appreciate the existence of experimental and empirical theoretical studies which have been done with respect to rain attenuation to improve service availability and microwave link planning.

In the 80s to date, prediction techniques have been explored for statistical estimation to derive attenuation probability on signal path lengths. There exist two approaches, based on the use of attenuation measurements collected over a greater number of samples at varying locations, frequencies, and signal path length. The manipulation of attenuation values derived from locally collected data from meteorological departments is usually another approach. Usually, this last approach is considered as its modelling is based on a large number of available data and gives more accurate results.

2.2 Wireless Communication and Technologies

Access networks made up of optical fiber and wireless technology is crucial for granting information availability. Each of these two technologies has drawbacks of its own. Optical fiber, for example, offers enormous bandwidth and blazingly fast speeds, yet this cable is not widespread due to cost. Wireless communication networks, on the other hand, have the potential to be everywhere, but their communication route is especially vulnerable to atmospheric and environmental interference. Large bandwidths are available for quick and effective communications over satellite and terrestrial lines at frequencies above 10 GHz [11] [17] [19].

Some of the benefits of the use of 5G technologies include high throughput and reduced latency. Wireless communication networks should have almost no interruptions for these technologies to be successfully implemented. Unfortunately, service interruptions tend to occur over communication networks operating at 7 GHz and above due to signal fading caused by raindrops. [19] [31]. In order to deliver a dependable service, link designers aim for links that are available for at least 99.99% over the course of a typical year or better.

2.2.1 Effects of the atmosphere and wave propagation

Communication systems operating (notably those with smaller elevation angles) at frequencies above 18 GHz may suffer considerably as a result of multiple simultaneous causes of attenuation due to atmospheric characteristics. Gas, rain, clouds, and tropospheric scintillation are a few of these sources of attenuation. The following formula is provided by ITU-R [11] for estimating the total attenuation arising from these different sources:

$$A_{total}(p) = A_G(p) + \sqrt{(A_R(p) + A_C(p))^2 + A_s^2(p)} \tag{2.1}$$

Where A_R is the rain attenuation, A_C is cloud attenuation, A_S is atmospheric scintillation attenuation, and p is the probability of exceeding attenuation in the range of 50% to 0.001% and where A_G is the attenuation due to gases (steam and oxygen). Note that A_c and A_C are considered at $p = 1$ [11].

2.3 Atmospheric signal propagation

The unpredictability of atmospheric properties that change from hourly, daily, monthly, or yearly degrades microwave signals as they travel through, notably at lower altitudes in the atmosphere [3]. As a result, understanding the statistics of the effects of one or more of these layers on electromagnetic signals is important for microwave system designers. For short-range communications, the millimeter and microwave bands offer the advantage of frequency reuse. However, these bands experience a significant signal loss due to atmospheric properties during wave propagation [11]. Other significant propagation limitations that have an impact are atmospheric effects due to clear air, dust storms, sand and fading owing to impediments, scintillation, beam spreading, and multipath. These are some factors that can have an impact on satellite and terrestrial network signal transmission.

The lower atmosphere is said to be inhomogeneous, hence, refractory and absorbent. In particular, in the millimeter and microwave wave ranges, these features have a significant impact on electromagnetic signal waves. Extremely refractive tropospheric layers are the main cause behind radio frequency wave signal degradation. Antenna decoupling, diffraction, diffusion and beam scattering are some of the effects addressed here [8] [20] [9] [12].

When electromagnetic wave encounters a barrier during its course of propagation, the wave is forced to take two or more paths to reach its destination, some of which may have been the result of several refractions and or reflections. Reflective materials tend to be rough due to diffusion at short wavelengths, so most of the signal is diffused into the material rather than reflected, weakening the signal at the receiver. The propagation medium is inhomogeneous hence likely to cause a signal's direction to diverge as it travels through the atmosphere. Scattering is the term used to describe this effect [20].

In the presence of clean air, electromagnetic signals are scatted, diffracted, and absorbed. As seen in Figure 2.1, oxygen and water molecules are the principal causes of these variables. Because of this, energy is also lost during the transmission of an electromagnetic pulse through uncontaminated air. The amount of water vapor present, the temperature, air pressure, and transmission frequency all affect how much the atmosphere affects an electromagnetic wave. According to estimates, nitrogen makes up 78% of the atmosphere's volume, followed by argon (0.9%), oxygen, O_2, (21%); carbon dioxide CO_2 (0.1%), and variable water H_2O vapor.

The water content level is constrained by the atmosphere's present temperature, resulting in very low amounts in polar regions and up to 4% in tropical areas. Condensation begins when the water vapour content exceeds 4%, and the extra water vapour is then expelled from the atmosphere [20]. Up to 100 GHz in the transmission bands, oxygen and water vapor among these substances show visible resonance.

Water vapor's attenuation of signals has a quadratic formula on its reliance on the density of water vapor at high concentrations greater than 12 gm^{-3}, four fundamental input parameters were given: temperature (°C), total pressure (kPa), frequency (GHz), and relative humidity (%) to analyze the impacts of signal propagation travelling via means of the environment [36][37]. Figure 2.1 depicts the particular attenuation for an atmospheric signal caused by gaseous absorption. Figure 2.1 shows 60 GHz and 118.74 GHz as the peak frequencies for oxygen absorption.

The absorption effect for water vapor peaks at 22 GHz and 183.3 GHz, respectively. Transmission windows are areas that become transparent to electromagnetic propagation between absorption peaks. Transmission windows can be seen in Figure 2.1 at the following GHz ranges: 35 GHz, 94 GHz, 140 GHz, and 220 GHz.

The free space equation, which is commonly used in wireless communication to relate transmitted power P_T and received power P_R, is provided by [3][20][41]:

$$\frac{P_R}{P_T} = \left[\frac{G_T G_R \lambda^2}{(4\pi d)^2}\right] g_T(\theta, \varphi) g_R(\theta', \varphi') \tag{2.2}$$

$g_T(\theta, \varphi)$ and $g_R(\theta, \varphi)$ are relative directional gains at spherical angles (θ, φ) respectively and G_T and G_R are transmitter and reception gains, λ is the wavelength of the electromagnetic wave, and d is the distance or range between two antennae. Equation 2.2 can be arranged and the transmission loss written as:

$$P_R = P_T \left[\frac{G_T G_R \lambda^2}{(4\pi d)^2}\right] g_T(\theta, \varphi) g_R(\theta' \varphi') \quad [watts] \tag{2.3}$$

Using logarithms on each aspects of the equation,

$$10log_{10}(P_R) = 10log_{10}\left[\frac{P_T G_T G_R g_T g_R}{(4\pi d)^2}\right] g_T(\theta, \varphi) g_R(\theta' \varphi') \quad [dB] \tag{2.4}$$

$$P_R = P_T + G_T + g_T + G_R + g_R + 20log_{10}(\lambda) - 20log_{10}(d) - 22 \tag{2.5}$$

Where P_T, G_T, g_T, g_R are in decibels.

The transmitted power minus the received power is the amount of power lost in the medium. Thus, this loss can be described as:

$$L = P_T - P_R = -(G_T + g_T + G_R + g_R + 20log_{10}(\lambda) - 20log_{10}(d) - 22) \quad [dB] \tag{2.6}$$

The distance, d, and wavelength are measured in the same units, while the antenna gain, G is expressed in decibels (dBi) In relation to an isotropic antenna.
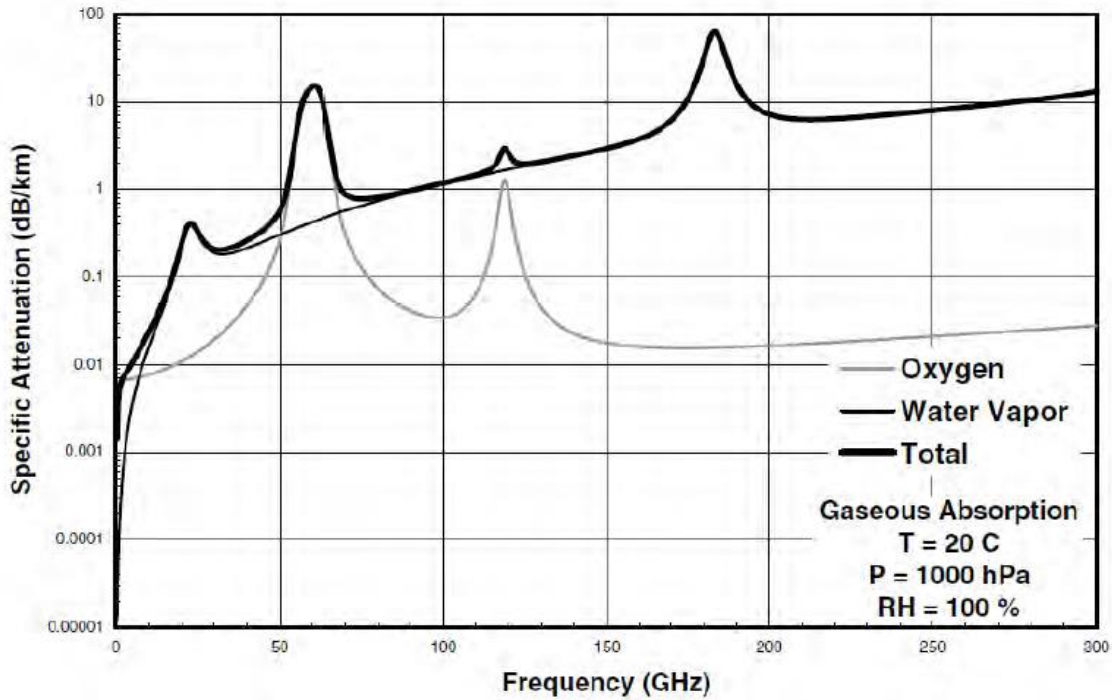
Figure 2.1 Specific attenuation in clear air with frequency dependence [3]

2.3.1 Hydrometeor effects on signal transmission

According to [40], humidity (or moisture) is evident on the horizon, even on sunny days. Hydrometeors, regardless of their shape, have a significant repercussion on electromagnetic waves exceeding 10 GHz [3] [20] [40]. The most common types of hydrometeors include fog, water vapor, clouds, and precipitation, including rain, snow, and hail. These hydrometeors transform into lossy dielectrics moving in the air, and rain is the main source of signal tempering when there is an electromagnetic wave [43]. Clouds do occur more frequently than rain, even though they might not have much of an impact on electromagnetic waves. They consist of suspended water droplets with a diameter of 0.01 cm or less. Therefore, specific attenuation brought on by clouds can be computed as follows, according to [45]:

$$\alpha_c = K_c M \quad [dB/km] \tag{2.7}$$

where M is the liquid water content expressed in g/m^3, and K_c, an attenuation constant that depends on temperature and frequency is also present. The atmospheric water vapor that is

condensed and is afloat in the atmosphere is what is commonly referred to as fog and can be a major worry for designers of point-to-point links when determining the most dependable linkages, especially along coastal regions [40] [45]. Accordingly, normalized fog attenuation is represented as follows:

$$A = -1.347 + 0.0372\lambda + \frac{18}{\lambda} - 0.22T[(dB/km)/(g/m^3)] \qquad (2.8)$$

Where T is the temperature and λ in $[mm]$ is the wavelength, which is true for -8 to 25C. Accordingly, therefore; empirical formula for determining attenuation occasioned by fog is as follows:

$$V = 0.024M^{-0.65} \qquad (2.9)$$

Where V is the visibility of the fog for drop sizes between $0.3\mu m$ and $10\ \mu m$, and M is the water content expressed in $[g/m3]$.

2.3.2 Rain's microstructural characteristics

A group of water droplets from the sky that return to the earth's ecosystems is what is known as rain. The percentage of rain's attenuating effect on a microwave signal can be better understood by studying microstructural features such as rainfall rate and size distribution, rainfall rate, and velocity. One of the most crucial factors affecting the microwave in this band is raindrop size and the distribution of rain drop sizes (DSD) [46]. A raindrop in free fall can take on a variety of shapes, including a sphere, an oblate-spheroid, a spheroid, and even a hamburger. A drop's base takes on a concave shape above 4 mm. Furthermore, Figure 2.2 provides a distinct representation of the fall velocities of various diameters in that larger drops fall with a greater velocity than the minute ones.
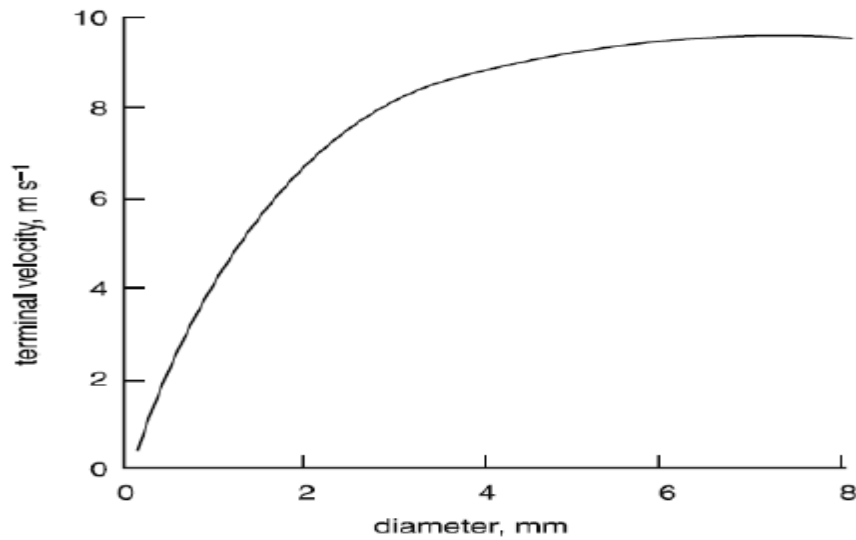
Figure 2.2 Raindrop diameter as a function of terminal velocity [47]

Convective and stratiform rain are two types of rain that can be distinguished from one another [7] [46]. Nimbostratus clouds, which are created when warm air and cooler air clash to create the latter type of rain, eventually fall as rain on Earth. Stratiform rain is distinguished by being prolonged, and widespread and occurs in conjunction with low rainfall rates. Contrarily, convective rain forms convective clouds (cumulonimbus) produced when hot, moist air rises and then fall back as rain to the earth over a particular area for a brief time [3]. This type of rain, connected to high rainfall levels, is common in the tropics.

2.3.3   Types of Rain
Rain is a local phenomenon; its consequence depends on the rain characteristics and spatial distribution [35]. Rain can be classified into five types:

❖ Stratified Rain: Widespread areas with low rain rates of about 25 mm/h and tiny small immersed showers, with a horizontal extent of hundreds of kilometers and a duration greater than one hour [34], [35].

❖ Convective Rain: Localized areas with relatively high rain rates, with strong ascending and descending wind currents that extend deeply into the troposphere. These areas have columnar shapes and sometimes extend up to the tropopause. Very high rain rates with horizontal regions of a few kilometers are possible, but they do not last very long (tens of

14

minutes at most). The more intense downpours in temperate climates are usually of this type [35].

- ❖ Orographic Rain: Caused entirely or mostly by the forced uplift of moist air over high ground [34].
- ❖ Monsoon Rain: Intense convection rain bands in a sequence followed by periods of stratified rain. This rain has bands typical widths of 50 km and lengths of over one hundred in length and yields heavy rainfall going for long hours daily [34]- [35].
- ❖ Tropical Storms Rain: Large systematized regions of rain which may extend over hundreds of kilometers. Tropical storms exhibit a number of spiral bands that terminates in zones of intense rain neighbouring the central region, which are known to be the eyes of the storm. Spiral bands similarly have regions with heavy convective rain [34]- [35].

2.4   Rain Rate Prediction Modelling

Presently, various analyses have been employed to estimate the effects of propagation through the rain. Physical modelling involving theoretical formulations has been attempted that require complete knowledge of the rain medium and all the boundaries, though this is not readily feasible. Other quasi-empirical methods are used today to address this uncertainty.

The methods make use of assumptions of propagation physics that affect the attenuation magnitudes and derive parameters from rain climatological data however it does not compare with attenuation data to regulate the derived parameters. On the other hand, empirical models use a summary of statistics of the path performance sourced from a collection of measurements that has always been from mid-latitude and continental climate locations.

The method involves extrapolating them with given occurrence probabilities to different frequencies and sites by using rain rate statistics and measured attenuation to set the model parameters. This is called modelling by regression. Regression modelling can be applied in attenuation prediction by using existing attenuation measurements and applying them to any attenuation equation to derive the regression coefficients [3,5–6]. It is useful if a large database of attenuation measurements is available and accessible, like those maintained by the ITU-R.

Also, sites like those in tropical regions lack these large attenuation databases. The other method is to use a physically randomly occurring scenario with similar rainfall features to model the attenuation parameters or a semi-empirical approach.

Several approaches have been suggested that the accuracy of the approach varies in the prediction of rain attenuation: we have analytical models used for the determination of the specific attenuation [12, 14–16], effective path length models [5–6, 17–20] and "Synthetic Storm" models [21–24]. Other ways of modelling include rain cell-shape profile models [25–32] and path-average rain rate models [3].

The variation in the methods depends on how the effective path length is computed. But, more specifically the accuracy of the approaches varies, whether or not attenuation is assumed to grow uniformly or not along the path. The growth of rain tempering with rain rates is not uniform in a given rain event [3, 5–6]. Some other models give predictions at some percentage of time e.g. the ITU-R model while others give predictions based on the full rain rate. Another class of models are improvements on the existing ones. The next section is a review of rain-fade modelling classes: specific attenuation, effective path length, rain cell-shape profiling methods, and the "Synthetic Storm" technique.

2.4.1   Rain Rate Prediction Models

The use of rain rate models for estimating point rainfall-rate cumulative distributions for a site is very beneficial. Previous studies propose several empirical models for predicting the point rainfall-rate cumulative distribution [52] [53]. Olsen (1999) underlined the importance of precise rainfall rate forecasts when estimating rain attenuation in order to avoid designing expensive or faulty systems due to under- or over-prediction. The work of Crane [3], which had a significant impact on the ITU-R zonal models, is also one of these models. Segal (1996) also created a model that impacted the definition of rainfall zones in countries like Canada, and ITU-R zonal models. To calculate the rain rate needed for fading calculations, Watson et al. [48] have developed a technique that provides accurate predictions of the severity of the rain.

Rain rate distribution should be calculated at an interval of one minute or less and be based on long-term data lasting about 10 years to be accurate. Although numerous weather services record data hourly and every five to thirty minutes, one-minute rain statistics are rarely available [8]. Longer integration intervals are known to exclude higher rate data and change the distribution [8] which has prompted academics to create solutions to the issue of converting from longer

integration periods to shorter counterparts. According to the functional principles outlined by Capsoni et al. (2008), the established conversion methods are divided into various classes:

Physical method: This method makes use of the monthly accumulation, annual accumulation, average annual accumulation, and annual rainfall rate. The models that are used the most frequently are the Crane model, Dutton-Dougherty model, ITU-R P.837-5, 2007, Rice-Holmberg model, EXCELL approach, and physical-stochastic method.[10] [53][55]

Analytical method: The one-minute equivalent of the rain rate's cumulative distribution (CDF) at integration time is calculated. Moupfouma, Karasawa, and Ito-Hosaya are a few well-known authors that have used this strategy.[5][6][7]

Empirical method: This method provides equal probability conversion between integration times. The most well-known authors are Watson, Segal, Chebil-Rahman, and Burgueno.

2.4.2   ITU-R Model

According to the context of ITU-R P. 530-17, it is recommended that the attenuation of the path beyond 0.01 percent of the time is obtained by getting the product of the ideal path distance and the specific attenuation A_s in (dB/Km). This is done while considering the space-time variability of rain intensity across the terrestrial path. These values got are then down-scaled through the use of an empirical formula to other proportions of time within the range of 0.01% and 1% whose detailed method can be obtained in the recommendation (ITU-R P. 530-17). This technique is supposed to be utilized globally. The consideration of the utilization of the rain attenuation entails all the operating links of frequency between 5GHz and not exceeding 100 GHz containing path lengths not higher than 60km. The below simple procedure is used in the measuring of the rain's attenuation in long-term statistics:

   a.   Get the rate of rain $R_{0.01}$ that is surpassed for 0.01 percent of time (having a time integration of 1 minute). In the event that this information is unavailable from the long-term measurements' local sources, and approximation can be obtained from the information contained in Recommendation ITU-R P.837-7.

   b.   Calculate the attenuation (specific), $A_S = \gamma R$ (dB/km) for the frequency, rain rate of interest, and polarization through the use of Recommendation ITU-R P.838-3.

   c.   Calculate the effectual path length l_{eff}, of the link by getting the product of the distance factor r and the actual path length l.

d. Compute the effective path length, l_{eff}, of the link by multiplying the actual path length l by a distance factor r. The factor estimation is expressed as [5].

$$l_{eff} = rl \tag{2.10}$$

where l is the path length (actual), and r is a path factor whose estimation is expressed as:

$$r = \frac{1}{0.477\, l^{0.633} R_{0.01}^{0.073\alpha}\, f^{0.123} - 10.579\,(1 - exp\,(-0.024l))} \tag{2.11}$$

Where f (GHz) is the frequency and α is the exponent in the specific attenuation model from Step 2. Maximum recommended r is 2.5, so if the denominator of Equation (2.11) is less than 0.4, use $r = 2.5$.

e. An estimation of the path attenuation exceeded 0.01% of the time expressed as:

$$A_{0.01} = \gamma R l_{eff} \tag{2.12}$$

f. The attenuation $A\%p$ (in dB) exceeded for other time percentages, p of the mean year may be calculated from the value of $A_{0.01}$ by using the following:

$$\frac{A_p}{A_{0.01}} = C_1 p^{-(C_2 + C_3 \log_{10} P)} \tag{2.13}$$

with:

$$C_1 = (0.07^{C_0})[0.12^{(1-C_0)}] \tag{2.14}$$

$$C_2 = 0.855 c_0 + 0.546\,(1 - c_0) \tag{2.15}$$

$$C_3 = 0.139 C_0 + 0.043\,(1 - C_0) \tag{2.16}$$

18

where:

$$C_0 = \begin{cases} 0.12 + 0.4[log_{10}(f/10)^{0.8}] \geq 10GHz \\ 0.12 \qquad\qquad f < 10GHz \end{cases} \tag{2.14}$$

g. By using the climate data itemised in the Recommendation ITU-R P.841, compute the yearly time percentages P that corresponds to worst time percentages P_w in the event that the worst-month statistics are desired. The figures of A surpassed for proportions of the time p annually will be surpassed for the percentages of time p_w that corresponds to the worst time on a worst-month basis.

The above-described extrapolation method is thought to be applicable worldwide and is valid for microwave path distance/lengths of 60km and frequency ranges up to 100 GHz [31]

2.4.3 Moupfouma Model

Moupfouma suggested an experiential model to be used for forecasting attenuation induced on a signal due to rain from the context of 1 min intensities of rain that have been documented in different wide geographical zones and percentages of time p that corresponds to such zones when these rates of rain are surpassed. The attenuation induced by rain on a path or LOS can be given by:

$$A(dB) = kR^\alpha l_{eff} \tag{2.15}$$

with

$$l_{eff} = rl \tag{2.16}$$

The denotation l (km) represents the path distance/length (actual); l_{eff} the effective path length and r a coefficient of path factor expressed as:

$$r = \frac{1}{1+cl^m} \tag{2.17}$$

The 1 min rain rate $R_{0.01}$ (mm/h) and the attenuation $A_{0.01}$ (dB) are supposed to be computed for the same percentage of time; where α and k are the coefficients of regression which depends on signal polarization and frequency

Using data collected 30 terrestrial radio links located in sampled countries i.e. Japan, US, Congo, and the European region. These links were operating in the range of 7-38GHz band with path distance of up to 58 km; c and m in the above equation were derived. It was noted that whereas m depended on the relationship between radio path distance and its regularity, c depended on the level of probability of interest for the available data. The resulting formula for the factor of path length is expressed as:

$$r = \frac{1}{1+0.03\left(\frac{p}{0.01}\right)^{-\beta l^m}} \tag{2.18}$$

with

$$m(f,l) = 1 + \Psi(F)\log_e l \tag{2.19}$$

And

$$\varphi(f) = 1.4 \times 10^{-4}F^{1.76} \tag{2.20}$$

$l < 50km$

$b = 0.45,$

f represents the frequency (GHz) and;

β indicates the coefficient of a regression that is provided by (2.21):

$$\left.\begin{array}{c} l < 50km \\ \beta = 0.45, for\ 0.001 \leq P \leq 0.01 \\ \beta = 0.6, for\ 0.01 \leq P \leq 0.1 \\ l \geq 50km \\ \beta = 0.36, for\ 0.001 \leq P \leq 0.01 \\ \beta = 0.6, for\ 0.01 \leq P \leq 0.1 \end{array}\right\} \tag{2.21}$$

2.4.4 Crane Global Model

Crane (1980) developed the Crane Global model (1st) and the 2-Component Crane model (2nd) as part of his contributions to rainfall research. The 2nd model used the path integration procedure and added the separately calculated debris and volume cell contributions to the connection

calculation. Here we use a closed probability distribution to predict the cumulative distribution function of precipitation while subjecting volume cells and debris (CDF) to separate procedures. The probability that an attenuation level was surpassed was determined using this model, and the calculated probability is the total of the probabilities for each component. Following is provided by Crane (1996) as the empirical rain rate distribution function:

$$P(r \geq R) = P_C(r \geq R) + P_D(r \geq R) - P_{CD}(r \geq R) \qquad (2.21)$$

With

$$P_C(r \geq R) = P_C e^{R/R_C} \qquad (2.22)$$

$$P_D(r \geq R) = P_N N\left(\frac{lnR - lnR_D}{S_D}\right) \qquad (2.23)$$

$$= \frac{P_N}{\sqrt{2\pi S_D}} \int_R^\infty exp\left[\frac{1}{2}\left(\frac{lnR/R_D}{S_D}\right)^2\right] \frac{dr}{r} \qquad (2.24)$$

$$P_{CD}(r \geq R) = P_C(r \geq R)P_D(r \geq R) \approx 0 \qquad (2.25)$$

2.4.5 Physical-Stochastic Model: EXCELL and Lavergnat-Golé Models

The physical-stochastic method improves on the physical method while adding statistical characteristics. It uses the physical characteristics of synthetic rain cells to imitate the counting process of a rain gauge running at a specific integration time (Capsoni et al, 2008). Rain's spatial profile is described by the EXCELL model. Even though the model's initial formulation was created for an elliptical rain cell, Capsoni et al. [14] model is distinguished by the Rain profile within the CELL as illustrated below in Figure 2.3. rain rate inclusion is extended in the Paraboni et al. (1998) a better model that simulates rain with no rate. The calculation of the rainfall rate time series R uses:

$$R = (R_M + R_{low})exp(-\rho/\rho_0) - R_{low} \qquad (2.26)$$

where R_m is peak rain rate, ρ is a distance from the peak, ρ_0 is a cell radius (at R_m/e) and

$$\rho_{max} = \rho_0 ln[(R_M + R_{low})/R_{low}] \qquad (2.27)$$
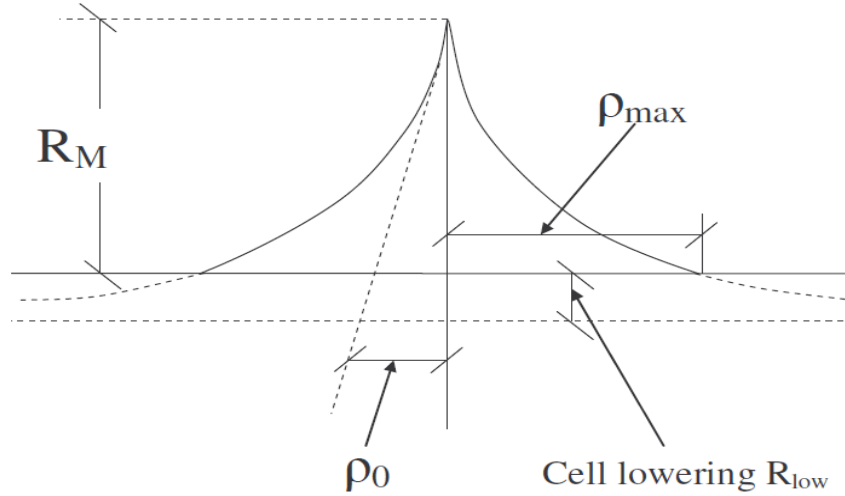
Figure 2.3 EXCELL model of rain cell [14]

The physical-stochastic category includes the Lavergnat and Golé model from 1998, which increases the total Pareto distributions by an exponentially falling term. Many scholars find the Lavergnat-Golé model to be an excellent choice because of its dependability, simplicity, and theoretical basis. The formula for changing the cumulative distribution from one integration time to another as of t_1 to a particular time of t_2 as provided in the Lavergnat-Gole statement:

$$P_2(R_2) = K^a P_1(R_1) \qquad (2.28)$$

$$R_2 = R_1/K^a \quad k \equiv t_2/t_1 \qquad (2.29)$$

The Ito and Hosoya approach was shown to have worse conversion accuracy than this one (2000). Using the database from the Kitami Institute of Technology (KIT), the parameter a is suggested for the entire planet. The following phrase is from Ito and Hosoya (2001):

$$a = 0.00219126|\emptyset| - 0.000205094|\lambda| - 0.001165957 R_{0.01C} + 0.000869955 R_{0.001C} +$$
$$0.00004927772M + 0.001336088D_{th} - 0.173738515\beta + 0.035580308 \qquad (2.30)$$

$$R_{0.001C} = 23.50390 M^{0.27896} \beta^{0.34162}$$

(2.31)

$$R_{0.01C} = 3.69786 M^{0.46613} \beta^{0.43482}$$

(2.32)

2.4.6 Karasawa-Matsudo Model

The proposed probabilistic distribution formulation by Moupfouma (1982) served as the foundation for the Karasawa-Matsudo model:

$$f(R|r,u) = \frac{r}{R} exp(-uR) \left\{ \frac{1}{R} + u \right\}$$

(2.33)

$$F(R|r,u) = \int_R^\infty f(R) dR = \frac{r}{R} \exp(-uR)$$

(2.34)

$$(p = F \times 100\%)$$

The Karasawa-Matsudo model (1990, 1991) redefines the climate variables supplied by the Moupfouma distribution model for the one-minute rain rate and provides the following new definitions based on Equations 2.33 and 2.34:

$$r_m = 7.24 \times 10^{-4} R_{m.,0.01} \quad U_m = 2.72/R_{h.,0.01}$$

(2.35)

On the other hand, the expression is provided by for a one-hour rain rate is:

$$r_h = 1.52 \times 10^{-3} R_{h.,0.01} \qquad U_h = 2.72/R_{h.,0.01}$$

(2.36)

This model, which utilizes an average of the top five one-hour rain rates each year (m_{1-5h}) which shows how the one-minute rain rate $R_{m,0.01}$ exceeded for 0.01% of the time.

$$R_{m,0.01} = a_{1-5h} m_{1-5h} \qquad (a_{1-5h} = 2.3)$$

(2.37)

Equations 2.35, 2.36, and 2.37 are used to express the one-minute rain rate distribution as:

$$F(R_m) = 7.24 \times 10^{-4} \frac{R_{m,0.01}}{R_m} exp \left(\frac{-1.98 R_m}{R_{m,0.01}} \right) \qquad (2.38)$$

2.4.7 Rice-Holmberg (R-H) rain rate model

In 1973, the R-H model was developed by Rice and Holmberg using extensive long-term data from more than 150 locations around the world. This model generates a rain rate distribution from the mode 1 thunderstorm rain and the "other rain" (mode 2). To create the overall distribution, the two modes are added together:

$$M = Mode\ 1 + Mode\ 2 \qquad [mm] \qquad (2.39)$$

According to Dissanayake et al., [52], the proportion of an average year for which the rain rate exceeds R mm/h at a medium site is given by:

$$P(R) = \frac{M}{87.6}\{0.03\beta e^{-0.03R} + 0.2(1-\beta)[e^{-0.258R} + 1.86e^{-1.63R}]\} \qquad (2.40)$$

where R is the clock minute rain rate in mm/h, is the thunderstorm component of M, β and M is the average yearly rainfall accumulation (in mm). Rice and Holmberg (1973) published global maps, which can be used to read the values of β and M, or they can be estimated using Dissanayake et al., [52], Rice and Holmberg, [53];

$$\beta = \frac{M_1}{M} \qquad (2.41)$$

where M_1 is the average annual amount of thunderstorm rain $[mm]$. Beta can also be calculated as:

$$\beta = \beta_0[0.25 + 2e^{-0.35}(1 + 0.125M)/U] \qquad (2.42)$$

$$\beta_0 = 0.03 + 0.97e^{-5\exp{(-0.004M_m)}} \qquad (2.43)$$

where U and M_m stand for, respectively, the greatest monthly precipitation recorded over the whole trial period and the average number of thunderstorm days anticipated over a typical year, an attenuation prediction property was added to the R-H model by Dutton and Dougherty (1974), which was missing from the original R-H (1973) model. It is described as follows:

$$
P(R) = \begin{cases} 0.0114\,(T_{11} + T_{12})\,e^{-\frac{R}{R_1}} & R < 5mm/h \\ 0.0114\,T_{21}\,exp\left(-\sqrt[4]{\frac{R}{R_{21}}}\right) & 5 \le R \le 30 \\ 0.0114\,T_{11}\,exp(R/\bar{R}_{11}) & R > 30 \end{cases} \tag{2.44}
$$

Where T_{11}, T_{21}, $\acute{R}_1$ and $\bar{R}$ are linear combinations of M, β and D = 24 + 3M, determined from regression equations. When compared to observed data, the R-H model has the flaw of consistently giving underestimated rainfall rates of 0.01% and lower [43].

2.4.8   Empirical Method

Longer integration times are usually adjusted to the required rain rate of one minute using the empirical technique. Its vast application stems from a useful hypothesis that contrasts the rates of precipitation for two different integration times at an equiprobable condition. In the case of Nigeria, Ajayi and Ofoche, Spain, Burgueno et al. Australia's Flavin, for Singapore, Ong and Zhu European data from Watson et al. In the case of China, Xiao et al. Malaysian researchers Chebil and Rahman, and Canadian researchers Segal are just a few of the studies that used this methodology in various regions.[4][48][60][61]

In theory, the power-exponential law and the power law are the two fundamental laws frequently applied in empirical approaches. The following is how the laws are stated in Emilian et al:

$$
R_1(P) = aR_T(P)^b \tag{2.45}
$$

where $R_1(P)$ and $R_T(P)$ at an equal percentage of exceedance (P), reflect the rain rate for an integration period of one minute and any other integration time (T), respectively. The constant values for the parameters a and b are shown in Table 2.1 together with the corresponding Integration times for the rain rate, t.

Table 2.1 For different integration times, the values of a and b ITU-R 837-5 [55]

τ	a	b
5 min	0.986	1.038
10min	0.919	1.088
20min	0.680	1.189
30min	0.564	1.288

2.5 Attenuation Induced by Rain

The specific attenuation induced because of rain A_s measured in dB/km or rain attenuation/unit length of distance is an important quantity that is central in the manipulation of statistics on rain tempering [36]. In space, the specific attenuation of rain builds upon the rain rate or the raindrop number at that particular point through the properties that characterize rain like the orientation of rain, wind advection velocity, spatial shape, size, raindrop water temperature, distribution sizes of the raindrops and the radiated electromagnetic wave properties (e.g., the signal separation, signal frequency, and the path of propagation of the signal) along a path at that point. Based on Mie Scattering theory, theoretically specific rain attenuation has been estimated by using water as a uniformly random distribution of raindrops modelled as spherical shapes or more complex shapes known as oblate-spheroid. Apart from the shape of the raindrops, the specific rain attenuation α also relies on the forward propagated radiated electromagnetic wave this wave is affected by refractive index of the raindrop water, signal frequency, rain drop water temperature; these parameters aid in the calculation of extinction cross section. An electromagnetic wave promulgates via a space medium that contains rain drops, the drops of rain absorb part of this signal, a portion is dissolute as heat and the rest are dispersed haphazardly. This part of the signal that is scattered introduces interfering signals or unwanted signals into the transmission channel. This unwanted signal may mask out the required signal leading to distortion of the initial. The figure below shows absorption and scattering effect when a radio wave is incident on a medium filled with rain.
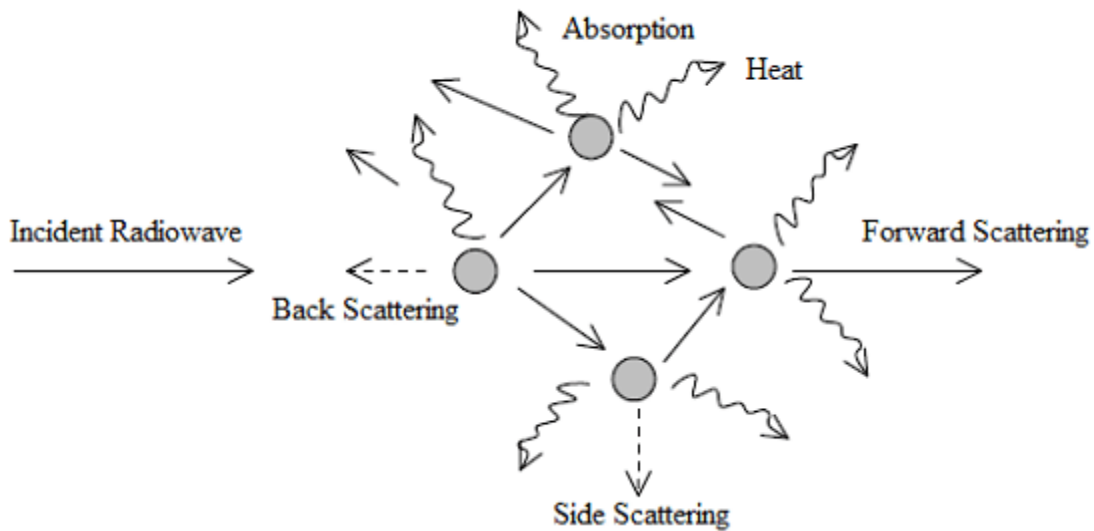
Figure 2.4 Incident electromagnetic radio wave in a medium filled with rain

At longer wavelengths comparable with the rain drop size, signal absorption will be significant; on the other hand, at shorter wavelengths, signal loss due to scattering will be substantial to the total attenuation experienced by a propagating radio wave passing through a medium full of rain is considered by summing up the total contributions from particular rain drops constituting that particular medium. The dimensions of rain drop vary considerably, hence, the particular attenuation is computed by assimilating contribution of each raindrop. Studies on rain attenuation make three basic assumptions, which are:

- The rain drops are presumed to be homogeneously spread in the area bound by the wave field as the exponential signal decay.
- It is an assumption that the raindrops are sphere-shaped or oblate spherical, leading to signal distortion. This signal distortion attenuation is due to losses in signal energy due to immersion and scattering by droplets from the occurrence of radio wave.
- It is assumed that the contribution due to the rain drops is independent from other drops and are summative in nature.

In the techniques of prediction where the utilization of a rain gauge is employed, rain rate cumulative distribution is computed at each specific point. Due to the challenge of spatial heterogeneous intensity of precipitation, we use the effective length path, the path is separated into

27

minor volumes of sphere-shapes and are considered to be homogeneously spread water drops. As radio signal propagates via the water drop it experiences a reduction on its amplitude. the effect on the signal due to rain is called rain attenuation.

Accordingly, Ippolito (1986), showed that the sum-total of attenuation (A) experienced by a signal in the path of its propagation, in (dB) could be represented as:

$$A(dB) = \int_0^l \alpha \, dl \tag{2.46}$$

α denotes a particular attenuation (dB/km) along the water drops path length in kilometres and the sum-total of the attenuation due to rain (A) is found by summing the definite attenuations throughout the path length. This path length is separated into diminished incremental capacity, and the precipitation is considered even. The mass of raindrops occurring in incremental is related to an equivalent attenuation referred to as specific attenuation.

When calculating attenuation of rain data for slant and terrestrial paths expressed as rain attenuation/unit length (dB/km), specific attenuation is an important factor. The specific attenuation is calculated using Mie scattering theory and a number of variables: the complex refractive index of rainwater at the terminal drop-velocity, the drop temperature, and the rain drop diameter dispersal [12–15]. The specific attenuation is then expressed as:

$$A_s = 4.343 \int_0^\infty Q_{ext}(D, \lambda, m) \times N(D) \, dD \tag{2.47}$$

where $Q_{ext}(D, \lambda, m)$ is the extinction cross-section, $N(D) \, dD$ is the raindrop number density with equivalent drop diameter D in the interval dD.

$Q_t(D)$ is a theoretical result determined from theory of classical scattering established by Mie for above 3 GHz frequencies, normally, Rayleigh approximation is used for frequencies in the range 1-3 GHz. The total $Q_t(D)$ is the sum of the contribution from absorption and scattering.

Empirical methods explored by Olsen et al approximated the relation between rain attenuation and the rate of rain R (mm/hr), where A_s the specific attenuation was found to depend on rate of rain

the polarization and frequency regression coefficients. The specific attenuation therefore takes the form:

$$A_s = kR^\alpha \tag{2.48}$$

The coefficients of regression are k and α where k is a factor depending on the wave frequency for a specific rain microstructure model and α is a factor dependent on polarization at a specific tilt angle[12-15].

We do note that actually, ITU-R continues to refine and improve on rain attenuation models by allowing recommendations to the preceding models [9]. In addition, new approaches to rain attenuation are encouraged so as to improve prediction results for attenuation in rain. In essence, progressive research work has been in the modelling of the path factor or the rain rate factor. Notably, the difference in these models depend on whether large data banks are used for fitting purposes or whether more physical analysis is infused with limited empirical information.
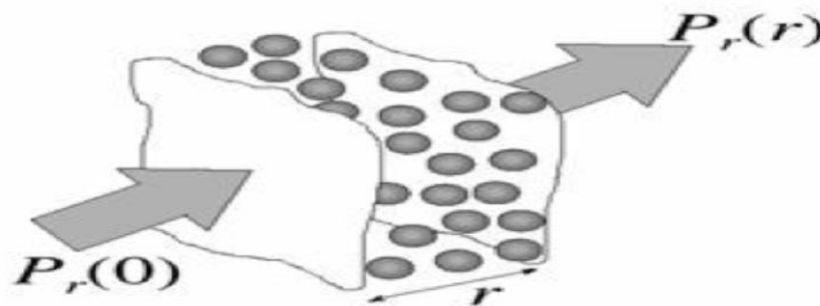
Figure 2.5 volume of sphere-shaped droplets that are evenly spaced [2]

2.6   Review of Existing Rain Rate Models

It is required to have prior information of the likelihood at which the rain rate surpasses to be able to determine the fade margin for a certain geographic region which depends on rain attenuation. Therefore, use of rain rate modelling is critical in envisaging rain attenuation. These rain rate models can be separated into two groups. These classes use either global or local models rain rate.

2.6.1 Global Rain Rate Models

Climate variables and geographic regions have the biggest effects on the methodology used in global rain rate models. In this situation, regional maps are useful for showing the distribution of precipitation at a specific percentage level exceedance, particularly for regions lacking monitoring stations. To build a worldwide rain rate climate model for communication networks, the planet was first separated to four classes or latitude bands namely sub-tropics, arctic, tropics, and mid-latitude. Eventually, there were eight labels to properly reflect changes in latitude and longitude. The study focuses on are Crane's and the ITU-R global models despite the global availability of various global rain rate models.

2.6.2 Crane's Global Rain Rate Model

According to Crane's work from 1980, the world was divided into eight areas, each with the letters A through H with various levels of moisture or dryness. The designation A denotes arctic dry, the designation H denotes tropical wet, and the designation H is further separated into E wet and E dry in the subtropics. The formation of more designations was prompted by a change rate of precipitation or rain with a smaller proportion of exceedance based on the data that was available. Based on the data that was provided, a change in rate of precipitation or rain with a smaller proportion of exceedance led to additional designations are being created. Region D was reclassified into D1, D2 and D3, with D1 being the driest and D3 being the wettest. Additional classifications of the B area, such as B1 and B2, were added to the global map after further research.

Figure 2.6 illustrates the cumulative distribution of rainfall for a rain climate model using Crane's notations. This model applies to rainfall attenuation calculation, particularly in places with limited local rainfall data. Three years of station data in total were used for area G, 3 years 178 stations of data were made available for region D2, and stations midway between areas G and D2 were used in other regions to compile these distributions. Three zones—America, Asia, Europe, and Africa—are identified on the regional rain climate map.
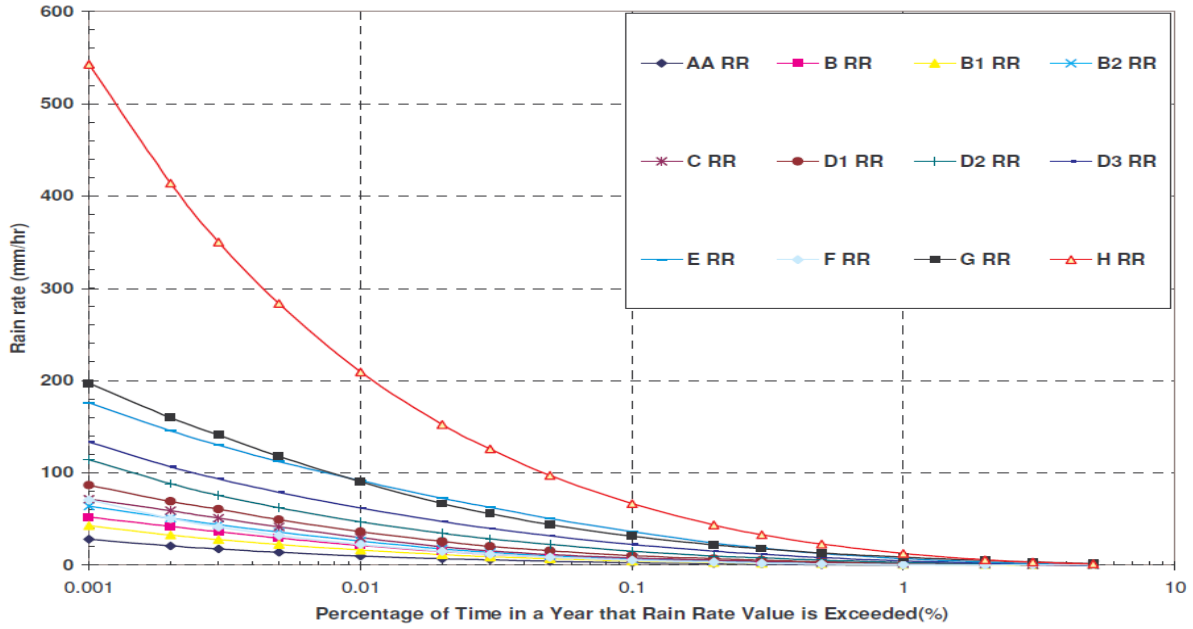
Figure 2.6 Crane's way of classifying the global rain climate zone [3]

Crane's global rainfall climate map is shown in Figure 2.7. On the map, it can be seen that Kenya is located in areas with a moist and moderate climate.
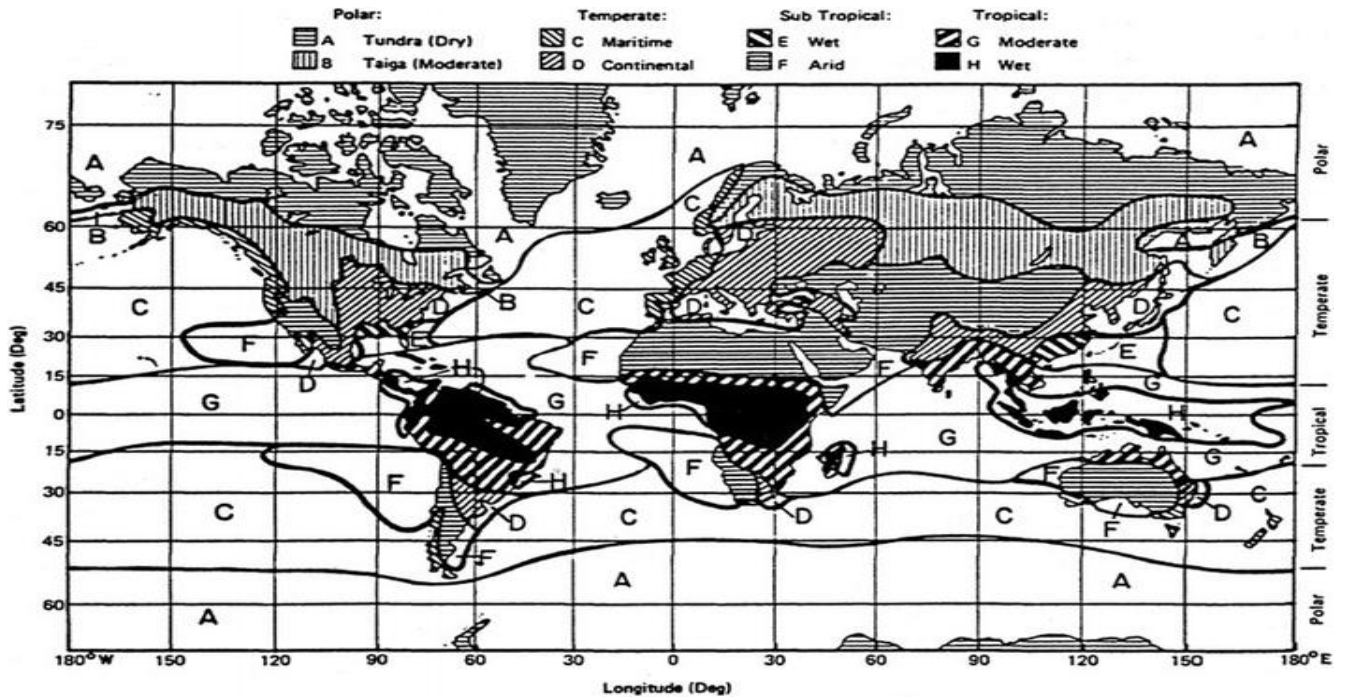
Figure 2.7 Global Crane rain climatic regions [8]

2.6.3 Global Rain Rate Model-ITU-R

As seen below in Figure 2.8, ITU-R provides the attributes of precipitation for propagation modeling, a trustworthy global climate model for rain rates. This model was originally created under CCIR in 1974, and it has since undergone a number of updates, including ITU-R P837-1 (1994), and ITU-R P.837-7 (2017). In order to calculate the fading margin for a given likelihood of exceedance, these suggestions are utilized to calculate the attenuation caused by rain at terrestrial and satellite communication systems.

This model's data are based on global measurements that are updated often, which lessens the discrepancy that is frequently seen when utilizing the model locally. The ITU-R rain climate map's rain rate distribution is applicable at percentage exceedances between 1% and 0.001%. The technique made use of customized database parameters, such as the location's latitude and longitude, P_{r6} M_c and M_s. The variables, P_{r6} M_c and M_s, respectively, stand for the likelihood of a six-hour period of rain, the amount of convective and stratiform rain that falls annually, and the probability of such rain.
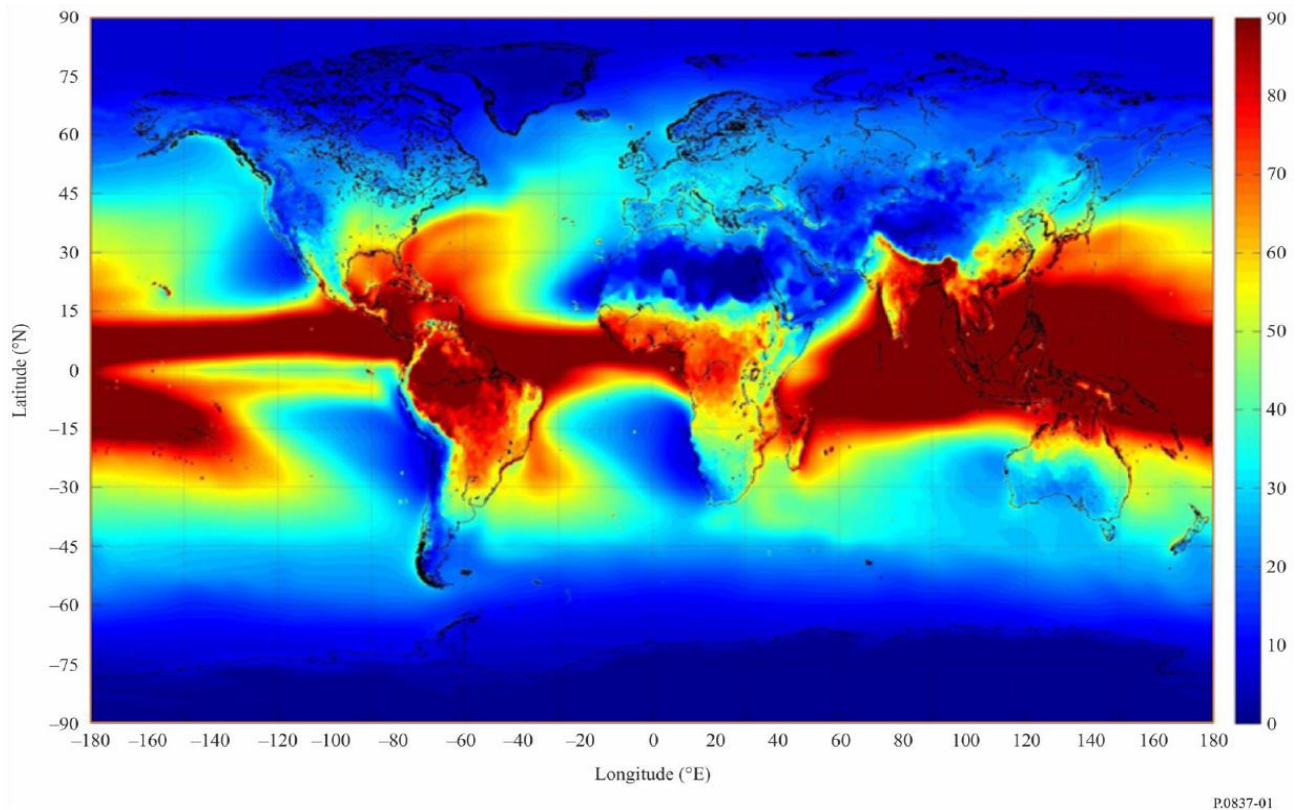
Figure 2.8 Rainfall rate exceeded for 0.01% of an average year [55]

2.6.4 Models for Localized Rain Rate

These particular models of rainfall rates were developed using empirical formulas and the results of considerable field data gathering. For instance, the 1973 Rice-Holmberg model, the 1979 and 1984 Dutton-Dougherty model, the 1996 and 2003 Crane two-component model, the 1982 Moupfouma-Dereffye model, the 1985 Moupfouma model, the 1993 and 1995 Moupfouma-Martin model, and the 1973 Seeber rain rate model all merit mentioning in this category. The two-component of rain rate model developed by Moupfouma, Crane and others these were given consideration in the earlier sections of this thesis. Below is a quick discussion of the Seeber model. [2-3] [5-8]

2.6.4.1 Seeber South Africa Rain Rate Model

Using an extreme-value theory, Seeber suggested a rain rate model using data collected in South Africa and the neighboring two islands. In conclusion, the theory roughly predicted the distributed cumulative rain rate based on the method used by Lin (1976 & 1978):

$$P(R \geq r) \approx \frac{1}{2} P_\circ . erfc \left[\frac{lnr - lnR_m}{\sqrt{2}\, S_R} \right] \tag{2.49}$$

where R_m, R, P_0, $\ln(\sim)$ and erfc $(\sim)$, represent for the median values of R during a rain event, the rain rate, the probability that rain would fall, the natural logarithm and the complementary error function, respectively. S_R stands for the standard deviation of $ln(R)$ during the rain event. The subsequent expressions serve as representations of the distribution parameters S, R_m and P_0:

$$S_R = \frac{P_\circ . N}{\alpha} . \emptyset \left[\Phi^{-1} \left(1 - \frac{1}{P_0 . N} \right) \right] \tag{2.50}$$

$$R_m = exp \left[U - S_R \Phi^{-1} \left(1 - \frac{1}{P_0 . N} \right) \right] \tag{2.51}$$

$$M = 8760 . e^{\frac{S_R^2}{2}} . R_m . P_o \tag{2.52}$$

Where $(\sim)$, and $\Phi^{-1}(\sim)$ respectively stand for the normal probability density function and the inverse of the normal probability density function's standard unit. In the formula, N is the number of rain gauge integration time intervals annually;

$$N = 8760/D \tag{2.53}$$

D is the integration time and is expressed in hours.

The increased fifteen minutes for integration used to collect the data on rain rate as well as the model's reliance on numerous factors while attempting to estimate the distributed accumulation of rain rate are its main drawbacks. In addition, the map's contour boundary cannot be adequately described by the number of stations utilized to create it.

2.6.4.2 Rain Rate Model by Moupfouma

Measurements from the study by Moupfouma and Dereffye were used to build a semi-empirical model, these were taken from tropical and equatorial climates that are seen in parts of the Congo. Three input variables are necessary for this model to compute the cumulative rain rate distribution. The main goal was to use a single function to express the rainfall rate distribution over the complete range of important values, this produced an all-encompassing probability statement with the following format:

$$P(R \geq r) = a\frac{e^{-ur}}{r^b} \tag{2.54}$$

Note that r must be more than 2 mm/hr, and that the constants a, b, and u rely on the integration time and the climatic conditions. The linear regression fitting technique was used to determine the constants. Moupfouma [5] suggests a very straightforward, semi-empirical global cumulative distribution of rain rate that is dependent only on the variable $R_{0.01}$. The parameters a and b were used to linearly regress the parameter $R_{0.01}$, which indicates the rain rate that is surpassed in 15 different locations for 0.01% of the time throughout the globe. The correlations are summarized in the following tables by Equations (2.55) and (2.56):

$$b = 8.22R_{0.01}^{-0.584} \tag{2.55}$$

The cumulative distribution of rain rate has a new general probability which is given by substituting Equation (2.55) into Equation (2.54) as follows:

$$P(R \geq R_{0.01}) = a\frac{e^{-uR_{0.01}}}{R_{0.01}^b} = 0.01\% \tag{2.56}$$

$$a = 10^{-4} \times R_{0.01}^b e^{uR_{0.01}} \tag{2.57}$$

$$u = 2.5 \times 10^{-2} \tag{2.58}$$

Here, both the value of a and the parameter b must be bigger than zero. By revising parameters b and u and eliminating parameter a, the Moupfouma and Martin model [7] improved upon the earlier models. It was discovered that u cannot have the value of a constant, this is depicted in Equation 2.58. They had an improvement that used the shape of the cumulative rain rate distribution, which depends on the point of interest's geographic features and local climatic conditions. It was discovered that rain rate distributions in tropical regions have a steeper slope and low values for the parameter u. With large values of the parameter u, it is less steep for temperate zones. The formula for the cumulative rain rate distribution is:

$$P(R \geq r) = \left(\frac{R_{0.01}+1}{r+1}\right)^b \times e^{[u \times R_{0.01}-1]-log_e(10^4)} \tag{2.59}$$

Where r (mm/hr) is the percentage of time P where the rain rate was exceeded. Parameter b is given by 2.60 considering the form of the rain rate's cumulative distribution

$$b = \left(\frac{r-R_{0.01}}{R_{0.01}}\right) \times log_e\left(1+\frac{r}{R_{0.01}}\right) \tag{2.60}$$

regarding the temperate and tropical zones, two primary zones —parameter u is provided in order to differentiate between the rain rate climates of different locations:

(a) For temperate zone:

$$u = \frac{log_e(10^4)}{R_{0.01}} \times \frac{1}{\left[1 \times \eta \times \left(\frac{r}{R_{0.01}}\right)^\beta\right]} \tag{2.61}$$

where $\eta = 4.56$ and $\beta = 1.03$ are constants that are positive.

(b) For tropical localities:

$$u = \frac{log_e(10^4)}{R_{0.01}} \times e^{-\lambda \times (r/R_{0.01})^\gamma} \tag{2.62}$$

with $\lambda = 1.066$ and $\gamma = 0.214$

Equations 2.54 through 2.62, according to Moupfouma and Martin [7], show behavior that is consistent with the probability law. The earlier work by Moupfouma and Martin (Moupfouma and Martin, 1993) was completed by the Moupfouma-Martin model (Moupfouma and Martin, 1995), which included the addition of a relationship that converts the rain rate at various integration periods to 1 min equivalent at a rain rate exceedance of 0.01% percentage. Expressed as follows:

$$R(1\ min)_{0.01} = (R(\tau\ min)_{0.01})^{\alpha} \tag{2.63a}$$

With:

$$\alpha = 0.987\big(\tau(min)\big)^{0.061} \tag{2.63b}$$

Provide that:

$$1min \leq \tau \leq 1hr \tag{2.63c}$$

2.7   Chapter Conclusion

A review of some of the existing rain rate models has been discussed in this chapter, with the introduction of statistical distribution processes which begin with the integration of the rainfall rate. The sampling period used by measuring devices to determine the rain rate is known as the integration time. It is necessary to calculate the cumulative distribution at a one-minute integration period to determine the terrestrial rain rate's attenuation. Further information has been given on the physical, empirical, and analytical conversion models that are currently in use globally. It is noted that, since these initial rain rate models were based on various integration times, the proposed conversion method will make it possible to transform the rain rate from 60-min integration time to 1-min integration time equivalents.

CHAPTER 3

3 RESEARCH METHODOLOGY

The techniques used to calculate the cumulative distributions for the percent exceedance and rain rate are described in depth in this chapter. It gives an overview of the data's origin and the procedure utilized to gather and process it.

3.1 Measurement of rain rate and cumulative distributions

For the best performance of wireless networks in an environment where rain is present, cumulative distributions provide a method of evaluation that may be used to calculate the likelihood that the rate of rainfall would surpass a certain percentage. These probabilities can be used by experts in design of communication systems to specify the minimum permissible amounts of base station fade margin to minimize network disruptions during wet weather. A value of rainfall rate comparable to 0.01% exceedance probability or link availability 99.99% is frequently of major concern for the sustainability of point-to-point or point-to-multi-point communication systems [6] [55]. $R_{0.01}$ is the common name for this considerable rate of precipitation, which is measured in millimeters per hour. Figure 3.1 displays an example cumulative distribution for different availability demands versus a performance metric.
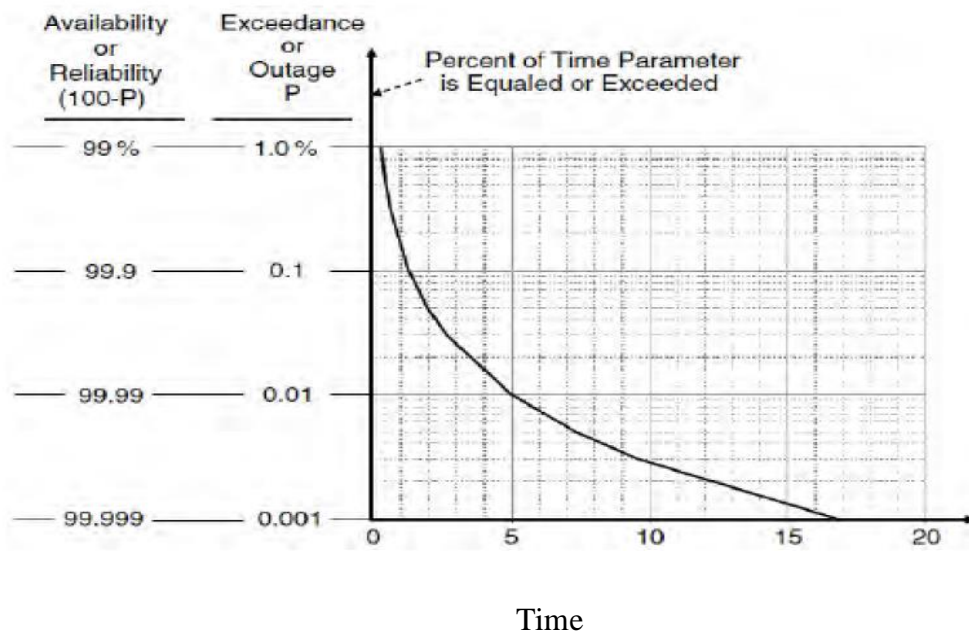
Figure 3.1: Percentage of time parameter is equaled or exceeded [20]

Ajayi and Ofoche [4] provided another illustration, who in Ile-Ife, Nigeria produced rainfall rate cumulative distributions, using rapid response rain sensors/gauges with a range of integration periods. These distributions' plots in Figure 3.2 show that shorter integration durations produce higher rainfall rates.
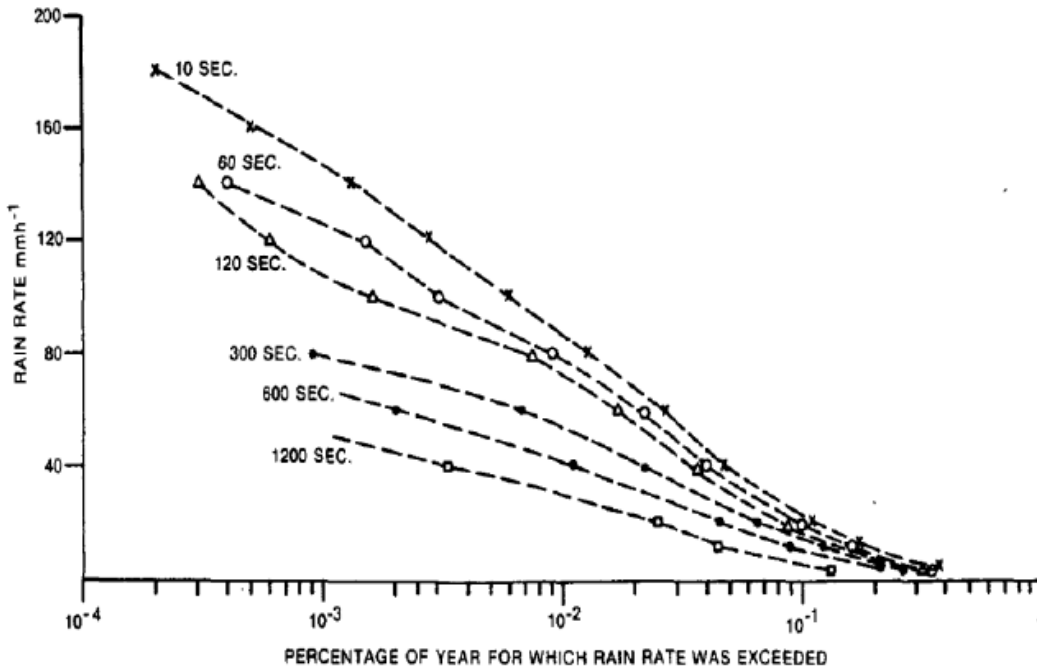
Figure 3.2: Rain distribution cumulatively at various integration times across Ile-Ife, Nigeria [4]

3.1.1 Rainfall rate measurements

Meteorological departments within various countries have long served as significant resources for rainfall observations and data. These agencies have records of measured rainfall information that have been gathered over quite extended periods. Instead, rain gauges, disdrometers, and radars can be utilized to undertake independent measurements to measure rainfall [3] [5] [28-30]. Due to its low cost and ease of installation, the rain gauge is the most often used of the three types of measuring equipment. The optical, tipping bucket, graduated cylinder sometimes referred to as standard gauges and weighing rain gauges are a few of the several types of rain gauges that may be used to measure rainfall. The images in Figure 3.3 below show the three most used kinds of rainfall measuring equipment.

Figure 3.3: Instruments for measuring rainfall include (***a***) disdrometer, (***b***) tipping bucket rain gauge, and (***c***) an optical rain gauge [63] [64]

The tipping bucket rain gauge is made up of a delivery pipe and a collecting funnel that gather rainwater and transfer it to the tipping bucket device. The bucket can be swung through its center to release the water once it is full. A reed switch magnetically closes and opens when the bucket is emptied, causing it to send the data recorder a pulse signal. $0.2\ mm, 0.5\ mm,\ and\ 1\ mm$ are the most often used calibration tips for tipping bucket rain gauges.

The disdrometer, on the other hand, uses two moving coils that move downward when they are struck by a raindrop falling from the sky and an electromechanical sensor that resembles a Styrofoam body. As a result of this downward motion, the sensor coil experiences a voltage, and the size of the voltage indicates the size of the raindrop that made contact [28-30].

To discover anomalies caused by particles travelling through an infrared light beam, an optical sensor is used in an optical rain gauge. In comparison to the tipping bucket rain gauge, the disdrometer is more sensitive to light rainfall rates (2 mm/h), while both instruments have varying degrees of precision and measurement error. A disdrometer's ability to monitor rainfall drop size dispersion in addition to rain rate measurements is another advantage of using it for data measurement. As a result, there has been a tremendous revolution in the study of raindrop size distribution. The rain gauge is still a useful and affordable equipment for data collection all around the world. The rainfall rate, measured in mm/h, is computed by comparing the amount of rain that falls on the earth's surface to its area and time.

In his work, Green [59] emphasized that, in addition to measuring the amount of rain falling, attenuation of rain is also influenced by the rate at which it is currently falling. For the scrutiny of rainfall statistics to be successful, it is necessary to provide crucial parameters like the rate of precipitation (R), the length of the propagation experiment (T), the amount of time (t) during which the rate of precipitation (R) exceeds that amount, and the percentage of time (P) during which the rate of precipitation (R) exceeds that amount (T). Equation 3.1 illustrates the relationship between these four parameters:

$$P(\%) = \frac{t}{T} \times 100 \tag{3.1}$$

Where t is given as

$$t = \sum_{i=1}^{N} \delta_{ti} \quad [minutes] \tag{3.2}$$

$$R = \frac{q}{P(\%)^V} \quad [mm/h] \tag{3.3}$$

where q and v are climatic zone dependent parameters.

The intensity of the rain (measured in mm/h) can be further broken down into several regimes, such as drizzle ($R < 5\ mm/hr$), widespread rain fall ($5\ mm/hr \leq R < 10\ mm/hr$), showers ($10\ mm/h \leq R < 40\ mm/hr$) and thunderstorm ($R \geq 40\ mm/hr$). Electromagnetic waves that interact with rainfall molecules will always be significantly attenuated; the signal will suffer more attenuation the shorter the wavelength it has. Most of the factors that affect how much rain will affect an electromagnetic wave include the size of the droplets, their density per volume, additionally known as the mean inter-drop distance and their velocity of fall.

3.2 Data Source

Kenya is a country in Eastern Africa. There are two rainy seasons in the country each year: the long rainy season, which runs from March to May, and the short rainy season, which runs from October to November. December to March is the sunniest month, whereas it is cooler from June through September. and frequently cloudier. Daily rainfall data from a few selected sites across Kenya were used to forecast the attenuation of the rain. These data were gathered over two years.

The METER ATMOS 41 Weather Station, that integrates weather sensors, twelve (12) of them into a single small instrument for measuring conditions in the atmosphere, this is what was used to gather the data. METER ATMOS 41 is a modular microenvironment weather station with no moving parts and a sleek tubular form factor. Temperature, relative humidity, vapor pressure, air pressure, wind speed and direction, sun radiation, precipitation, and lightning are only a few of the 12 climatic variables that the ATMOS 41 weather station measures.

It has a flare hole in the rain gauge with a 3.75-inch diameter that releases raindrops, which then fall through the dropper. Although the droplet size decreases as the intensity of the rain increases, the ATMOS 41 firmware has an algorithm that automatically adjusts for this. It accurately measures light rainfall and heavy condensation that other rain gauges might miss with a resolution of 0.017mm.
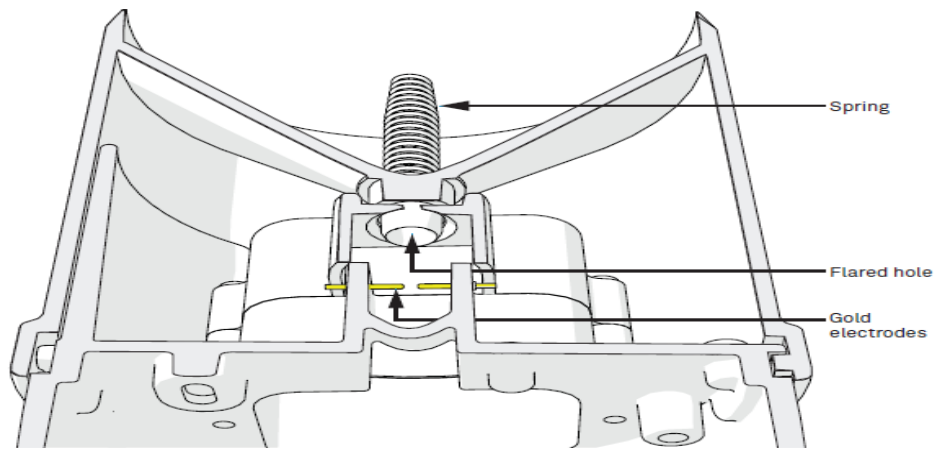
Figure 3.4: Rain Gauge [62]

Figure 3.5: ATMOS 41 all-in-one weather station [62]

The TU Delft/Oregon State University TAHMO (Trans-African Hydro-Meteorological Observatory) Project produced the two years' worth of 60-minute rainfall data. Data about the weather in real time was gathered from several sites in Kenya. Table 3.1 provides a summary of the samples stations chosen for this study.

Table 3.1 Rain Data sites

Site ID	Name	Latitude	Longitude
TA00063	Kapsabet Boys High School	0.203	35.117
TA00171	Maseno University	-0.003	34.597
TA00141	Sacho High School	0.388	35.787
TA00031	Homa Bay High School	-0.538	34.46
TA00056	Murang'a High School	-0.722	37.146
TA00066	Alliance Girls High School	-1.265	36.662
TA00134	Nairobi University	-1.274	36.81
TA00025	Kenya Meteorological Department	-1.302	36.76
TA00166	Chuka University	-0.32	37.659
TA00307	Wajir Girls	1.748	40.034
TA00067	Makueni Boys School	-1.794	37.621
TA00131	Shimo la Tewa School	-3.96	39.744
TA00068	Base Titanium Mine	-4.373	39.441
TA00072	Likoni School for the Blind	-4.079	39.657
TA00065	Mukumu Girls High School	0.218	34.768

KENYA MAP
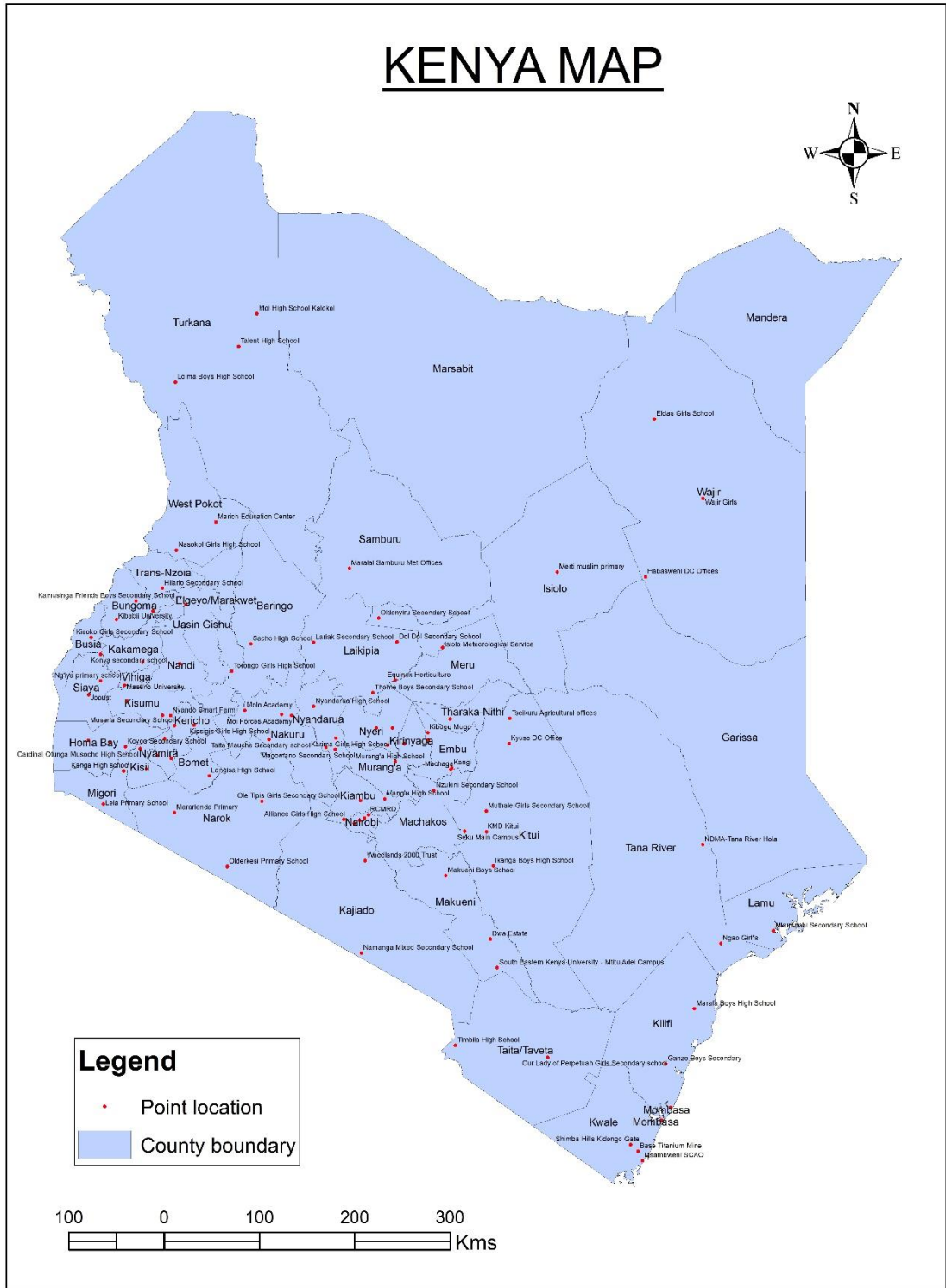
Figure 3.6: Geographical Locations of sites on Kenyan Map

3.3 Conversion of 60-min rainfall rate to 1-minute integration time

It is essential to transform the available rainfall data in mm into rainfall rate because rainfall attenuation is equivalent to rainfall rate in millimeter per hour (mm/hr) rather than rainfall in millimeter (mm).

The time elapsed between each rainfall data record is known as the integration time τ. There are two methods for changing a rainfall distribution with an integration time of τ -min to 1 min. Both the first and second methods are predicated on an equal probability, P, and an equal rate of precipitation, R. In this thesis, the following techniques are discussed:

3.3.1 Segal method

Segal made the suggestion for a representative equal probability-based technique in 1986 [10]. The conversion factor, $\rho\tau$ (P) such as in (3.4) and (3.5) is subject to power law using this approach.

$$\rho_\tau(p) = \frac{R_1(P)}{R_\tau(P)} \tag{3.4}$$

$$\rho_\tau(p) = aP^b \tag{3.5}$$

The rainfall rates that are equally likely to be surpassed are $R_1(P)$ and $R_\tau(P)$, for integration times of $1 - min$ and $\tau\, min$, respectively. Based on rainfall data gathered over a period of ten years at 47 locations across Canada, Segal presented a regression coefficient $a\, and\, b$.

3.3.2 Burgueno et al. Method

Based on 49 years' worth of data on the rainfall rate collected in Barcelona, Spain, Burgueno et al. proposed a conversion method in [11]. The rate of 1-min rainfall is calculated using (3.6).

$$R_1(P) = AR_\tau{}^b(P) \tag{3.6}$$

For integration times of 1 min and min, respectively, $R_1(P)$ and $R_\tau(P)$ are the rainfall rates that are, with equal chance, exceeded. The conversion variables are $a\, and\, b$.

3.3.3 Emiliani et al. Method

ITU-R P.837-5 was proposed to be expanded by Emiliani et al. in [12]. A power law conversion method is used to generate a new set of coefficient values based on an extended database of three

different kinds of Köppen climatic regions. The publication also extends the potential global applications of the approach by including the updated conversion coefficients for 60 minutes. The investigation revealed that for integration times between 5 and 30 minutes, the proposed coefficients outperformed ITU-R P.837-5. But as integration time increased, conversion performance decreased. Table 3.2 includes a list of the coefficients proposed by Segal, Burgueno et al., and Emiliani et al.

Table 3.2 Coefficient values for Segal, Emiliani and Burgueno method

τ	Segal method		Burgueno et al. Method		Emiliani et al. Method	
	a	b	a	b	a	b
60	1.759	-0.054	0.92	1.24	0.509	1.394

3.3.4 Chebil & Rahman Method

Based on rain the occurrences of rain events taken between 1991 and 1998 in Malaysia a conversion technique from 60-min to 1-min was proposed by Chebil & Rahman in [5]. The majority of the 82 stations in the Malaysia Peninsular that have 60-minute rainfall records are collected from the Malaysia Meteorological Department (MMD) for a period of 12 years.

Convective disturbance rain events were taken into consideration when developing the model. The strait form rainfall is not used. The method applies the probability conversion factor to change $60-min\ to\ 1-min$ using ratio of rainfall rates surpassed with equivalent probability P for the integration time of $1\ min$, $R_1(P)$ and $60\ min$, $R_{60}(p)$ as given in (3.7) and (3.8).

Strait form rainfall is not taken into account. The approach uses the ratio of rainfall rates surpassed with equal probability P for the integration times of $1\ min$, $R_1(P)$, and $60\ min$, $R_{60}(P)$ as stated in (3.7) and (3.8) to convert 60 min to 1 min.

$$CF_{60} = \frac{R_1(P)}{R_{60}(P)} \tag{3.7}$$

$$CF_{60} = aP^b + ce^{(dP)} \tag{3.8}$$

Rewriting Equation (3.7) with the regression coefficients given in $a, b, c, and\ d$ yields $R_1(P)$ (3.9).

45

$$R_1(P) = R_{60}(P)[0.72P^{-0.041} + 1.141\exp(-2.57P)] \tag{3.9}$$

3.3.5 ITU-R P.837-6 Annex 3

Capsoni and Luini created the EXCELL Rainfall Statistics Conversion (EXCELL RSC) model that is contained in ITU-R P.837-6 Annex 3 [14]. The physical foundations of the system were built on the virtual motion of artificial rain cells. Based on the yearly local mean wind speeds that were acquired from the ERA-15 database on a global scale, a virtual rain gauge was generated from the characteristics from the local input data.

The site's coordinates, the integration time of the source rainfall statistics, and the cumulative distribution rain rate value (mm/h) are all required local input data.

3.4 Specific Attenuation

When we obtain rain rate measurements, it is imperative that we manipulate these data and obtain the results; which we then do a comparative analysis between these outputs and the results obtained from existing prediction models. This would enable the development of region-specific models that would improve on link reliability. Attenuation due to rain through a terrestrial length path can be expressed as the multiplication of definite attenuation (dB/km) and the effectual radio wave path distance of propagation (km). Therefore, the effective length of path is obtained from the understanding of the connection dimension and the horizontal dispersal of the rainfall along the path. It means therefore that the attenuation of rain A (dB) beyond ∂ per cent of time is computed as;

$$A_{0.01} = l_{eff}\gamma R \tag{3.10}$$

ITU-R P.838-3 recommendation establishes the process of particular attenuation from rain intensity. Hence specific attenuation, l_{eff}(dB/km) is got from the rate of rain R (mm/h) surpassed at p per cent of the time through the use of law-power relationships as follows;

$$A_s = kR^{\alpha} \tag{3.11}$$

The denotation ∂ and k are dependent upon the electromagnetic wave's polarization and frequency. ITU-R P. 838-3 recommendation tables contains the constants where they appear [10].

They can also be got through interpolation where we consider the linear of a and logarithmic scale of k [3]. To deal with the temporal and unique variation of rain features, some strategies are required. There are numerous models for predicting the attenuation of rain along a path, and each of these models suggests a different method. Models like the ITU-R model, the Moupfouma model, the Crane Global model, the Silva Mello model, and others are examples of rain attenuation prediction models for terrestrial microwave prediction. [2] [3] [5-7] [9-11]

3.5 Data Collection and Processing

Ajayi et al. (1983) created a table for the power law conversion coefficients based on rainfall observations made in Ile-Ife, Nigeria, between September 1979 and December 1981 using a quick response rain gauge with a 10-second integration period. For conversion from 60 minutes of integration time data, it has been determined by linear extrapolation that = 11.565 and by logarithmic extrapolation, =0.7982 [4, 11]. These conversion variables are utilized to analyze our data because Ile-Ife is a tropical location and Kenya is in the tropical region.

In theory, the power-exponential and the power laws are the two fundamental laws frequently applied in empirical approaches. The following describes how the laws are stated in Emilian et al (2009).

$$R_1(P) = aR_T(P)^b \tag{3.12}$$

Where $R_1(P)$ and $R_T(P)^b$ are, the rain rate for a one-minute integration time and any integration time (T) respectively at equal percentage of exceedance (P), a and b values for 60 to 1 minute integration time is used as per Emilian et al (2009). It follows that,

$$R_{0.01} = \alpha R_{60}(P)^\beta \tag{3.13}$$

3.6 Chapter Conclusion

In this chapter, the techniques for measuring rainfall rate are discussed, a method of evaluation that could be applied to determine the percentage of rainfall rate exceedance likelihood for successful wireless network functioning in a rain-affected environment is presented. The source

of data used in this thesis is also acknowledged and the equipment used at the stations where these data was collected from.

CHAPTER 4

4   RESULTS AND ANALYSIS

This chapter analyzes rainfall data from TAHMO. ITU-R analysis findings are presented, and MATLAB is used to depict the graphs.

4.1   The results and Analysis

The conclusions following the findings were drawn from the analyses detailed below:

(i) The rain data obtained was for $5 - minutes,$ so we used the Ile Ife conversion factors to get the 1-minute rain rate data.

(ii) The data was manipulated to determine the % exceeded, this was done by determining the occurrence frequency based on the range.

(iii) The probability of occurrence was calculated, from which the average mean was determined by multiplying the rain range and probability of occurrence.

(iv) Using the probability of occurrence % rain exceeded was determined a graph of rain range and % percentage exceeded was used to determine $R_{0.01}$

4.2   1-minute sampling rate in Kenya

For each of the ten sites, $R_{0.01}$ has been calculated and is shown in Table 4.1. According to the findings, the lowest $R_{0.01}$ was recorded at Habaswein in Wajir and the highest $R_{0.01}$ was recorded at Mukumu Girls in Kakamega. The ITU-R map shows that the rain rate for the Habaswein area is about 40mm/hr and the Mukumu area is roughly 50mm/hr, indicating that the figures are far lower.

Table 4.1 Climate information for the chosen areas

Station	Latitude	Longitude	$R_{0.01}mm/hr$	ITU-R $R_{0.01}mm/hr$
Muranga	-0.722	34.146	50	
Kamusinga	0.794	34.705	40	
Kebabii	0.521	34.256	42	50
Mukumu	0.218	34.768	65	
Habaswein	-1.123	34.398	30	

Maseno	-0.003	34.597	63	
Cardinal Otunga	-0.599	34.744	62	
Wajir	1.748	40.034	30	
Lariak	0.402	36.377	20	
Chuka	-0.32	37.659	48	

For the 10 locations listed in table 4.1, a plot of percent exceedance VS. rain rate (mm/h) is as depicted in Figure 4.1 and 4.2. from these two graphs, the various $R_{0.01}$ for the locations is determined then these results presented in a manner seen in table 4.1 above.
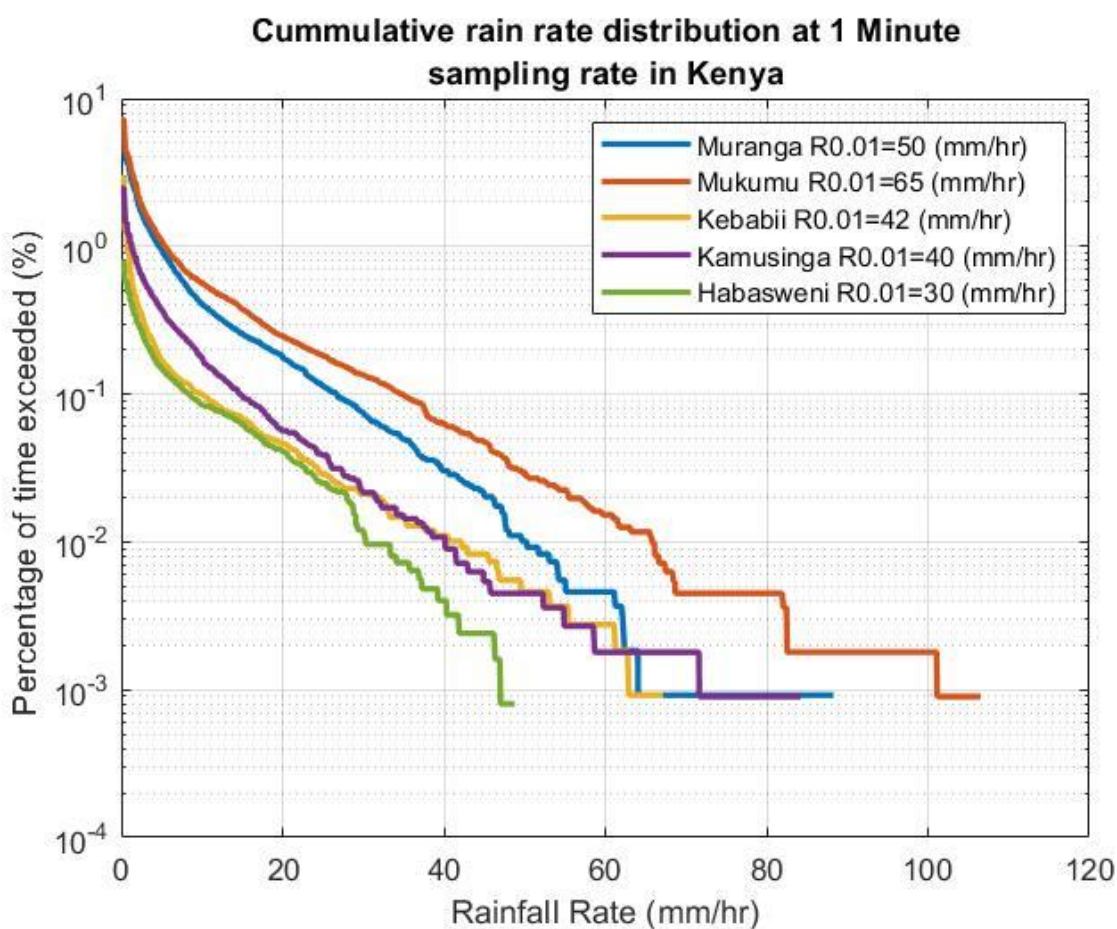
Figure 4.1: distribution of the overall rainfall rate for a one-minute sample rate in Kenya
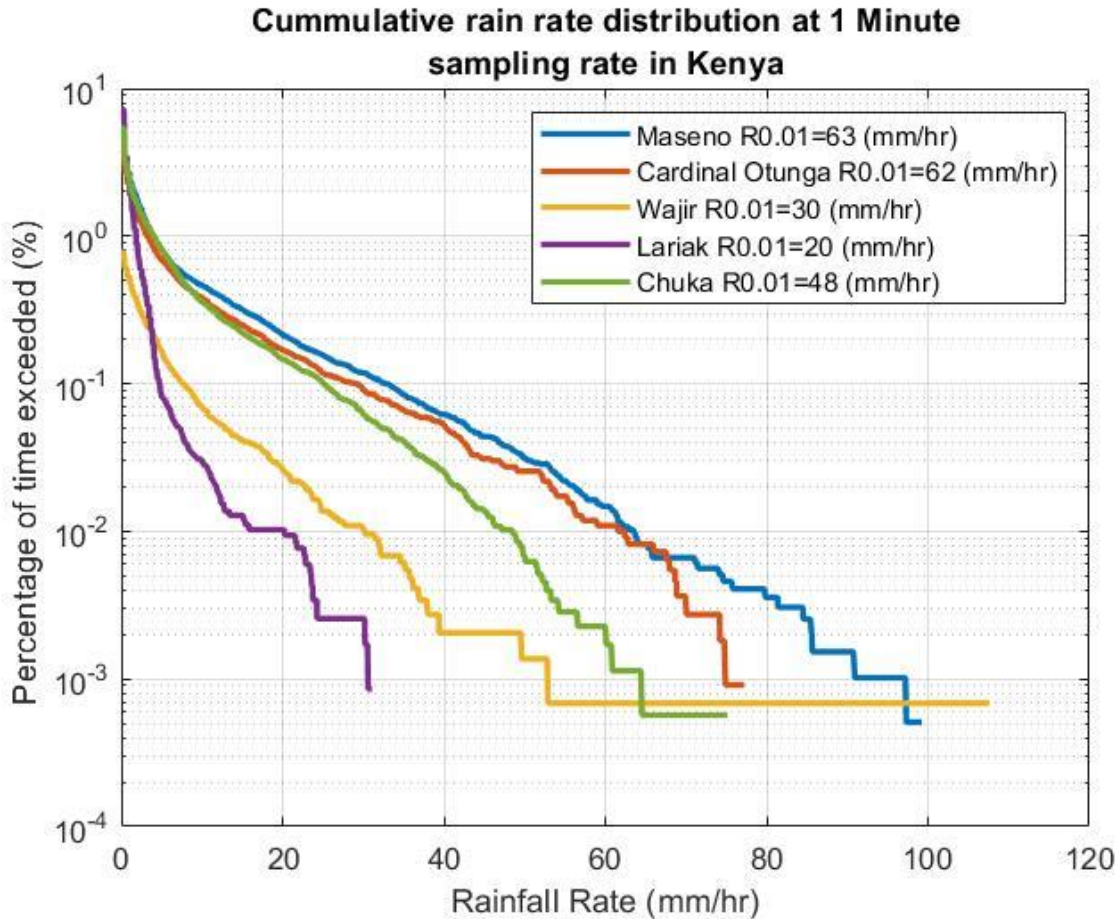
Figure 4.2: distribution of the overall rainfall rate for a one-minute sample rate in Kenya

4.3 Results on Specific attenuation for horizontally and vertically polarized signals.

The specific attenuation for both horizontally and vertically polarized signals for the five sites was determined and are tabulated as shown in table 4.2 and 4.3 respectively.

The computed distributed specific attenuation of rainfall against frequency is shown in Figures 4.3 and 4.4 for five locations in Kenya: Kamusinga, Muranga, Kebabii, Mukumu, and Habaswein. In actuality, they are typical places that capture the majority of the nation. The particular specific rain attenuation for each of the five locations is shown in Figure 4.3 for horizontal polarization and in Figure 4.4 for vertical polarization. For frequency ranges up to 60 GHz, the specific attenuation rises rapidly; then, from 60 GHz to 100 GHz, it rises more gradually, as can be seen in both figures.

For frequencies up to 150 GHz, their values stay nearly constant. After that, it gradually drops for the remaining propagation frequency. Figure 4.3 shows that at 60 GHz, for a horizontally polarized signal, the maximum measured specific attenuation of 21 dB is seen at Mukumu, meanwhile the minimum is predicted to be 12 dB in Habaswein. At the frequency of 60 GHz, Mukumu has the largest specific rain attenuation of 19 dB, whereas Habaswein has the lowest at 11 dB, according to Figure 4.4. As a result, it's quite evident that the specific rain attenuation for vertical polarization is less than that of horizontal polarization. This is attributed to the fact that raindrops have a not spherical in shape and they are flattened at the base, which causes signals transmitted with horizontal polarization to be highly attenuated than those transmitted in a vertically polarized manner.

Table 4.2 Specific attenuation for horizontally polarized

Frequency	Specific Attenuation Horizontal Polarization				
	Kamusinga	*Muranga*	*Kebabii*	*Mukumu*	*Habaswein*
	$R_{0.01}=40$	$R_{0.01}=50$	$R_{0.01}=42$	$R_{0.01}=65$	$R_{0.01}=30$
0	0	0	0	0	0
10	1.25	1.66	1.33	2.31	0.87
20	4.52	5.72	4.75	7.55	3.33
30	7.94	9.82	8.32	12.59	6.05
40	10.86	13.18	11.33	16.55	8.46
50	13.02	15.59	13.54	19.27	10.31
60	14.49	17.20	15.05	21.02	11.63
70	15.49	18.25	16.06	22.13	12.54
80	16.15	18.93	16.72	22.81	13.16
90	16.59	19.37	17.16	23.24	13.58
100	16.88	19.66	17.46	23.51	13.88
120	17.21	19.96	17.78	23.76	14.22
150	17.36	20.07	17.92	23.80	14.40
200	17.24	19.88	17.79	23.51	14.35
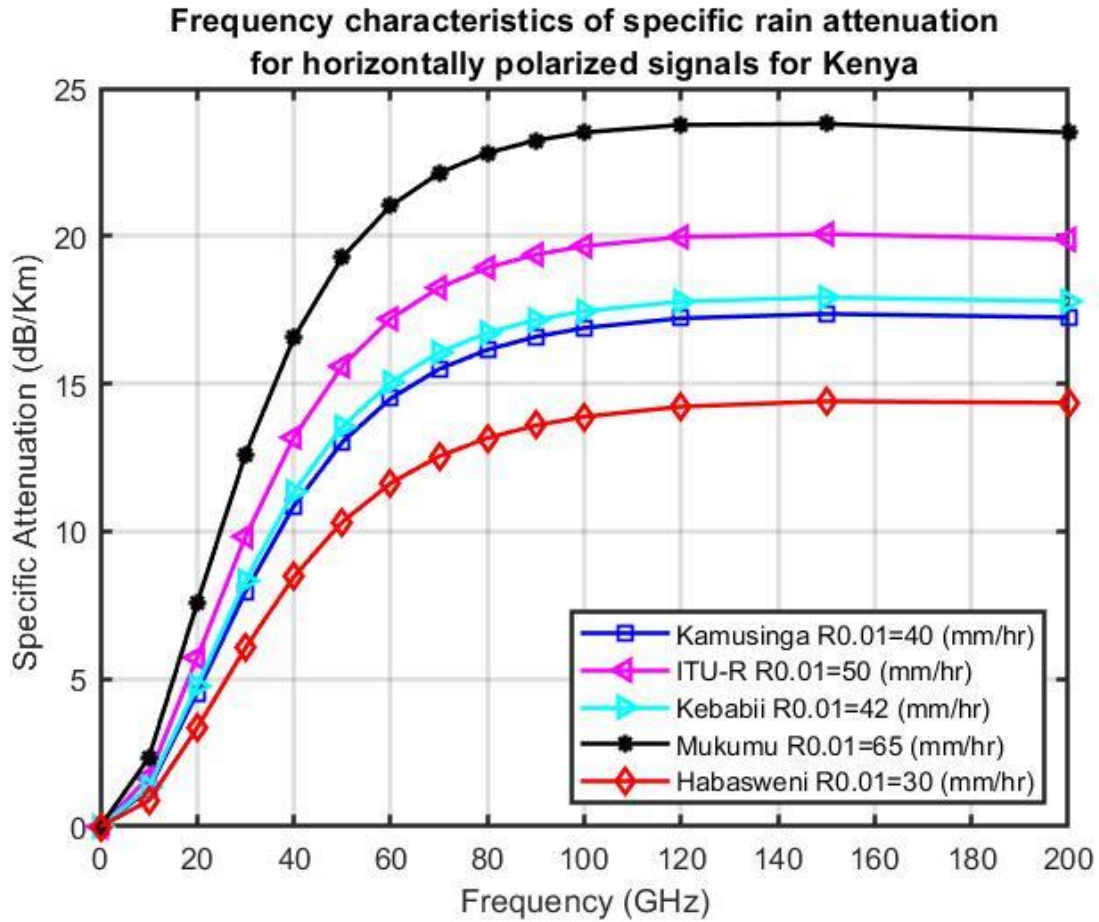
Figure 4.3: specific rain attenuation VS. frequency characteristics for horizontally polarized signals in Kenya

Table 4.3 Specific attenuation for vertically polarized signals

Frequency	Specific Attenuation Vertical Polarization				
	Kamusinga	Muranga	Kebabii	Mukumu	Habaswein
	40	50	42	65	30
0	0	0	0	0	0
10	1.00	1.31	1.06	1.80	0.70
20	3.63	4.52	3.81	5.86	2.73
30	6.64	8.14	6.94	10.35	5.11
40	9.54	11.52	9.94	14.37	7.49
50	11.80	14.07	12.26	17.29	9.41
60	13.47	15.92	13.97	19.38	10.86
70	14.68	17.24	15.20	20.83	11.92

80	15.55	18.19	16.09	21.86	12.70
90	16.16	18.84	16.71	22.57	13.26
100	16.59	19.29	17.14	23.04	13.65
120	17.07	19.78	17.63	23.53	14.11
150	17.26	19.94	17.81	23.63	14.33
200	17.06	19.66	17.60	23.22	14.22
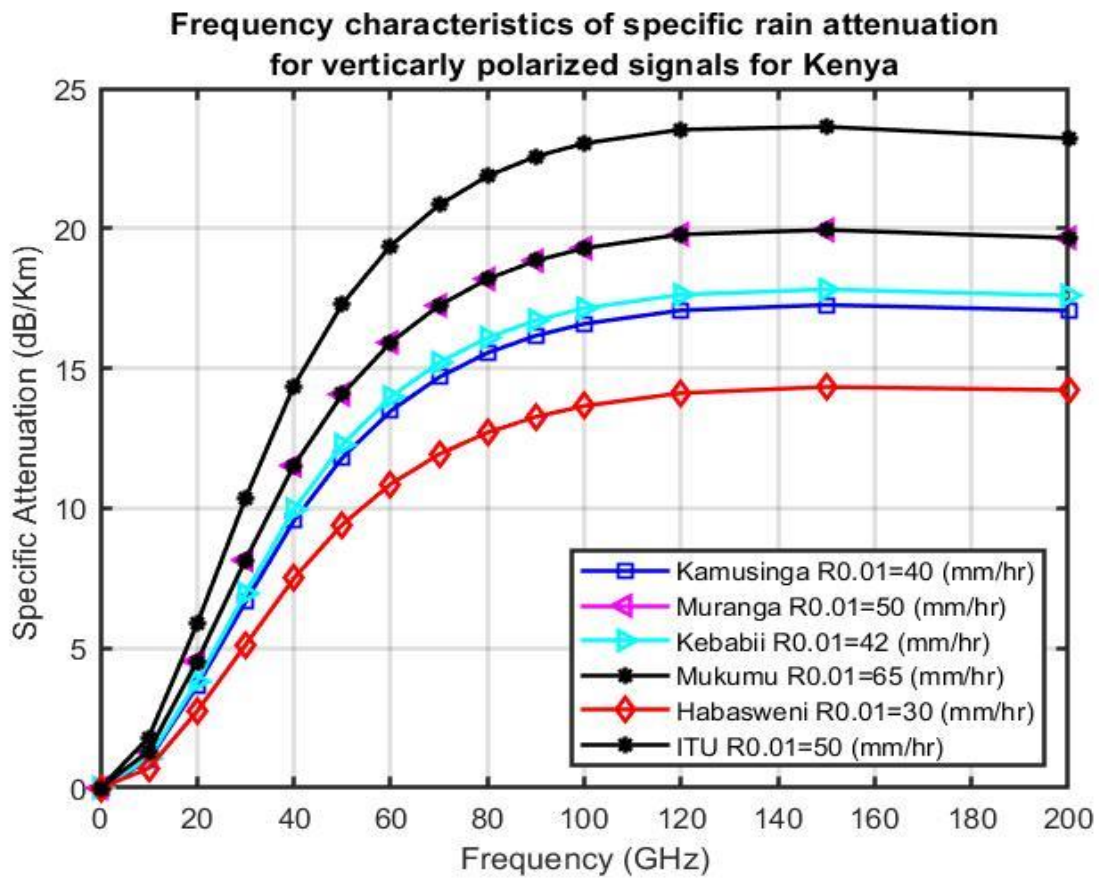
Figure 4.4: specific rain attenuation VS. frequency characteristics for vertically polarized signals in Kenya

4.4 Results on Specific attenuation for circularly polarized signals

It can be seen from Figure 4.4 even despite adverse weather circumstances, circular polarized signal is more robust to rain attenuation, circular polarized antennas mitigate on signal absorption given that they broadcast on all planes thereby increasing your chances of establishing a successful link. Additionally, circular polarized antennas transmit and receive in all planes, transferring the signal strength to the new plane without losing any of the original signal strength.
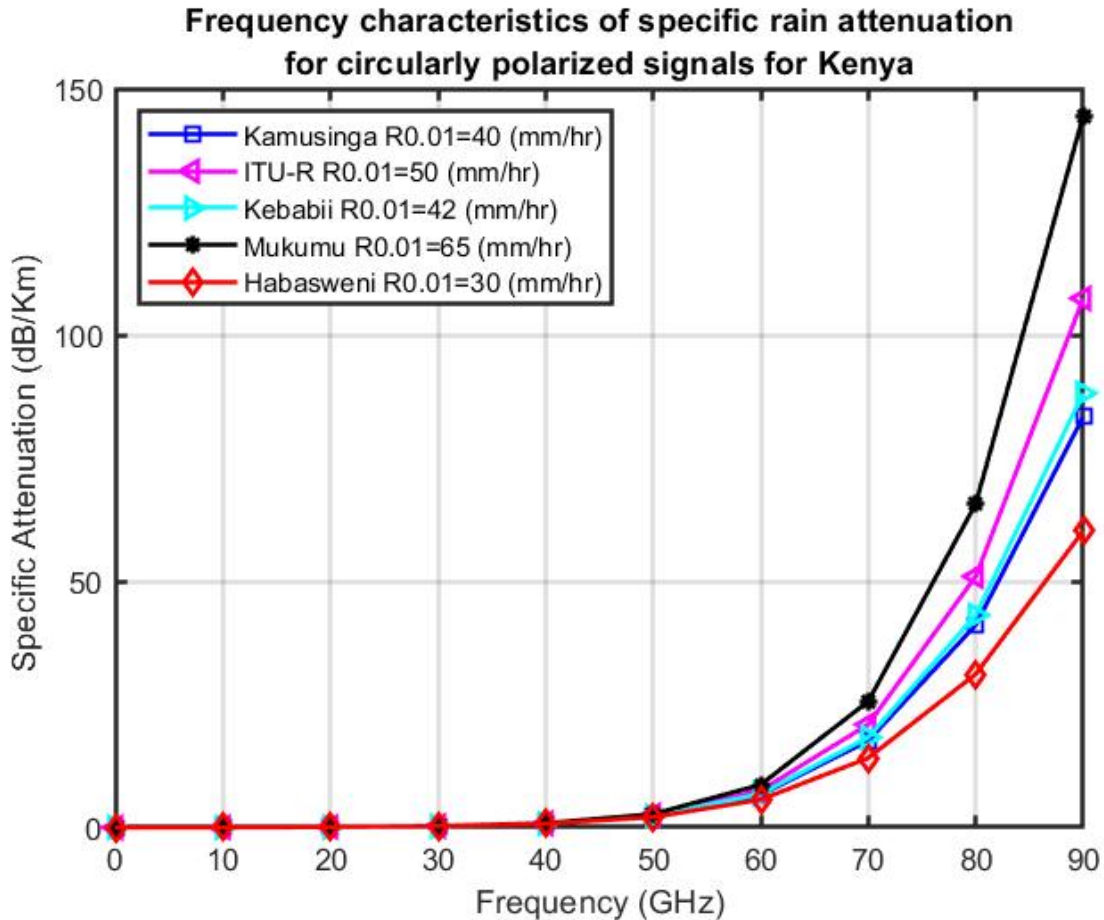
Figure 4.5: specific rain attenuation VS. frequency characteristics for circularly polarized signals in Kenya

Although circularly polarized systems also experience reflected signals, these signals are returned in the opposite direction, mainly avoiding interference with the signal that is already in motion. As a result, circularly polarized signals are significantly better at passing through and bending around obstacles, such as rain.
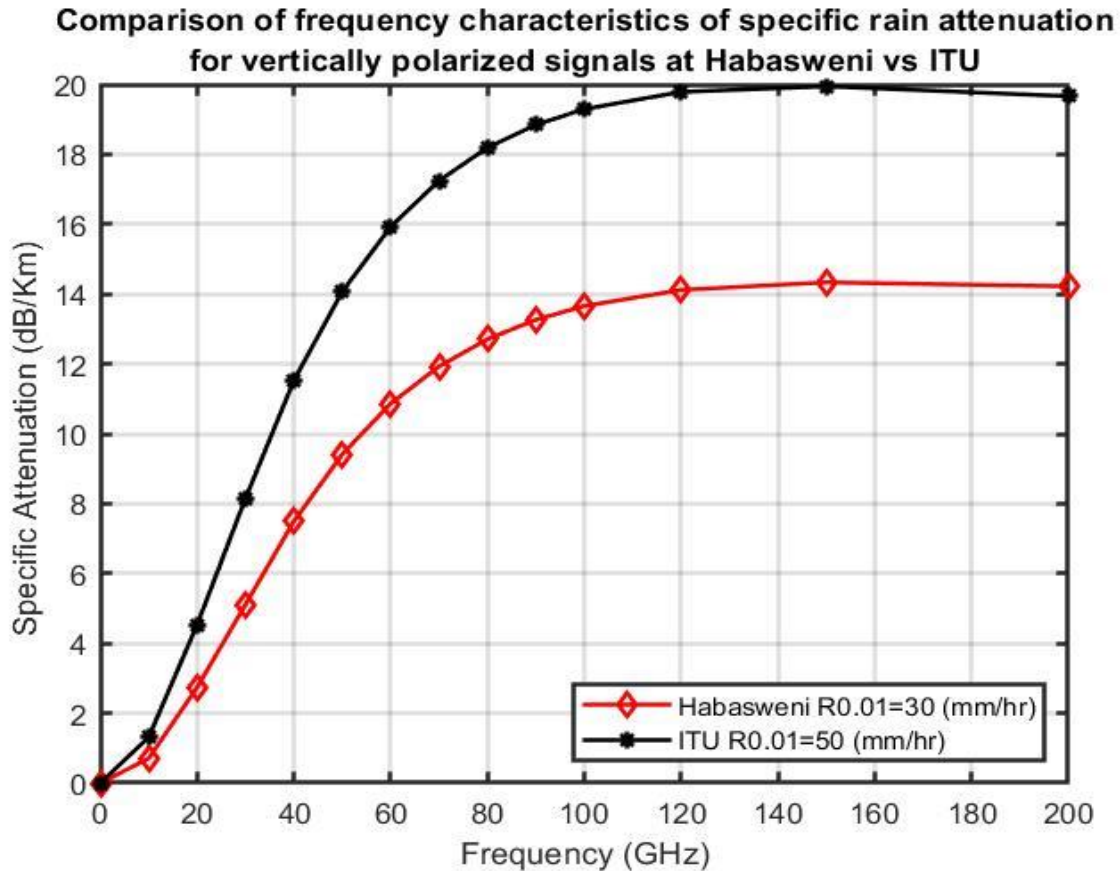
Figure 4.6: comparison of specific rain attenuation VS. frequency characteristics for vertically polarized signals at Habaswein VS. ITU-R

A comparison is drawn for two extreme locations with different values with reference to ITU-R as shown in figure 4.6 and 4.7 looking at one particular frequency of 40GHz it is evident that the specific attenuation at Habaswein is seen to be much lower that is 7.5dB/Km than the one postulated by ITU-R which can be seen to be 11.5 dB/Km. Similarly, looking at Figure 4.7 for a vertically polarized signal at Mukumu specific attenuation is seen to be about 14 dB/Km while ITU-R returns a much lower value of about 11dB/Km.

It therefore means that ITU-R underestimates the specific attenuation at Mukumu and over estimates the same at Habaswein.
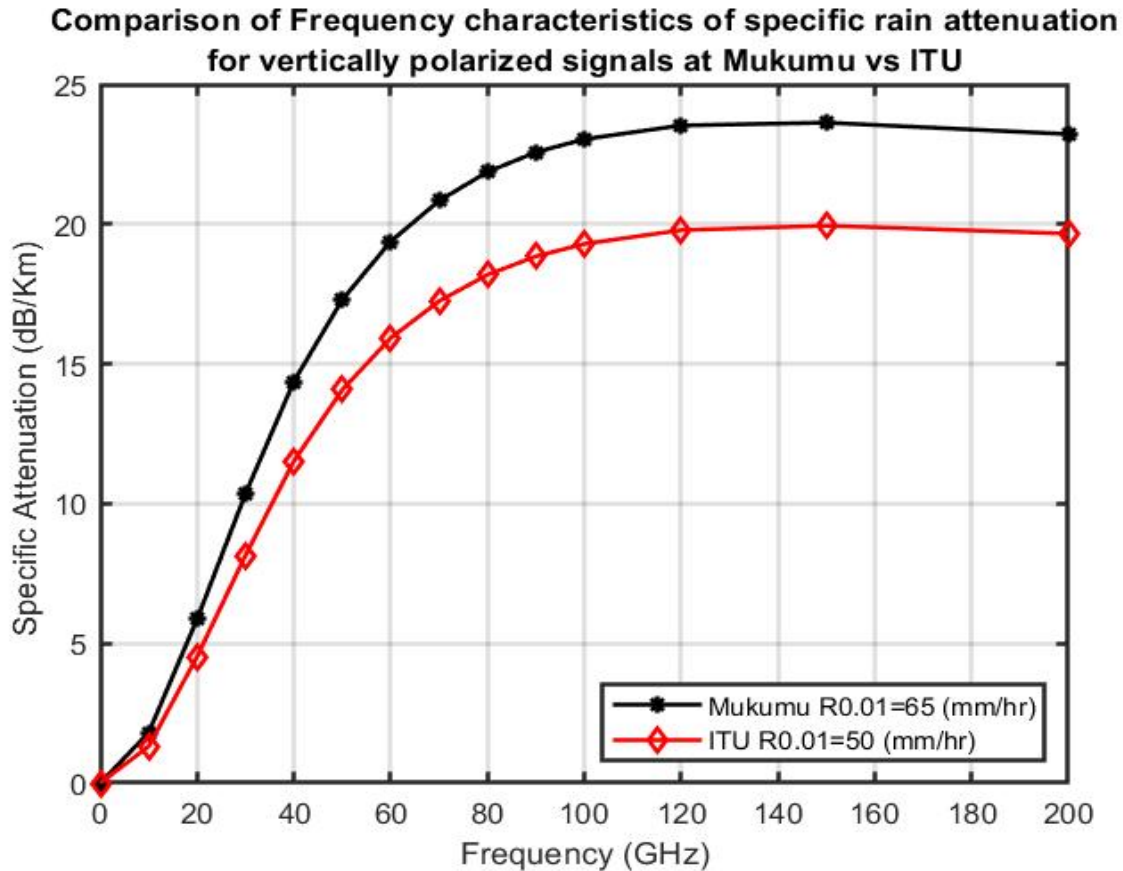
Figure 4.7: comparison of specific rain attenuation VS. frequency characteristics vertically polarized signals at Mukumu VS. ITU-R

4.5 Determining the attenuation due to rainfall

The ITU-R model [5] states that there are five processes involved in the prediction of rainfall attenuation:

a. Get the rate of rain $R_{0.01}$ that is exceeded for 0.01 percent of the time (having a time integration of 1 minute). In the event that this information is unavailable from the long-term measurements' local sources, and approximation can be got from the information contained in Recommendation ITU-R P.837-7.

b. Calculate the attenuation (specific), $A_S = \gamma R$ (dB/km) for the frequency, rain rate of interest and polarization through the use of Recommendation ITU-R P.838-3.

c. Calculate the effectual path length l_{eff}, of the link by getting the product of the distance factor r and the actual path length l.

57

d. Compute the effective path length, l_{eff}, of the link by multiplying the actual path length l by a distance factor r. The factor estimation is expressed as [5].

$$l_{eff} = rl \tag{4.1}$$

where l is the path length (actual), and r is a path factor whose estimation is expressed as:

$$r = \frac{1}{0.477\,l^{0.633}\,R_{0.01}^{0.073\alpha}\,f^{0.123} - 10.579\,(1 - exp\,(-0.024l))} \tag{4.2}$$

where f (GHz) is the frequency and α is the exponent in the specific attenuation model from Step 2. Maximum recommended r is 2.5, so if the denominator of Equation (4.2) is less than 0.4, use $r = 2.5$.

e. An estimation of the path attenuation exceeded for 0.01% of the time expressed as:

$$A_{0.01} = \gamma R l_{eff} \tag{4.3}$$

f. The attenuation $A\%p$ (in dB) exceeded for other time percentages, p of mean year may be calculated from the value of $A_{0.01}$ by using the following:

$$\frac{A_p}{A_{0.01}} = C_1 p^{-(C_2 + C_3 log_{10}P)} \tag{4.4}$$

with:

$$C_1 = (0.07^{c_0})[0.12^{(1-c_0)}] \tag{4.5}$$

$$C_2 = 0.855c_0 + 0.546(1 - c_0) \tag{4.6}$$

$$C_3 = 0.139C_0 + 0.043(1 - C_0) \tag{4.7}$$

where:

58

$$C_0 = \begin{cases} 0.12 + 0.4[log_{10}(f/10)^{0.8}] \geq 10GHz \\ 0.12 \qquad\qquad f < 10GHz \end{cases} \tag{4.8}$$

g. By using the climate data itemised in the Recommendation ITU-R P.841, compute the yearly time percentages P that corresponds to worst time percentages P_w in the event that the worst-month statistics are desired. The figures of A surpassed for proportions of the time p annually will be surpassed for the percentages of time p_w that corresponds to the worst time on a worst-month basis.

The above-described extrapolation method is thought to be applicable worldwide and is valid for microwave path distance/lengths of 60km and frequency ranges up to 100 GHz [31]

We determined the attenuation that would occur due to rain on a terrestrial line of site at 20GHz microwave frequency. Using the ITR − R we determined the path factor at that frequency, the using the already calculated $R_{0.01}$ we determined the specific attenuation at that frequency. Finally, the path attenuation was determined by getting the product of specific attenuation, path factor and the distance. This has been done for the five sites and the results are as shown in tables 4.4 to 4.9

Table 4.4 Kamusinga Path Attenuation

Distance	Path factor	Specific attenuation	Attenuation
1	1.977	3.63	7.18
5	1.112	3.63	20.20
10	1.007	3.63	36.61
20	0.993	3.63	72.20
30	0.922	3.63	100.53
40	0.777	3.63	112.96
50	0.621	3.63	112.98
60	0.492	3.63	107.43

Table 4.5 Muranga Path Attenuation

Distance	Path factor	Specific attenuation	Attenuation
1	1.931	4.52	8.743
5	1.072	4.52	24.269
10	0.957	4.52	43.354
20	0.920	4.52	83.304

30	0.841	4.52	114.306
40	0.708	4.52	128.315
50	0.571	4.52	129.234
60	0.456	4.52	124.012

Table 4.6 Kebabi Path Attenuation

Distance (km)	*Path factor*	*Specific attenuation*	*Attenuation*
1	1.967	3.812	7.500
5	1.103	3.812	21.029
10	0.996	3.812	37.988
20	0.976	3.812	74.466
30	0.903	3.812	103.334
40	0.761	3.812	116.084
50	0.610	3.812	116.294
60	0.484	3.812	110.818

Table 4.7 Mukumu Path Attenuation

Distance (km)	*Path factor*	*Specific attenuation*	*Attenuation*
1	1.87934446	5.860630751	11.01414396
5	1.02837234	5.860630751	30.13455276
10	0.90424556	5.860630751	52.99449334
20	0.84555909	5.860630751	99.11019206
30	0.76220434	5.860630751	134.009945
40	0.64110276	5.860630751	150.2906625
50	0.52012887	5.860630751	152.4141617
60	0.41976416	5.860630751	147.6049641

Table 4.8 Habaswein Path Attenuation

Distance (km)	*Path factor*	*Specific attenuation*	*Attenuation*
1	2.03914916	2.737095034	5.581345043
5	1.16698316	2.737095034	15.9707191
10	1.07900661	2.737095034	29.53343635
20	1.1051202	2.737095034	60.49638024
30	1.04938771	2.737095034	86.16821706
40	0.88570068	2.737095034	96.96987739
50	0.70102351	2.737095034	95.93839879
60	0.54779989	2.737095034	89.96282184

Table 4.9 Path Attenuation for Vertically Polarized Signals

Distance (km)	Kamusinga	Muranga	Kebabii	Mukumu	Habaswein
1	7.18	8.743	7.500	11.01414396	5.581345043
5	20.20	24.269	21.029	30.13455276	15.9707191
10	36.61	43.354	37.988	52.99449334	29.53343635
20	72.20	83.304	74.466	99.11019206	60.49638024
30	100.53	114.306	103.334	134.009945	86.16821706
40	112.96	128.315	116.084	150.2906625	96.96987739
50	112.98	129.234	116.294	152.4141617	95.93839879
60	107.43	124.012	110.818	147.6049641	89.96282184
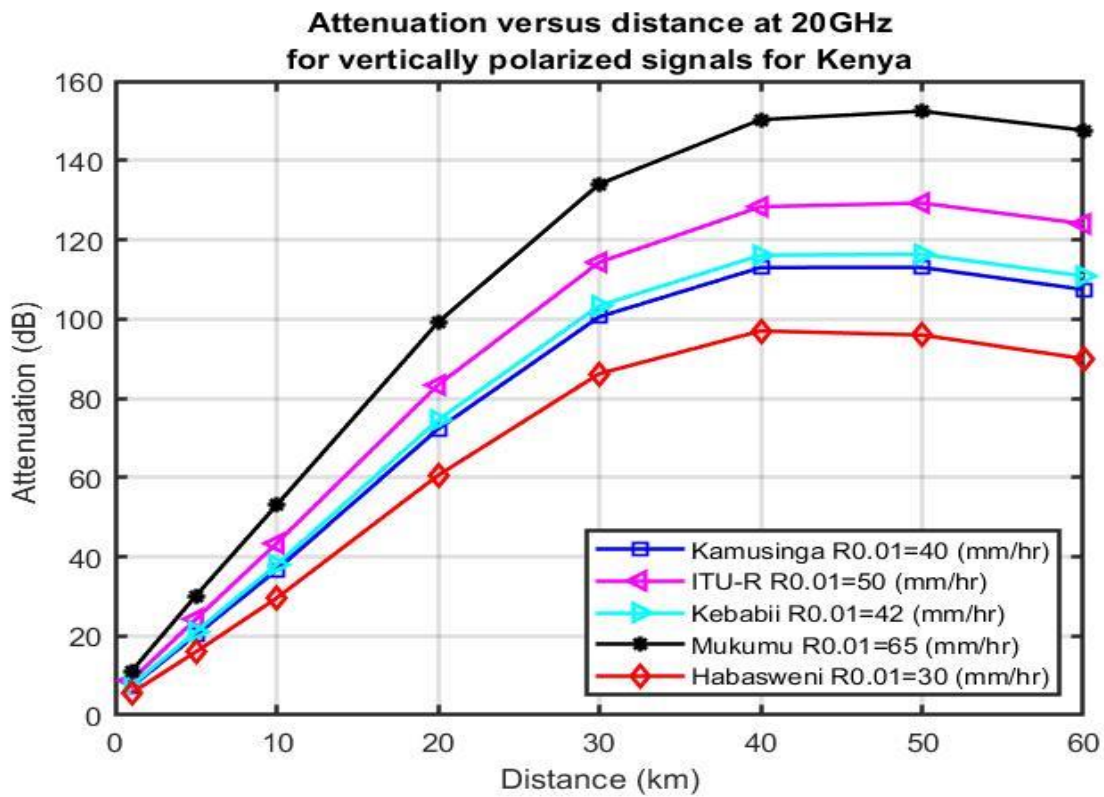
Figure 4.9: path attenuation for vertically polarized signals

Table 4.10 path attenuation for horizontally polarized signals

Distance (km)	Kamusinga	Muranga	Kebabii	Mukumu	Habasweni
1	8.630253753	10.63660257	9.033661837	13.60390442	6.593855391
5	23.8081436	28.93895013	24.8441163	36.44411841	18.53799466
10	42.24344228	50.58971077	43.93418962	62.69351063	33.59043664
20	80.21496109	93.67375907	82.94580996	113.0881227	66.21378282
30	109.3533603	125.9937606	112.7231456	150.0757015	92.17903223

40	122.7035083	141.2528651	126.4590647	168.1077929	103.5749169
50	123.9607021	143.6008962	127.9422831	171.969977	103.6037536
60	119.4355268	139.530209	123.5129191	168.5161768	98.52877321

In Figures 4.9 and 4.10, the rain path attenuation for horizontal and vertical polarizations for the five (5) locations in Kenya across various distances is depicted. These two figures show that the attenuation of rain increases dramatically up to a distance of 30 km, then less significantly up to a distance of 40 km, therefore; eventually the attenuation becomes nearly constant. Since the effective path length does not decrease as the true path length grows, the rain attenuation becomes non-uniform as the distance increases.
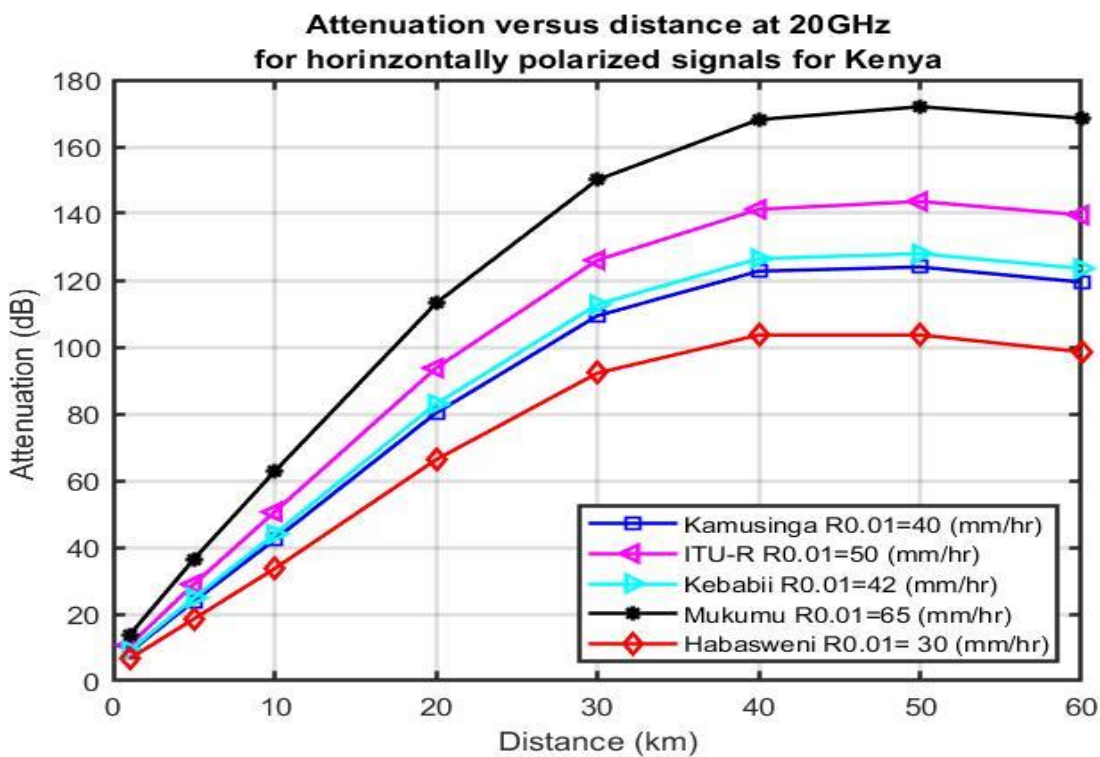
Figure 4.10: path attenuation for horizontally polarized signals

The maximum rain attenuation, measured in decibels (dB), occurs in Mukumu at 134 dB, while the lowest is in Habaswein at 86 dB, as demonstrated in Fig. 4.9 with vertical polarization at a distance of 30 km. The horizontal polarization attenuation distribution in Figure 4.10 is also similar, with Mukumu having the highest value at 150 dB and Habaswein having the lowest value

at 92 dB at a distance of 30 km. In line with what has already been established, a comparison of the two plots shows that vertical polarization attenuates rain less than horizontal polarization.
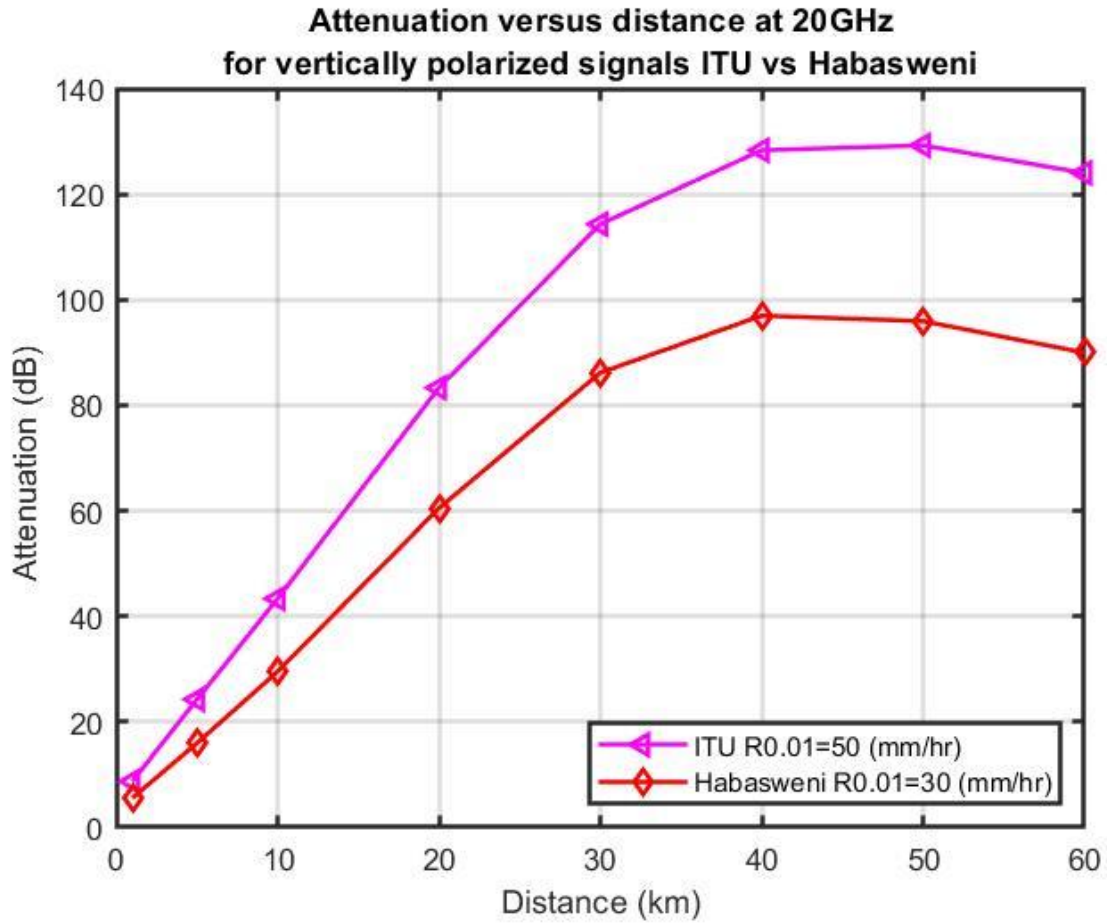
Figure 4.11: comparison for path attenuation for vertically polarized signals Habasweni VS. ITU-R
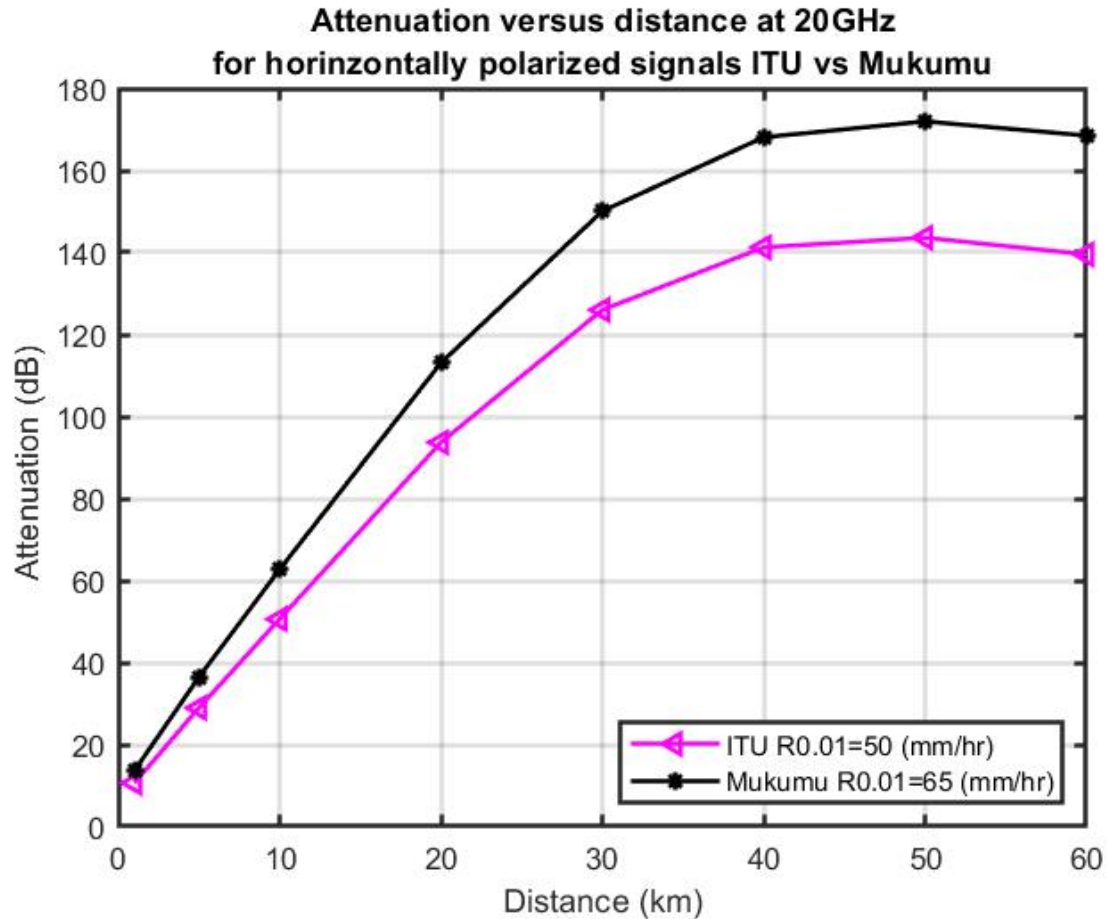
Figure 4.12: comparison for path attenuation for vertically polarized signals Mukumu VS. ITU-R

From figure 4.12 illustrates how the ITU-R rain rate value underestimates the attenuation due to rain for Mukumu which is situated in the western part of the country and experiences a lot of rainfall. For a point-to-point 10km Line of Sight Link at 20Ghz it can be seen that attenuation at Mukumu is 62 dB using the determined rain rate of 65 (mm/hr) while ITU-R returns a value of 52 dB.
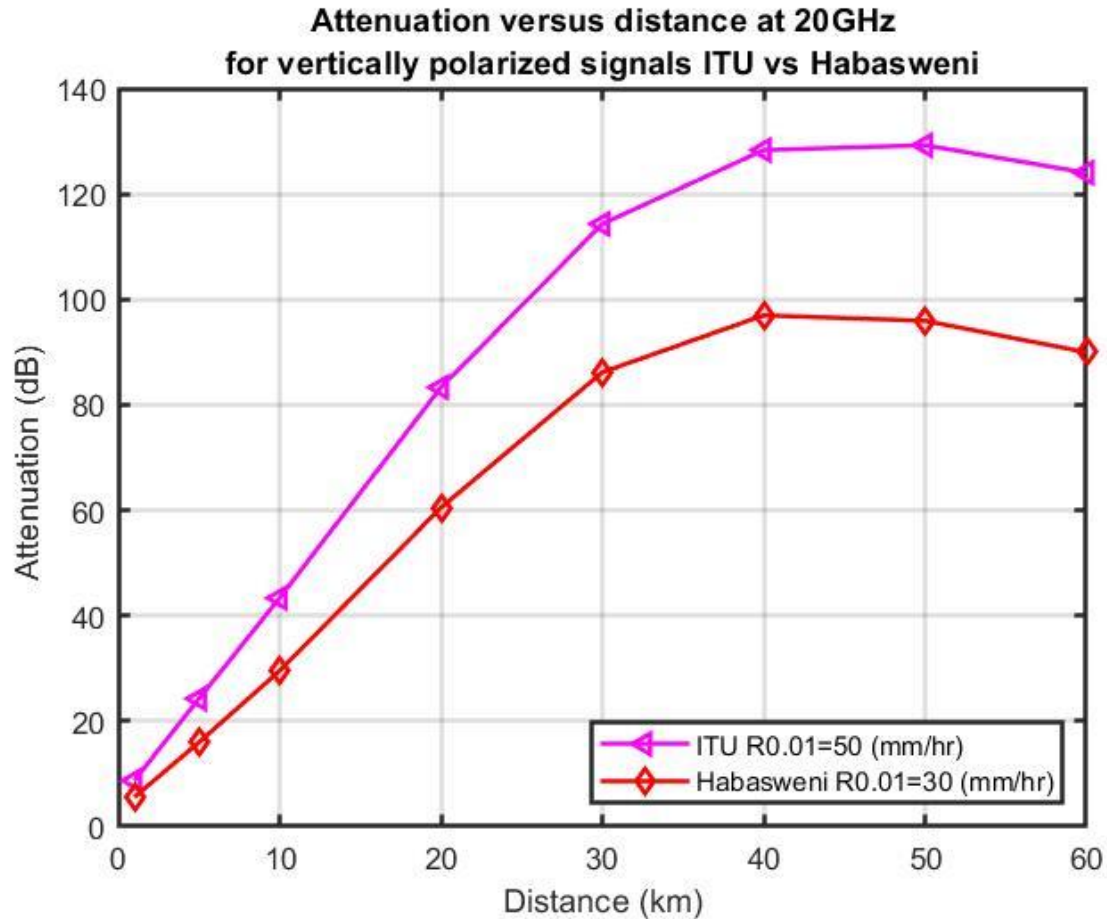
Figure 4.13: comparison for path attenuation for horizontally polarized signals Mukumu VS. ITU-R

Similarly, from figure 4.13, the ITU-R rain rate value overestimates the attenuation due to rain for Habaswein which is situated in the northern part of the country and experiences minimal rainfall. For a point to point 10km Line of Sight Link at 20Ghz it can be seen that attenuation at Habaswein is 28 dB using the determined rain rate of 30 (mm/hr) while ITU-R gives a value of 43 dB.

4.6   Fade Margin Analysis

Because rain falls at different times of the year and at different rates, the rain fade margin needed to take rain attenuation into account varies throughout time. The fading depth is shown in Figures 4.15 and 4.16 at various time intervals.
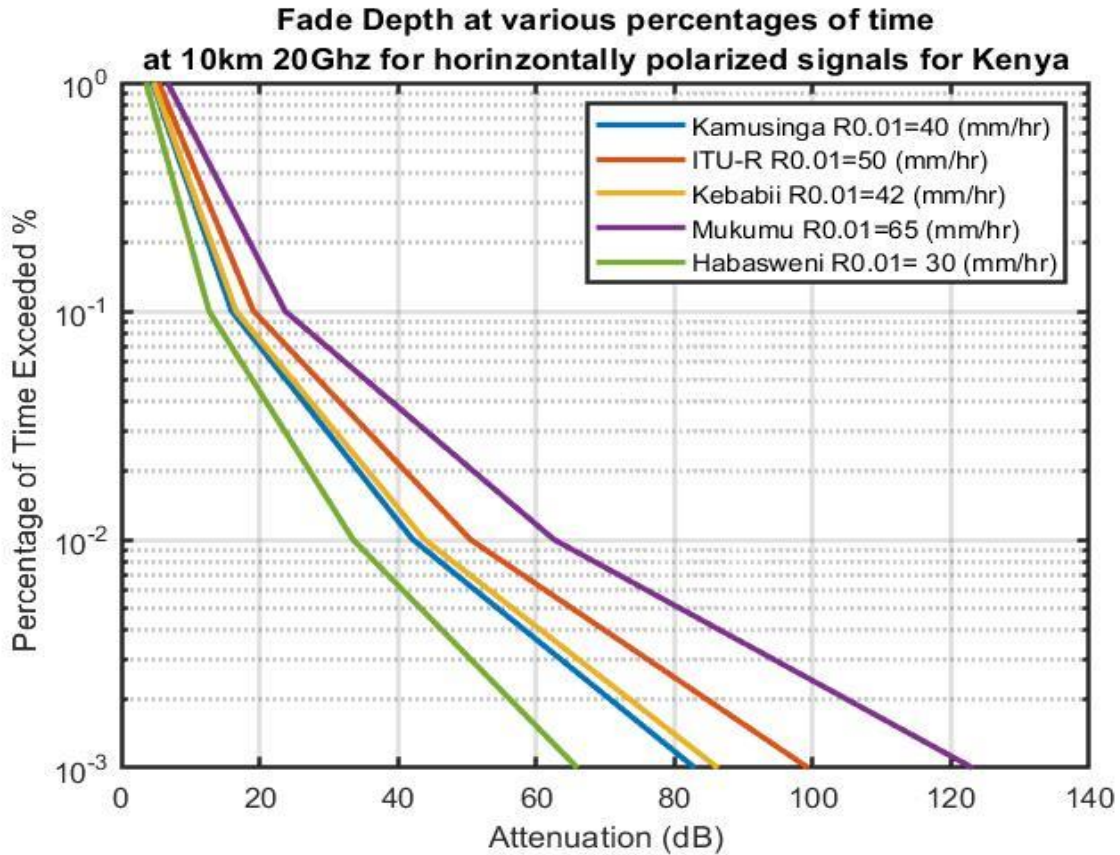
Figure 4.15: Annual rain attenuation exceeded for different percentages of time at 20 GHz
frequency with link length of 10 km using horizontal polarization

The rain attenuation values for a horizontally polarized signal at various percentages of time at 20 GHz in a 10 km channel length are shown in Figure 4.15. The highest fade depth was measured in Mukumu to be 62 dB at 0.01% of the time (99.99% availability), while the minimum was measured in Habaswein to be 32 dB.
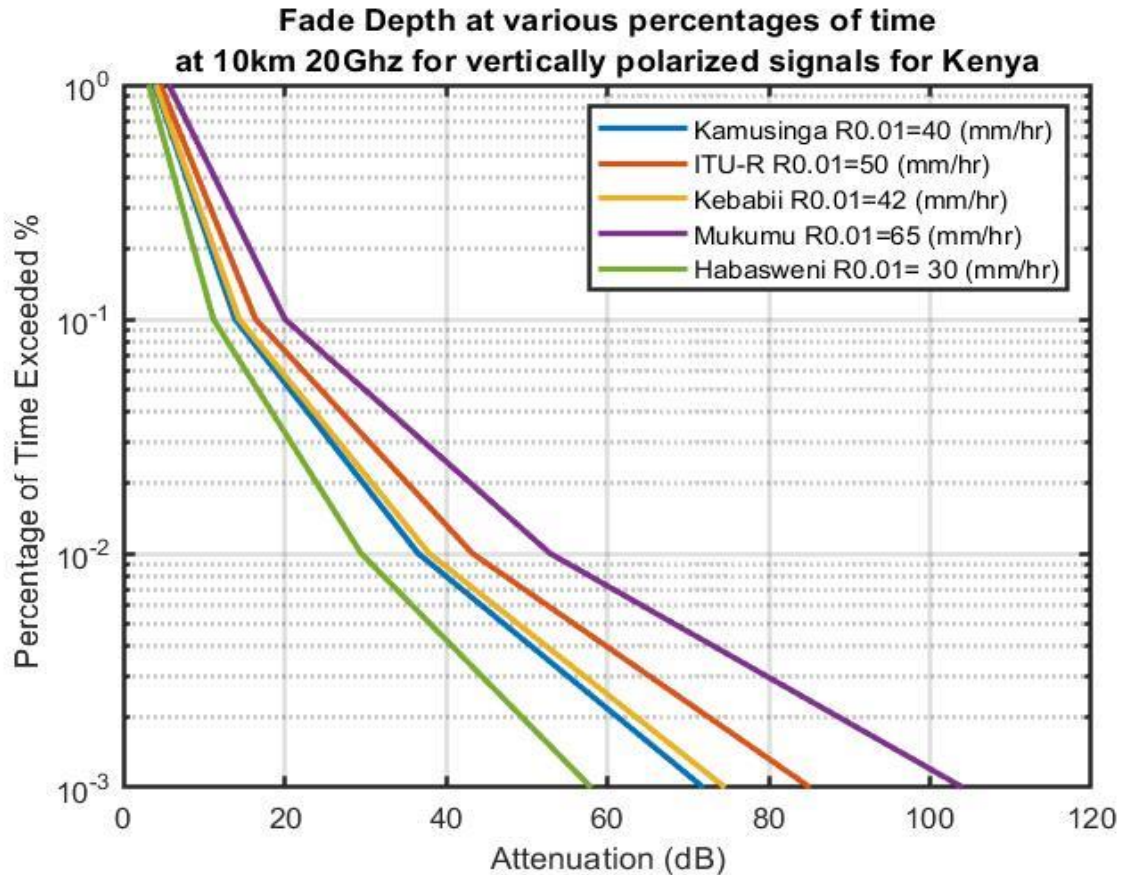
Figure 4.16: Annual rain attenuation exceeded for different percentages of time at 20 GHz frequency with link length of 10 km using vertical polarization

An equal distribution of rain fade is seen for vertical polarization Figure 4.16 with the highest value of 54 dB in Mukumu and the lowest value of 28 dB in Habaswein at the same operating frequency and link distance. The two graphs can be compared, and a vertically polarized signal has a lower attenuation of rain compared to a horizontally polarized signal.

Table 4.11 Attenuation at different % of time

Attenuation Exceedance	Polarization	Kamusinga	Muranga	Kebabii	Mukumu	Habaswein
$A_{0.001}$	Vertical	71.920	85.154	74.615	104.088	58.007
	Horizontal	82.971	99.364	86.292	123.138	65.976
$A_{0.01}$	Vertical	36.546	43.271	37.915	52.892	29.476
	Horizontal	42.162	50.492	43.849	62.572	33.525
$A_{0.1}$	Vertical	13.845	16.393	14.364	20.0378	11.166
	Horizontal	15.972	19.128	16.612	23.705	12.701
A_1	Vertical	3.910	4.629	4.056	5.659	3.153
	Horizontal	4.511	5.402	4.691	6.695	3.587

4.7 Contour map for $R_{0.01}$

Figure 4.17: Contour map of rain fade at 0.01%-time exceedance for Kenya

Figure 4.17 show a contour map of $R_{0.01}$ that has been calculated and determined from the two year rainfall data, this maps extrapolates values for other regions based on the data provided and

can be helpful in determining attenuation at particular locations within the country. From the figure the western part of the country has higher values compared to northern and coastal regions that experience less rainfall

4.8   Chapter Conclusion

Based on the available rain rate statistics, the particular specific rain attenuation for the ten locations has been determined. Additionally, the path attenuation (dB) for specific five out of these places was calculated based on the determined rain rate and the current models. This chapter also determined the fade margins which have been presented. Finally, a contour map is presented that has values for $R_{0.01}$ for Kenya.

CHAPTER 5

5   CONCLUSION AND FUTURE RESEARCH WORK

This chapter summarizes the thesis's findings, contributions, and suggestions for additional research.

5.1   Conclusion

Design engineers need more precise data on rainfall rates surpassed for a portion of an annual average to design and implement more dependable microwave systems communications with fewer link outages. This information is essential for estimating the attenuation caused by rainfall on microwave and millimeter networks that operate at higher frequencies of more than $10\ GHz$. In Chapter 3, rainfall rate conversion models for 5 locations over Kenya were successfully established utilizing the power-law function and cumulative distributions derived from measured data. The ITU-R model was employed to calculate $R_{0.01}$.

The results were examined in Chapter 4 and the following conclusions were made: The attenuation is seen to be greatest at Mukumu, then in descending order Muranga, Kamusinga, Kebabii, and Habaswein. Additionally, it should be noted that because raindrops are not spherical and are flattened at the base, vertical polarization has a lower specific rain attenuation than horizontal polarization. Thus, the horizontally polarized waves exhibit greater attenuation than the vertically polarized waves. This chapter calculates the particular attenuation for the chosen locations using the $R_{0.01}$ results, and then determines the path loss attenuation at $20 GHz$ for the five sites. Because raindrops are not spherical and are flattened at the base, the results obtained reveal that horizontal polarization has a higher specific rain attenuation than vertical polarization.

Additionally, it is discovered that the vertically and circularly polarized signals are less affected by precipitation than the horizontally polarized signal. Therefore, it is more cost-effective to use vertical polarization in heavily rainy areas like Mukumu. Specific attenuation is determined for different frequencies similarly, rain attenuation is also calculated for various distances, the results are properly presented. Due to the non-uniformity of the rain's distribution along the link, it is discovered that shorter link paths are more affected by rainfall than longer ones.

5.2 Contribution of research work

Results in this thesis shows that using actual rain data collected over a period of time can give results that are quite specific and of course accurate to the particular geographical area. This minimizes errors and link outages that might occur due to underestimation of attenuation due to rain, similarly there will be cost benefits to Mobile Network Operators (MNOs) as there will be limited over design of microwave links. This means that, the results determined would enable radio network and link designers to build networks that are cost effective, robust and resilient to attenuation due rain.

5.3 Recommendations for Further Research Work

For more definitive findings on rainfall rates can be determined if data of rainfall can be obtained which is measured at shorter integration time of 30 second or less.

Based on the data available, the worst month statistical analysis should be taken into consideration; this can be determined by using the ITU-R recommendation, and the results should be compared to identify the deviations.

REFERENCES

[1] Olsen, R. L., D. V. Rogers, and D. B. Hodge, "The aR^b relation in the calculation of rain attenuation," *IEEE Transaction on Antennas and Propagation*, vol. 26, 318-329, 1978.

[2] R.K. Crane, "Prediction of attenuation by rain," IEEE *Trans. Comm.*, vol. 28, pp. 1717–1733, 1980

[3] Crane, R.K, "A two-component rain model for the prediction of attenuation statistics," *Radio Science,* vol. 17, N.6, 1371-1387, 1982.

[4] G.O. Ajayi and E.B.C. Ofoche, "Some tropical rainfall rate characteristics at Ile-Ife for microwave and millimeter wave application," *J. of Climate and Applied Meteor.*, vol. 23, pp. 562–567, 1983.

[5] F. Moupfouma, "Improvement of a rain attenuation prediction method for terrestrial microwave links," *IEEE Trans. Antennas Propag.*, vol. 32, pp. 1368–1372, 1984.

[6] F. Moupfouma, "Rainfall-rate distribution for radio system design," *IEEE proceedings*, vol. 134, pp. 527-537, Feb. 1987.

[7] Moupfouma F. "Rain induced attenuation prediction model for terrestrial and satellite earth microwave links," IEEE, vol.42, 539-550, 1987.

[8] C. K. Crane, "Electromagnetic Rain Propagation through rain", John Wiley & Sons, Inc. 1996.

[9] "Propagation prediction techniques and data required for the design of terrestrial line-of-sight systems," Recommendation ITU-R 530-17, 2017.

[10] "Characteristics of precipitation for propagation modelling," ITU-R, Geneva, 2017, ITU-R Rec. P.837- [1-7].

[11] "Propagation data and prediction methods required for the design of Earth-space telecommunication systems," Recommendation, Geneva ITU-R P.618-11, 2013.

[12] Goldhirsh, J., 1983: "Rain cell size statistics as a function of rain rate for attenuation modelling ".IEEE Trans. Antennas Propag., 31 , 799–801

[13] Asiyo, M. and Thomas J. O. Afullo, 2013: "Statistical Estimation of fade depth and outage probability due to multipath propagation in Southern Africa," Progress in Electromagnetics Research B, Vol. 46, 251-274.

[14] C. Capsoni, F. Fedi, C. Magistroni, A. Paraboni, A. Pawlina: "Data and theory for a new model of the horizontal structure of rain cells for propagation applications," *Radio Science*, vol. 22, n°3, pp. 395-404, 1987.

[15] A. Pawlina-Bonati, "Essential knowledge of rain structure for radio applications based on available data and models," *Proceedings of Radio Africa 99, Gaborone, Botswana,* October 1999, pp. 96-106.

[16] M. Binaghi and A. Pawlina Bonati, "Statistical dependence of rain occurrence in multiple site case modelled with dynamical radar derived parameters," *Proc. ISAP 92, Int. Symp. On Antennas and Propag.,* pp. 1053–1056, Sapporo (Japan), Sept. 1992.

[17] Drufuca G, Zawadzki I, "Statistics of rain gauge data," *Journal of Applied Meteorology*, vol. 14, December, pp. 1419- 1429, 1975.

[18] S. Begum, C. Nagaraja, I. Otung, "Analysis of rain cell size distribution for application in site diversity," *IEEE Antennas & Propag.*, pp.1–5, 2006.

[19] Emilio Matricciani, Apolonia Pawlina Bonati, "Rain cell size statistics inferred from long term point rain rate: model and results," *Proc. Third Ka band utilization conference*, Sorrento, Italy,September, 1997.

[20] Ippolito, L. J. Jr., 2008: " Satellite Communications Systems Engineering: Atmospheric Effects, Satellite Link Design and System Performance", John Wiley and Sons Ltd, UK.

[21] Sauvageot H. and Mesnard Frederic, "The relation between the area-average rain rate and therain cell size distribution parameters," *Journal of Atmospheric Science*, vol.56, pp. 57-70, Jan. 1999.

[22] T. G. Konrad, "Statistical models of summer rain showers derived from fine-scale radar observations," *J. Appl. Meteor.,* vol. 17**,** pp. 171–188, 1978.

[23] R. S. Teno´rio, H. Sauvageot, and S. Ramos-Buarque, "Statistical studies of rain cell size distribution using radar data during squall line episodes in West Africa," *Proc. Third Int. Symp. on Hydrological Applications of Weather Radar,* Sao Paulo, Brazil, 518–526,1995.

[24] K. Naicker and S. H. Mneney, "Propagation measurements and modelling for terrestrial line-of-Sight links at 19.5 GHz," *IEEE Africon, Gaborone, Botswana,* vol. 01, pp.95–100, Sept.2004.

[25] Assis Mauro S., L. A. R. da Silva Mello and Jorge L. Cerqueira, "Rain attenuation research in Brazil," URSI GA 2005.

[26] Peter Odero Akuon, "Rain cell size attenuation modelling for terrestrial and satellite radio links," *Master's Thesis*, December 2011, pp. 40-47.

[27] Akuon P. O. and Afullo T. J. O., "Negative power law attenuation estimation for rainy Earth-Space radio links," *Proc. of PIERS symposium*, Kuala Lumpur, Malaysia, pp. 270-276, 27th – 30th March. 2012.

[28] Akuon P. O. and Afullo T. J. O., "Path reduction factor modelling for terrestrial links based on rain cell growth," *Proc. of IEEE Africon conference*, Livingstone, Zambia, pp. 1-6, 13-15th Sept. 2011. ISBN: 978-1-61284-991-1.

[29] Akuon P. O. and Afullo T. J. O., "Rain cell size statistics from rain gauge data for site diversity planning and attenuation prediction," *Proc. of Southern Africa Telecommunication Networks and Applications Conference (SATNAC),* East London, South Africa, pp. 213-216, 4-7th Sept., 2011. ISBN: 978-0-620-50893-3.

[30] Akuon P. O. and Afullo T. J. O., "Rain cell sizing for the design of high capacity radio link systems in South Africa," *Progress in Electromagnetics Research, PIER B*, vol. 35, pp. 263-285, 2011.

[31] "Propagation data and prediction methods required for the design of terrestrial line of sight systems," Recommendation ITU-R P.530-17 (12/2017), December 2017.

[32] Harry E. Green, "Propagation impairment on Ka-band SATCOM links in Tropical and Equatorial Regions", *IEEE Antennas and Propagation Magazine*, Vol. 46, No.2, April 2004, pp. 31-44.

[33] G.O Ajayi, S.Feng, S.M. Radicella, B.M Reddy (Ed), "Handbook on Radiopropagation Related to Satellite communications in Tropical and Subtropical Countries" *ICTP, Trieste, Italy* 1996, pp.2-14

[34] C.G.S. Migliora, M.S. Pontes and L.A.R. Silva Mello, "Rain Rate and attenuation Measurements in Brazil," *Preprint of URSI Comm. F Open Symposium on regional Factors in Predicting Radiowave Attenuation Due to Rain*, Rio de Janeiro, Brazil, Dec. 1990, pp.8-13.

[35] M.G. Zhang, D.Z. Hu, "Investigation of Rain Attenuation and Rain Rates Statistics in China and its Neighbouring Area," Paper Submitted for [15], 1995

[36] Goldrish J. and Vogel, WJ., "Report A2A-98-U-0-021," *Applied Physics Laboratory*, John Hopkins University, Laurel, M.D, 1998.

[37] Liebe, H.J., G.A. Hufford and T. Manabe (1991): "A model for the complex permittivity of water at frequencies below 1 THz" Inter. J. of Infrared and Millimeter Waves, 12 (7), 659–678.

[38] G. O. Ajayi, "Physics of Tropospheric Radiopropagation" *ICTP, Trieste, Italy*, Feb1989, pp. 11-12

[39] Crane, R. K. (2003) "Propagation Handbook for Wireless Communication System Design", *CRC Press, New York*

[40] Tamošiunaite, M., S. Tamošiunas, M. Žilinskas and M. Tamošiuniene, (2011) "Atmospheric Attenuation due to Humidity, in Electromagnetic Waves, ed Vitaliy Zhurbenko", *ISBN: 978-953-307-304-0, InTech,* Croatia, pp. 157-172

[41] Carlos Salema: Microwave Radio Links from Theory to Design, John Wiley & Sons, Inc., 2003, Chapter two

[42] Elbert, B. R., (2004) "Satellite Communication Applications Handbook," *Artech House*, USA

[43] Crane, R. K. (1996) "Electromagnetic Wave Propagation through Rain", Wiley Interscience, New York

[44] Born, M., and E. Wolf, ""Principles of Optics, New York: Pergamon Press, 1964.

[45] Freeman, R. L., (2007) "Radio System Design for Telecommunications," John Wiley and Sons, New York

[46] Kumar, L.S. and Y.H. Lee, 2010: "Shape Slope parameter distribution modelling for electromagnetic scattering by rain drops," Progress In Electromagnetics Research B, Vol. 25, 191-209

[47] Goddard, J, W. F. (2011) "Propagation in Rain and clouds, in Propagation of Radiowaves ed. Les Barclay," Institution of Electrical Engineers, UK.

[48] Watson, P.A., V. Sathiaseelan and B. Potter, 1982: "Development of a Climatic map of rainfall attenuation for Europe," *No. 300, 134, Post Graduate School of Electrical and Electronic Engineering,* University of Bradford, U.K.

[49] Blanchard, D. C., "The behavior of water drops at terminal velocity in air," *Trans. Amer. Geophys. Union*, Vol. 31, pp. 836–842, 1950

[50] Brentha, T., and A. S. Joseph, "Cloud statistics measured with the Infrared Cloud Imager (ICI)" *IEEE Trans. Geosci. Remote Sens.,* Vol. 43(9), pp. 2000–2007, 2005.

[51] Das, S., A. Maitra, and A. K. Shukla, "Rain Attenuation Modeling In The 10-100 GHzFrequency Using Drop Size Distributions For Different Climatic Zones In Tropical India" *Prog. Electromagn. Res. B*, vol. 25, 211–224, 2010.

[52] Dissanayake A., J. Allnutt and F Haidara, 1997: "A prediction Model that combines Rain Attenuation and other propagation impairments along earth-satellite paths," *IEEE Transactions and Propagation*, Vol. 45, No. 10, Oct.

[53] Rice, P.L. and N.R. Holmberg (1973), "Cumulative Time Statistics of Surface-Point

Rainfall Rates," *IEEE Transactions on Communications*, Vol. COM-21, No. 10, 1131-1136.

[54] Brentha, T., and A. S. Joseph, "Cloud statistics measured with the Infrared CloudImager (ICI)" *IEEE Trans. Geosci. Remote Sens.,* Vol. 43(9), pp. 2000–2007, 2005.

[55] Recommendation ITU-R P.837-5 "Characteristics of precipitation for propagation modelling."

[56] Erma, V. A., "Exact solution for the scattering of electromagnetic waves fromconductors of arbitrary shape". *II. General case, Phys. Rev.*, Vol. 176, pp. 1544–1553, 1968b.

[57] Basili, P., P. Ciotti, G. d'Auria, P. Ferrazzoli, and D. Solimini, "Case study of intense scintillation events on the OTS path,"*IEEE Trans. Antennas Propag.,* Vol. 38, pp. 107–113, 1990.

[58] P.O. Akuon. "Rain Cell Ratio Technique in path attenuation for Terrestrial Radio Links" *World Academy of Science, Engineering and Technology International Journal of Electronics and Communication Engineering* Vol:13, No:6, 2019

[59] Green, H.E., "Propagation on Ka-Band SATCOM Links in Tropical and Equatorial Regions," *IEEE Antennas and Propagation Magazine*,Vol. 46, No.2, 31-43, 2004

[60] Segal, B. (1986). The influence of raingage integration time on measured rainfall-intensity distribution functions. J. Atmos. Oceanic Technol., 3, 662–671.

[61] Chebil, J., & Rahman, T. A. (1999). Rain rate statistical conversion for the prediction of rain attenuation in Malaysia. Electronics Letter, 35, 1019-21.

[62] van de Giesen, Nick & Hut, Rolf & Selker, John. (2014). The Trans-African Hydro-Meteorological Observatory (TAHMO). Wiley Interdisciplinary Reviews: Water. 1. 10.1002/wat2.1034.

[63] Mary N. Ahuna, Thomas J. Afullo, Akintunde A. Alonge, "30-Second Integration Time Power Law Conversion Model for Rainfall Attenuation in South Africa", Paper presented at the IEEE Fifth International Conference on Wireless Communications, Vehicular Technology, Information Theory and Aerospace & Electronic Systems, Hyderabad, India, December 13-16, 2015.

[64] Mary N. Ahuna, Thomas J. Afullo and Akintunde A. Alonge, "30-Second and One-Minute Rainfall Rate Modelling and Conversion for Millimetric Wave Propagation in South Africa", SAIEE African Research Journal, Vol. 107, pp. 17-29, March 2016.

Appendix A: Data analysis in a typical site on the rain data

Appendix A.1 Microsoft Excel Interface showing typical analysis

Rain Range	% Rain Exceeded Muranga	% Rain Exceeded Mukumu	% Rain Exceeded Kebabii	% Rain Exceeded Kamusinga	% Rain Exceeded Habasweni
0.001	5.383469981	7.226243287	2.905945191	2.473212843	0.775131596
0.002	5.383469981	7.226243287	2.905945191	2.473212843	0.775131596
0.003	5.383469981	7.226243287	2.905945191	2.473212843	0.775131596
0.004	5.383469981	7.226243287	2.905945191	2.473212843	0.775131596
0.005	5.383469981	7.226243287	2.905945191	2.473212843	0.775131596
0.006	5.383469981	7.226243287	2.905945191	2.473212843	0.775131596
0.007	5.383469981	7.226243287	2.905945191	2.473212843	0.775131596
0.008	5.383469981	7.226243287	2.905945191	2.473212843	0.775131596
0.009	5.383469981	7.226243287	2.905945191	2.473212843	0.775131596
0.01	5.383469981	7.226243287	2.905945191	2.473212843	0.775131596
0.011	5.383469981	7.226243287	2.905945191	2.473212843	0.775131596
0.012	5.383469981	7.226243287	2.905945191	2.473212843	0.775131596
0.013	5.383469981	7.226243287	2.905945191	2.473212843	0.775131596
0.014	5.383469981	7.226243287	2.905945191	2.473212843	0.775131596
0.015	5.383469981	7.226243287	2.905945191	2.473212843	0.775131596
0.016	5.383469981	7.226243287	2.905945191	2.473212843	0.775131596
0.017	5.383469981	7.226243287	2.905945191	2.473212843	0.775131596
0.018	5.383469981	7.226243287	2.905945191	2.473212843	0.775131596
0.019	5.383469981	7.226243287	2.905945191	2.473212843	0.775131596
0.02	5.383469981	7.226243287	2.905945191	2.473212843	0.775131596
0.021	5.383469981	7.226243287	2.905945191	2.473212843	0.775131596
0.022	5.383469981	7.226243287	2.905945191	2.473212843	0.775131596
0.023	5.383469981	7.226243287	2.905945191	2.473212843	0.775131596
0.024	5.383469981	7.226243287	2.905945191	2.473212843	0.775131596
0.025	5.383469981	7.226243287	2.905945191	2.473212843	0.775131596
0.026	5.383469981	7.226243287	2.905945191	2.473212843	0.775131596
0.027	5.383469981	7.226243287	2.905945191	2.473212843	0.775131596
0.028	5.383469981	7.226243287	2.905945191	2.473212843	0.775131596

ID	Name	Country	Latitude	Longitude	Ro.o1
TA00001	Lela Primary School	Kenya	-1.123	34.398	47.788
TA00018	Koyoo Secondary School	Kenya	-0.582	34.607	59.101
TA00019	Osodo Secondary School	Kenya	-0.524	34.256	41.722
TA00020	Woodlands 2000 Trust	Kenya	-1.653	36.862	21.305
TA00021	Kipsombe Secondary School	Kenya	0.758	35.174	41.989
TA00023	Dwa Estate	Kenya	-2.389	38.041	31.814
TA00024	Mang'u High School	Kenya	-1.072	37.046	46.266
TA00025	Kenya Meteorological Department	Kenya	-1.302	36.76	32.579
TA00026	Moi Forces Academy	Kenya	-0.287	36.17	36.567
TA00028	Equinox Horticulture	Kenya	0.046	37.143	62.101
TA00029	Karima Girls High School	Kenya	-0.501	36.587	15.967
TA00030	Ole Tipis Girls Secondary School	Kenya	-1.095	35.892	41.254
TA00031	Homa Bay High School	Kenya	-0.538	34.46	59.534
TA00056	Murang'a High School	Kenya	-0.722	37.146	50.318
TA00057	St. Scholastica Catholic School	Kenya	-1.253	36.856	21.226
TA00061	Kipsigis Girls High School	Kenya	-0.379	35.251	46.467
TA00063	Kapsabet Boys High School	Kenya	0.203	35.117	48.335
TA00064	Kamusinga Friends Boys Secondary School	Kenya	0.794	34.705	40.194
TA00065	Mukumu Girls High School	Kenya	0.218	34.768	65.845
TA00066	Alliance Girls High School	Kenya	-1.265	36.662	53.282
TA00067	Makueni Boys School	Kenya	-1.794	37.621	36.594
TA00068	Base Titanium Mine	Kenya	-4.373	39.441	44.463
TA00108	Nzukini Secondary School	Kenya	-0.992	37.507	48.007
TA00129	Timbila High School	Kenya	-3.391	37.718	44.686
TA00130	Our Lady of Perpetuah Girls Secondary school	Kenya	-3.498	38.586	47.788
TA00131	Shimo la Tewa School	Kenya	-3.96	39.744	39.274
TA00132	Ganze Boys Secondary	Kenya	-3.551	39.695	37.296
TA00133	Mkunumbi Secondary School	Kenya	-2.298	40.694	41.789
TA00134	Nairobi University	Kenya	-1.274	36.81	35.058
TA00140	Torongo Girls High School	Kenya	0.131	35.607	36.594
TA00141	Sacho High School	Kenya	0.388	35.787	57.851
TA00146	Greenergia	Kenya	-0.148	34.623	66.351
TA00147	Kisoko Girls Secondary School	Kenya	0.449	34.282	50.617
TA00155	Namanga Mixed Secondary School	Kenya	-2.523	36.829	48.335
TA00156	Ikanga Boys High School	Kenya	-1.701	38.068	32.057
TA00157	South Eastern Kenya University - Mtitu Adei Campus	Kenya	-2.657	38.107	45.242
TA00158	Muthale Girls Secondary School	Kenya	-1.185	38.001	41.902
TA00166	Chuka University	Kenya	-0.32	37.659	48.553
TA00171	Maseno University	Kenya	-0.003	34.597	63.635
TA00172	Isiolo Meteorological Service	Kenya	0.354	37.588	39.504
TA00173	Longisa High School	Kenya	-0.855	35.396	33.144
TA00174	Oldonyiru Secondary School	Kenya	0.63	36.988	32.178

TA00182	RCMRD	Kenya	-1.222	36.893	37.529
TA00183	Olderkesi Primary School	Kenya	-1.711	35.565	106.802
TA00185	Mararianda Primary	Kenya	-1.203	35.067	44.015
TA00186	Kyuso DC Office	Kenya	-0.55	38.213	44.574
TA00187	Tseikuru Agricultural offices	Kenya	-0.314	38.22	35.181
TA00189	Machaga	Kenya	-0.795	37.666	25.183
TA00190	University of Embu	Kenya	-0.517	37.456	31.205
TA00196	Baricho High school	Kenya	-0.552	37.228	35.771
TA00247	Maralal Samburu Met Offices	Kenya	1.098	36.714	37.996
TA00250	Kangi	Kenya	-0.779	37.677	47.568
TA00258	Kibugu Mugo	Kenya	-0.447	37.451	50.833
TA00261	Marafa Boys High School	Kenya	-3.032	39.959	51.701
TA00281	Marich Education Center	Kenya	1.537	35.457	37.296
TA00283	Dedan Kimathi University of Technology	Kenya	-0.404	36.966	39.389
TA00288	Kibisi Secondary School	Kenya	0.698	34.865	54.587
TA00307	Wajir Girls	Kenya	1.748	40.034	30.225
TA00316	Konya secondary school	Kenya	0.29	34.371	56.489
TA00317	Ng'iya primary school	Kenya	0.04	34.372	57.013
TA00354	Talent High School	Kenya	3.193	35.675	41.903
TA00355	Moi High School Kalokol	Kenya	3.501	35.848	36.711
TA00356	Loima Boys High School	Kenya	2.857	35.08	21.091
TA00358	Eldas Girls School	Kenya	2.494	39.582	33.024
TA00359	Habaswein DC Offices	Kenya	1.015	39.495	30.348
TA00360	KMD Kitui	Kenya	-1.38	38.003	52.345
TA00374	Jooust	Kenya	-0.093	34.26	44.128
TA00377	Dol Dol Secondary School	Kenya	0.406	37.161	28.738
TA00378	Karatina University (Itiati campu)	Kenya	-0.405	37.117	33.504
TA00379	Lariak Secondary School	Kenya	0.402	36.377	20.279
TA00386	Merti muslim primary	Kenya	1.061	38.666	50.617
TA00387	Kanga High school	Kenya	-0.81	34.589	50.293
TA00388	St.Clare Gekendo High School	Kenya	-0.505	34.974	40.879
TA00389	Mwongori Nyamira Count	Kenya	-0.691	35.037	47.239
TA00394	Nyando Smart Farm	Kenya	-0.288	35.03	58.268
TA00413	Kibabii University	Kenya	0.62	34.521	42.242
TA00414	Murungaru Secondary School	Kenya	-0.587	36.493	36.829
TA00416	Magomano Secondary School	Kenya	-0.607	36.581	42.667
TA00440	St Charles Ichuni High School	Kenya	-0.277	36.075	47.129
TA00441	Cardinal Otunga Musocho High School	Kenya	-0.599	34.744	62.408
TA00442	St Johns Nyamagwa	Kenya	-0.792	34.805	46.688
TA00444	Ngao Girl"s	Kenya	-2.42	40.204	40.308
TA00445	Koome Island HQ	Kenya	-0.081	32.733	51.701
TA00453	NDMA-Tana River Hola	Kenya	-1.495	40.03	24.666
TA00469	Nyambaria Boys	Kenya	-0.666	34.908	51.163

TA00473	Taita Mauche Secondary school	Kenya	-0.512	35.957	34.467
TA00480	Seku Main Campus	Kenya	-1.376	37.798	28.238

Appendix B: Code Listing

Appendix B.1 Main code for specific attenuation on horizontally polarised signals

```
F = [0 10 20 30 40 50 60 70 80 90 100 120 150 200 ]; %
Frequency

%Kamusinga
Kam = [0 1.256724823 4.520037931 7.948911698 10.86346528
13.02114672 14.49901406 15.49466874 16.15102156 16.59273081
16.88900901 17.21717773 17.36467208 17.24628478 ];

%Muranga
Mur = [0 1.663664581 5.722114991 9.822608166 13.18312697
15.59521215 17.20017149 18.25419563 18.93003737 19.37368261
19.6629349 19.96688016 20.07242985 19.88582089 ];

%Kebabii
Keb = [0 1.336217826 4.759210681 8.325411772 11.33302533
13.54498916 15.05084899 16.06001092 16.72153658 17.16452212
17.4600175 17.7840904 17.92366909 17.79174576 ];

%Mukumu
Muk = [0 2.31368355 7.550434003 12.59801409 16.55165801
19.27982524 21.0265397 22.13370375 22.81508895 23.24526194
23.51260434 23.7666843 23.80097575 23.51051654 ];

%Habaswein
Hab = [0 0.875345911 3.33508435 6.050667402 8.464650172
10.31926482 11.63282981 12.5433862 13.16152115 13.58815239
13.88220388 14.22337438 14.40560064 14.35356074 ];

figure

plot(F, Kam, 'bs-','linewidth',1.5);
hold on;
plot(F, Mur, 'm<-','linewidth',1.5);
hold on;
```

```matlab
plot(F, Keb, 'c>-','linewidth',1.5);
hold on;
plot(F, Muk, 'k*-','linewidth',1.5);
hold on;
plot(F, Hab, 'rd-','linewidth',1.5);
grid on;

title({"Frequency characteristics of specific rain
attenuation"; "for horizontally polarized signals for
Kenya"});
ylabel('Specific Attenuation (dB/Km) ');
xlabel('Frequency (GHz)');
legend('Kamusinga','Muranga','Kebabii',
'Mukumu','Habaswein',"location","southeast");
set( gca, 'fontsize', 10 ,'linewidth',1.5);
```

Appendix B.2 Main code for specific attenuation on vertically polarised signals

```matlab
F = [0 10 20 30 40 50 60 70 80 90 100 120 150 200]; %
Frequency

%Kamusinga
Kam = [0 1.00036403 3.633432117 6.6457753 9.548369932
11.80374796 13.47453519 14.6803781 15.55259061 16.16652731
16.59127193 17.07293624 17.26552722 17.06741345 ];

%Muranga
Mur = [0 1.312084724 4.526310477 8.147320597 11.52224641
14.07011992 15.92431019 17.24478624 18.19044236 18.8474268
19.29475664 19.78591077 19.94535906 19.6624545 ];

%Kebabii
Keb = [0 1.061489688 3.81225685 6.948472874 9.948846845
12.26586061 13.9757815 15.20636184 16.09458368 16.71808397
17.1480303 17.63243235 17.81889814 17.60386712 ];

%Mukumu
Muk = [0 1.804975944 5.860630751 10.35222476 14.37106175
17.29747102 19.3802164 20.83857149 21.86970315 22.57353186
23.04209608 23.5321283 23.63293337 23.22266188 ];

%Habaswein
```

```matlab
Hab = [0 0.705151671 2.737095034 5.110802312 7.494080026
9.41197247 10.86387236 11.92872269 12.70817695 13.2650492
13.6571043 14.11679823 14.33489306 14.22063759 ];

figure

plot(F, Kam, 'bs-','linewidth',1.5);
hold on;
plot(F, Mur, 'm<-','linewidth',1.5);
hold on;
plot(F, Keb, 'c>-','linewidth',1.5);
hold on;
plot(F, Muk, 'k*-','linewidth',1.5);
hold on;
plot(F, Hab, 'rd-','linewidth',1.5);
grid on;

title({"Frequency characteristics of specific rain
attenuation"; "for vertically polarized signals for
Kenya"});
ylabel('Specific Attenuation (dB/Km) ');
xlabel('Frequency (GHz)');
legend('Kamusinga','Muranga','Kebabii',
'Mukumu','Habaswein',"location","southeast");
set( gca, 'fontsize', 10 ,'linewidth',1.5);
```

Appendix B.3 Main code Attenuation versus distance at 20GHz for horizontally polarised signals

```matlab
F = [1 5 10 20 30 40 50 60]; % Frequency

%Kamusinga
Kam = [8.630253753 23.8081436 42.24344228 80.21496109
109.3533603 122.7035083 123.9607021 119.4355268 ];

%Muranga
Mur = [10.63660257 28.93895013 50.58971077 93.67375907
125.9937606 141.2528651 143.6008962 139.530209 ];

%Kebabii
```

```
Keb = [9.033661837 24.8441163 43.93418962 82.94580996
112.7231456 126.4590647 127.9422831 123.5129191 ];

%Mukumu
Muk = [13.60390442 36.44411841 62.69351063 113.0881227
150.0757015 168.1077929 171.969977 168.5161768 ];

%Habaswein
Hab = [6.593855391 18.53799466 33.59043664 66.21378282
92.17903223 103.5749169 103.6037536 98.52877321 ];

figure

plot(F, Kam, 'bs-','linewidth',1.5);
hold on;
plot(F, Mur, 'm<-','linewidth',1.5);
hold on;
plot(F, Keb, 'c>-','linewidth',1.5);
hold on;
plot(F, Muk, 'k*-','linewidth',1.5);
hold on;
plot(F, Hab, 'rd-','linewidth',1.5);
grid on;

title({"Attenuation versus distance at 20GHz"; "for
horinzontally polarized signals for Kenya"});
ylabel('Attenuation (dB) ');
xlabel('Distance (km)');
legend('Kamusinga','Muranga','Kebabii',
'Mukumu','Habaswein',"location","southeast");
set( gca, 'fontsize', 10 ,'linewidth',1.5);
```

Appendix C: Table C-1 Frequency-dependent coefficients for estimation of specific rain attenuation [ITU-R P.838-3, 2005]

Frequency (GHz)	k_H	α_H	k_V	α_V
1	0.0000259	0.9691	0.0000308	0.8592
1.5	0.0000443	1.0185	0.0000574	0.8957
2	0.0000847	1.0664	0.0000998	0.9490
2.5	0.0001321	1.1209	0.0001464	1.0085
3	0.0001390	1.2322	0.0001942	1.0688
3.5	0.0001155	1.4189	0.0002346	1.1387
4	0.0001071	1.6009	0.0002461	1.2476
4.5	0.0001340	1.6948	0.0002347	1.3987
5	0.0002162	1.6969	0.0002428	1.5317
5.5	0.0003909	1.6499	0.0003115	1.5882
6	0.0007056	1.5900	0.0004878	1.5728
7	0.001915	1.4810	0.001425	1.4745
8	0.004115	1.3905	0.003450	1.3797
9	0.007535	1.3155	0.006691	1.2895
10	0.01217	1.2571	0.01129	1.2156

Frequency (GHz)	k_H	α_H	k_V	α_V
11	0.01772	1.2140	0.01731	1.1617
12	0.02386	1.1825	0.02455	1.1216
13	0.03041	1.1586	0.03266	1.0901
14	0.03738	1.1396	0.04126	1.0646
15	0.04481	1.1233	0.05008	1.0440
16	0.05282	1.1086	0.05899	1.0273
17	0.06146	1.0949	0.06797	1.0137
18	0.07078	1.0818	0.07708	1.0025
19	0.08084	1.0691	0.08642	0.9930
20	0.09164	1.0568	0.09611	0.9847
21	0.1032	1.0447	0.1063	0.9771
22	0.1155	1.0329	0.1170	0.9700
23	0.1286	1.0214	0.1284	0.9630
24	0.1425	1.0101	0.1404	0.9561
25	0.1571	0.9991	0.1533	0.9491
26	0.1724	0.9884	0.1669	0.9421
27	0.1884	0.9780	0.1813	0.9349
28	0.2051	0.9679	0.1964	0.9277
29	0.2224	0.9580	0.2124	0.9203
30	0.2403	0.9485	0.2291	0.9129
31	0.2588	0.9392	0.2465	0.9055
32	0.2778	0.9302	0.2646	0.8981
33	0.2972	0.9214	0.2833	0.8907
34	0.3171	0.9129	0.3026	0.8834
35	0.3374	0.9047	0.3224	0.8761
36	0.3580	0.8967	0.3427	0.8690
37	0.3789	0.8890	0.3633	0.8621
38	0.4001	0.8816	0.3844	0.8552
39	0.4215	0.8743	0.4058	0.8486
40	0.4431	0.8673	0.4274	0.8421
41	0.4647	0.8605	0.4492	0.8357
42	0.4865	0.8539	0.4712	0.8296
43	0.5084	0.8476	0.4932	0.8236
44	0.5302	0.8414	0.5153	0.8179
45	0.5521	0.8355	0.5375	0.8123
46	0.5738	0.8297	0.5596	0.8069
47	0.5956	0.8241	0.5817	0.8017
48	0.6172	0.8187	0.6037	0.7967

Frequency (GHz)	k_H	α_H	k_V	α_V
49	0.6386	0.8134	0.6255	0.7918
50	0.6600	0.8084	0.6472	0.7871
51	0.6811	0.8034	0.6687	0.7826
52	0.7020	0.7987	0.6901	0.7783
53	0.7228	0.7941	0.7112	0.7741
54	0.7433	0.7896	0.7321	0.7700
55	0.7635	0.7853	0.7527	0.7661
56	0.7835	0.7811	0.7730	0.7623
57	0.8032	0.7771	0.7931	0.7587
58	0.8226	0.7731	0.8129	0.7552
59	0.8418	0.7693	0.8324	0.7518
60	0.8606	0.7656	0.8515	0.7486
61	0.8791	0.7621	0.8704	0.7454
62	0.8974	0.7586	0.8889	0.7424
63	0.9153	0.7552	0.9071	0.7395
64	0.9328	0.7520	0.9250	0.7366
65	0.9501	0.7488	0.9425	0.7339
66	0.9670	0.7458	0.9598	0.7313
67	0.9836	0.7428	0.9767	0.7287
68	0.9999	0.7400	0.9932	0.7262
69	1.0159	0.7372	1.0094	0.7238
70	1.0315	0.7345	1.0253	0.7215
71	1.0468	0.7318	1.0409	0.7193
72	1.0618	0.7293	1.0561	0.7171
73	1.0764	0.7268	1.0711	0.7150
74	1.0908	0.7244	1.0857	0.7130
75	1.1048	0.7221	1.1000	0.7110
76	1.1185	0.7199	1.1139	0.7091
77	1.1320	0.7177	1.1276	0.7073
78	1.1451	0.7156	1.1410	0.7055
79	1.1579	0.7135	1.1541	0.7038
80	1.1704	0.7115	1.1668	0.7021
81	1.1827	0.7096	1.1793	0.7004
82	1.1946	0.7077	1.1915	0.6988
83	1.2063	0.7058	1.2034	0.6973
84	1.2177	0.7040	1.2151	0.6958
85	1.2289	0.7023	1.2265	0.6943
86	1.2398	0.7006	1.2376	0.6929

Frequency (GHz)	k_H	α_H	k_V	α_V
87	1.2504	0.6990	1.2484	0.6915
88	1.2607	0.6974	1.2590	0.6902
89	1.2708	0.6959	1.2694	0.6889
90	1.2807	0.6944	1.2795	0.6876
91	1.2903	0.6929	1.2893	0.6864
92	1.2997	0.6915	1.2989	0.6852
93	1.3089	0.6901	1.3083	0.6840
94	1.3179	0.6888	1.3175	0.6828
95	1.3266	0.6875	1.3265	0.6817
96	1.3351	0.6862	1.3352	0.6806
97	1.3434	0.6850	1.3437	0.6796
98	1.3515	0.6838	1.3520	0.6785
99	1.3594	0.6826	1.3601	0.6775
100	1.3671	0.6815	1.3680	0.6765
120	1.4866	0.6640	1.4911	0.6609
150	1.5823	0.6494	1.5896	0.6466
200	1.6378	0.6382	1.6443	0.6343
300	1.6286	0.6296	1.6286	0.6262
400	1.5860	0.6262	1.5820	0.6256
500	1.5418	0.6253	1.5366	0.6272
600	1.5013	0.6262	1.4967	0.6293
700	1.4654	0.6284	1.4622	0.6315
800	1.4335	0.6315	1.4321	0.6334
900	1.4050	0.6353	1.4056	0.6351
1 000	1.3795	0.6396	1.3822	0.6365

Appendix D: Published Works

Rain Attenuation Prediction for Terrestrial Links at Microwave and Millimeter Bands over Kenya

1st Joseph Onaya
Department of Electrical and Information Engineering
University of Nairobi
Nairobi, Kenya
joseph.onaya@gmail.com

2nd Peter O. Akuon
Department of Electrical and Information Engineering
University of Nairobi
Nairobi,Kenya
akuon@uonbi.ac.ke

3rd Vitalis Oduol Kalecha
Department of Electrical and Information Engineering
University of Nairobi
Nairobi,Kenya
vkoduol@uonbi.ac.ke

Abstract—The equatorial and tropical regions are usually characterized with high amount of rainfall; this usually affect transmission links operating at microwave and millimetre wave bands. The rainfall being a natural and time-varying phenomenon, its induced attenuation increases with frequency and varies from year to year and from region to region. In this paper, a comprehensive analysis of rainfall attenuation is estimated for five sites namely Muranga, Kamusinga, Mukumu, Kebabii and Habasweni. Rainfall rate exceeded for 0.01% of the time is obtained using long term rainfall measurements obtained from Trans-African Hydro-Meteorological Observatory (TAHMO) for a period of two years. The specific attenuation due to rain is predicted at vertical and horizontal polarization for frequency from 1– 100 GHz. Then by using International Telecommunication Union Recommendation (ITU-R), it is found from predictions that the rain attenuation is higher in Mukumu which is located in the western part of Kenya that ordinarily experiences a lot of rain fall. It is also seen that a horizontal polarized signal is more attenuated than vertical polarised signal. Conclusively, the Western Part of Kenya will suffer more from rain-induced network outages compared to other parts of the country. This study will provide useful inputs in the deployment of terrestrial and across the entire Country of Kenya.

Index Terms—specific attenuation, rain rate, effective path length, drop size

I. INTRODUCTION

There is continuous growth in the telecommunications (TLC) sector which has seen the introduction of more data thirsty products and services in the wireless domain of TLC systems. These products and services need to be supported by

Microwave links play a very important role in wireless telecommunications system using radio frequency (RF) as the main medium of transmission. Synchronous Digital Hierarchy (SDH) is usually used to employ Point to Point (Multi Point) microwave link while most back bone and last mile terrestrial systems of communication employ Parallel Digital Hierarchy (PDH). TLC engineers in most cases take keenly the following design parameters of a microwave link, (a) system reliability, (b) economical design, (c) present and future frequency selection and planning, (d) in order to minimize the number of additional microwave sites to save on frequency fees, and (e) flexible, multilevel and adaptable telecommunications systems. Microwave links are prone to many sources of signal interference due to attenuation along the line of sight; microwave propagation path usually is occasioned by the physical variations that occur in the troposphere and tropopause. We do have hydrometeors namely raining, fogging, moisture and oxygen in the path of the radio signal (path of propagation) which causes significant signal energy loss through signal absorption. Amongst these hydrometeors, the signal loss due to attenuation in its propagation path is majorly caused by rain. This has been realised to be a significant microwave link design challenge for mostly operated at higher frequencies usually above 10 GHz [9-13]. Equatorial regions experience excessive rainfall most times of the year, therefore attenuation due to rain is quite significant when it comes to propagation losses during signal transmission. This usually degrades the

thirsty products and services in the wireless domain of TLC systems. These products and services need to be supported by the bandwidth-limited radio network. Nevertheless, in radio network systems there is still frequency spectrum under-utilization especially in the higher bands of frequency. This is because high frequency signals are adversely attenuated by rain through absorption and scattering mechanisms [1-6]. Therefore, there is need for TLC design engineers to estimate and provide for the expected amount of rain attenuation in a radio link situated anywhere in the world during the link planning phase. This process requires the knowledge of characteristics of rain rates and rain attenuation [7-8].

due to rain is quite significant when it comes to propagation losses during signal transmission. This usually degrades the radio wave propagation along the transmission path. This shows clearly that attenuation due to rain definitely impacts negatively the length of path of the terrestrial microwave links and therefore at higher frequencies the use of which is greatly limited on these terrestrial links, point to point microwave transmission systems. In order to mitigate the effects of path attenuation in rain, exact rain information is vital for an RF engineer. Rain rates exceeded at 0.01% of the year is necessary in computing specific attenuation for these radio links.

Interestingly, most African regions rely on ITU-R maps

to determine rain rates exceeded 0.01% of the time [ITU-R P.837]. There has been limited measurement campaigns to obtain in situ measurements from the region. However, recent studies in South African and Nigeria show that the elaborate and useful ITU-R data may underestimate the real rain rate values, especially in equatorial and subtropical areas. It is therefore necessary to carry out rain rate measurements in these locations in order to compare with those from ITU-R and inform policy decision for network operators and regulators in the communications sector. ITU-R P.530 recommends rain rate information over 1-minute integration time. However, the equipment used for this kind of data are not easily affordable. Luckily, ITU-R also recommends conversion factors for different integration times. Therefore, the data presented in this paper were collected and converted into 1-minute integration time as discussed later in the paper.

II. II. METHODOLOGY

A. Data Collection and Processing

Kenya is located in the Eastern part of Africa bisected horizontally by the Equator and vertically by longitude 38° E, Kenya is bordered to the north by South Sudan and Ethiopia, to the east by Somalia and the Indian Ocean, to the south by Tanzania, and to the west by Lake Victoria and Uganda. The Country experience's two rainy seasons per year the long rainy season lasts from March to May, while the short rainy season lasts from October to November. The sunniest time of year is December to March, while June to September is cooler and

TABLE I
CLIMATIC PARAMETERS FOR THE SELECTED LOCATIONS

Station	Latitude	Longitude	$R_{0.01} mm/hr$	$R_{0.01} mm/hr // ,ITU$
Muranga	-0.722	34.146	50	
Kamusinga	0.794	34.705	40	
Kebabii	0.521	34.256	42	40
Mukumu	0.218	34.768	65	
Habasweni	-1.123	34.398	30	

December to March, while June to September is cooler and often more overcast. For the prediction of Rain attenuation in Kenya, daily rainfall data for a select five stations across the nation were used, these data were collected for a period of two years. These daily rainfall data was converted into average accumulation of (mm/hr). Table 1 presents the climate parameters, the geographic coordinates, the data collection period of the stations where rainfall data were collected in Kenya.

In principle, the two main laws commonly used in empirical methods are the power law and the power-exponential law. In Emilian et al (2009), the laws are expressed as follows:

$$R_1(P) = \alpha R_T(P)^b \qquad (1)$$

Where $R_1(P)$ and $R_T(P)$ are, the rain rate for a one-minute integration time and any integration time (T) respectively at equal percentage of exceedance (P), a and b values for 60 to 1 minute integration time is used as per Emilian et al (2009). It follows that

lasts from October to November. The sunniest time of year is December to March, while June to September is cooler and often more overcast. For the prediction of Rain attenuation in Kenya, daily rainfall data for a select five stations across the nation were used, these data were collected for a period of two years. These rainfall data were converted into average accumulation of (mm/hr). Table 1 presents the climate parameters, the geographic coordinates, the data collection period of the stations where rainfall data were collected in Kenya.

The data provided was collected using ATMOS 41 Weather station which has 12 weather sensors combined into a single, compact device for atmospheric conditions. It contains a 9.31-cm diameter rain gauge, which has a flared hole that forms the rain into drops, these drops then pass through the drip counter. As the rain intensity increases, the drops become smaller, but the ATMOS 41 firmware contains an algorithm to automatically compensate for drop size as the rain increases. It has a 0.017 mm resolution means it can accurately measure small rainfall and even heavy dew events that other rain gauges could miss.

III. RAIN RATE DISTRIBUTION IN KENYA

Kenya is located in the Eastern part of Africa Bisected horizontally by the Equator and vertically by longitude 38° E, Kenya is bordered to the north by South Sudan and Ethiopia, to the east by Somalia and the Indian Ocean, to the south by Tanzania, and to the west by Lake Victoria and Uganda. The Country experience's two rainy seasons per year the long rainy season lasts from March to May, while the short rainy season lasts from October to November. The sunniest time of year is

equal percentage of exceedance (P), a and b values for 60 to 1 minute integration time is used as per Emilian et al (2009). It follows that,

$$R_{0.01} = \alpha R_{60} (P)^{\beta} \qquad (2)$$

$R_{0.01}$ is the rainfall rate exceeded for 0.01% of the time and coefficients α and β are 11.565 and 0.7982 respectively as used in Ile Ife Nigeria [11]

$R_{0.01}$ has been determined for the five sites and is presented in Table 1. The results show that the highest $R_{0.01}$ is 65 mm/hr at Mukumu Girls situated in Kakamega and the lowest is 30 mm/hr at Habasweni located in Wajir. Tha rain rate from ITU map for Mukumu area is about 50mm/hr and for Habsweni about 40mm/hr which shows that the values are much lower. A plot of % exceedance versus rain rate (mm/h) for the five locations is as shown in figure 1

IV. RF LINK PLANNING

RF link between a transmitter and a receiver undergoes several fade phenomena, due to multipath effects, rain, fog and scintillation effects. The gain of both transmit and receive antennas, branching losses, route diversity gains and multipath fading determine the amount of power received at the receiver. This informs the fade margin required so that the received signal level will be above the receiver threshold. The path attenuation can be modelled through a link budget

A. Link Budget

In order to determine the link budget, the following fade phenomena are normally taken into account. The received signal level (RSL) is determined as follows:

Figure 1. Cummulative rain rate distribution at 1 Minute sampling rate in Kenya
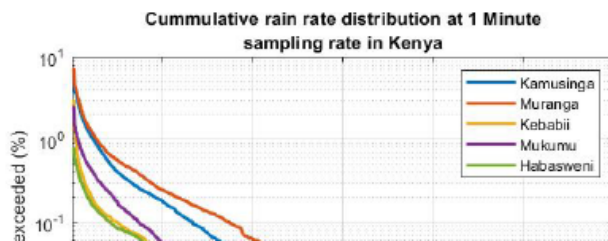
C. Specific Rain Attenuation

The radio waves propagating through rain are subject to attenuation caused by raindrops of various sizes. The scattering of the signal by these rain drops can be modelled via Mie scattering. The signals may also be absorbed, especially by larger raindrops if the carrier frequency is high. The term specific attenuation or attenuation coefficient, which expresses the attenuation per unit of path length is obtained from
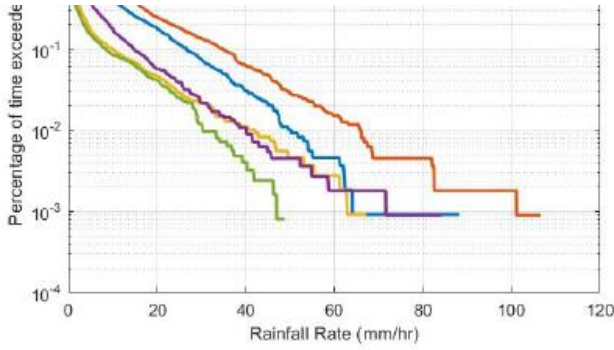
Fig. 1. Rain rates exceedance curves for 5 locations

specific attenuation or attenuation coefficient, which expresses the attenuation per unit of path length is obtained from $R_{0.01}$[14][15]

$$A_s = kR^\alpha \qquad (5)$$

k and α are the coefficients of regression where k is a factor dependent on the wave frequency for a particular microstructure model of the rain and the α factor depends on the polarization at a given tilt angle, frequency and temperature [17-21].
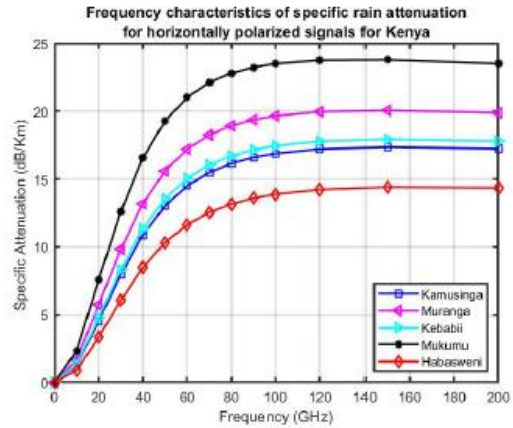
$$RSL = P_t + G_t + G_r - FSL - A_g - L_r - L_t - (A_r + A_w) \qquad (3)$$

Where; P_t is the transmitted power,
G_t is the gain of the transmitter,
G_r is the receiver gain,
Free space loss (FSL),
A_g is the attenuation due to gas,
A_r is the attenuation due to rain,
A_w is the wet antenna loss (both transmitter and receiver terminals),
L_t is the loss in transmit-systems and
L_r is the loss in the receive-systems.
The free-space loss is determined as;
$FSL = (32.4 + 20log_{10}L + 20log_{10}f)$
where f (GHz) is the frequency used in the link and L is the link path length in km. It is therefore necessary to determine the attenuation due to rain, A_r

B. Path Attenuation for Rain

For terrestrial links, ITU-R 530 specifies path attenuation as the product of specific attenuation per km, ITR-R 838, and the effective path length, L_{eff}.
The effective path length is the product of the real actual length and a path factor, r. Therefore, the path attenuation is written as follows;

$$A_r = A_s rL \qquad (4)$$

where specific attenuation is specified under ITU-R 838. The path factor can be modelled in several ways, such as that of IUT-R, rain cell model and other effective rain rate models [17-21].

Fig. 2. Specific Attenuation for horizontal polarization

Fig. 3. Specific attenuation for vertical polarization

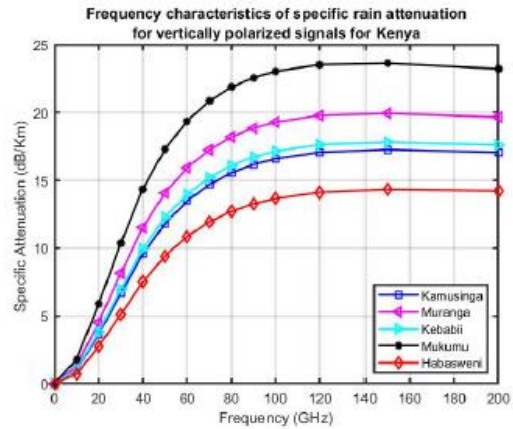ITU-R, rain cell model and other effective rain rate models [17-21].

Fig. 3. Specific attenuation for vertical polarization

In Figure 2 and 3 the distribution of specific attenuation of rain versus frequency are for horizontally and vertically polarized signals is determined for the five sites that is Habasweni, Lela, Mukumu, Kebabii, Muranga and Kamusinga. The specific attenuation increases sharply for 0–50 GHz, followed by a more gradually increment for 50–100 GHz. For all locations in it is seen that the specific attenuation found from measurement is higher than ITU predicted values.

V. CONCLUSION

In this paper, $R_{0.01}$ at one minute integration time is determined by the help of rainfall data collected for more than a year from selected five sites in Kenya. Then by using ITU model, the specific attenuation due to rain is predicted at vertical and horizontal polarization for frequency from 1–100 GHz. It is observed that the attenuation is maximum in Mukumu located in Western part of Kenya which experiences large amounts of rainfall and least in Habasweni located in the Northern part of the Country which experiences least amount of rainfall.

VI. ACKNOWLEDGMENT

REFERENCES

[1] R.K. Crane, "Prediction of attenuation by rain," IEEE Trans. Comm., vol. 28, pp. 1717–1733, 1980.

[2] Crane, R.K, "A two-component rain model for the prediction of attenuation statistics," Radio Science, vol. 17, N.6, 1371-1387, 1982.

[3] G.O. Ajayi and E.B.C. Ofoche, "Some tropical rainfall rate characteristics at Ile-Ife for microwave and millimeter wave application," J. of Climate and Applied Meteor., vol. 23, pp. 562–567, 1983.

[4] F. Moupfouma, "Improvement of a rain attenuation prediction method for terrestrial microwave links," IEEE Trans. Antennas Propag., vol. 32, pp. 1368–1372, 1984.

[5] F. Moupfouma, "Rainfall-rate distribution for radio system design," IEEE proceedings, vol. 134, pp. 527-537, Feb. 1987.

[6] Moupfouma F. "Rain induced attenuation prediction model for terrestrial

[15] ITU-R 838-2, Specific Attenuation Model for Rain for Use in Prediction Models, Vol. 2003, P Series, International Telecommunication Union, Geneva, Switzerland, 2005.

[16] Fashuyi, M. O., P. A. Owolawi, and T. O. Afullo 'Rainfall ratemodelling for LoS radio systems in South Africa," Trans. of South African Inst. of Elect. Engineers, Vol. 97, 7481, 2006.

[17] Moupfouma, F. and L. Martin, "Modelling of rainfall rate cumulative distribution for the design of satellite and terrestrial communication systems," International Journal for Satellite Communication, Vol. 13, 105–115, 1995.

[18] Rice, P. and N. Holmberg, "Cumulative time statistics of surface-point rainfall rates," IEEE Transactions on Communications, Vol. 21, No. 10, 1131–1136, October 1973.

[19] ITU-R P.837-[1-7], "Characteristics of precipitation for propagation modelling," ITU P Series, Geneva.

[20] Sirven, P., J. F. Gontanegre, and C. Prioul, G´eographie du Rwanda, Editions A, DeBoeck, Brussels, Belgium, 1974

[21] P.O. Akuon.,Rain Cell Ratio Technique in path attenuation for Terrestrial Radio Links, 2019